THE OHIO STATE UNIVERSITY

Project HyBuJet

Student Authors: T. Ramsay, B. Collet, K. Igar, D. Kendall, D. Miklosovic, R. Reuss, M. Ringer, and T. Scheidt

Supervisor: Dr. G. M. Gregorek
Assistant: R. L. Reuss
Department of Aeronautical & Astronautical Engineering

Universities Space Research Association
Houston, Texas 77058

Subcontract Dated November 17, 1989
Final Report
RF Project 767919/722941

May 1990

HYPERSONIC BUSINESS JET

(HyBuJET)

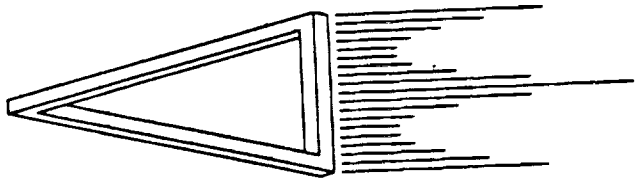

PROJECT: HyBuJET

by:

Tom Ramsay
Bill Collet
Karyn Igar
Dewayne Kendall
Dave Miklosovic
Robyn Reuss
Mark Ringer
Tony Scheidt

We would like to thank the following people for their continual support and information on this project:

Bob Boyd
Dr. Michael Bragg
Dr. Stephen Corda
Dr. Gerald Gregorek
Don Hallock
Jim Hartsel
Carol Hopf
Phil Weissman

TABLE OF CONTENTS page

LIST OF FIGURES

page

LIST OF TABLES

LIST OF SYMBOLS

a	acceleration
A	active cooling area
A_c	capture area
A_t	throat area
A_i	local cooling area
AR	aspect ratio
b	span
c	mean aerodynamic chord
C_D	drag coefficient
C_{Dw}	wavedrag coefficient
C_f	skin friction coefficient
$\frac{C_f}{c}$	$\frac{\text{elevon chord}}{\text{mean aero chord}}$
C_l	roll coefficient
$C_{l\alpha}$	2D lift curve slope
C_L	lift coefficient
C_M	moment coefficient
C_n	yaw coefficient
C_P	pressure coefficient
C_{Pc}	silicon coolant specific heat (0.43)
C_{Pf}	liquid hydrogen specific heat (2.2)
C_Y	side force coefficient
D	drag
F_c	postulated function defined by Spalding
h	heat transfer coefficient
L	lift

M	moment
P	pressure
P_R	Prandtl Number (0.7)
q	dynamic pressure
r_o	radius of curvature
R	gas constant
S	planform area
SFC	specific fuel consumption
T	temperature
U	velocity
V	volume coefficient
W	weight

GREEK

α	angle of attack
β	side slip angle
Γ	anhedral angle
δ	deflection angle
ϵ	emissivity
η	spanwise location
Λ	leading edge sweep angle
ρ	density
σ	Boltzman's constant

SUBSCRIPTS

0	stagnation conditions
a	aileron

atm	atmospheric conditions
aw	adiabatic wall
e	elevator
i	inboard local position
le	leading edge stagnation line
o	outboard local position
p	roll rate
q	pitch rate
r	yaw rate, recovery
t	turbulent
vs	vertical surface
w	wall
α	rate of angle of attack change
β	side slip angle
δ	local free stream conditions
∞	free stream conditions

1. INTRODUCTION

The business world of today moves at a rapid pace, and commercial aviation is being hard pressed to keep up. It is no longer acceptable for executives to spend countless hours flying all over the world. While the Concorde is a step in the right direction, its transatlantic range cannot connect all of the important business centers of today. In order to meet the needs of the coming decades, a longer range hypersonic business jet is proposed (project HyBuJET). HyBuJET is designed to cover transpacific routes in a fraction of the time it takes today.

In order to obtain a workable initial concept, the complex interplay of aerodynamics, atmospheric heating, thrust, fuel selection, weight, etc. need to be evaluated for an acceptable conceptual design to be presented. Previous hypersonic commercial designs have tended toward large, 250+ passenger aircraft. In order to keep weights and costs down a smaller 10 passenger business jet will be investigated.

The requirements for this project were set at a cruise Mach number of 4-6, accommodations for 10 passengers/2 crew, a range of 6000 nm, and take-off/land from a conventional 10,000 ft runway.

2. SUMMARY

The initial design requirements we set at the beginning of this project were to design for cruise conditions, acceptable (or possibly augmented) subsonic performance, adequate room for passengers, and engine-airframe integration. In order to optimize for cruise conditions, a waverider configuration was chosen for the high lift-to-drag ratio and low wave drag. The leading edge and lower surface of a waverider was mapped out from a known flow field (see section on waveriders for more information) and optimized for a cruise Mach number of 6, a cruise altitude of 100,000 ft, and a span of 90 ft. The shockwave generated by a waverider remains attached along the entire leading edge, allowing for a larger compression along the lower surface. A waverider generating code MAXWARP (Maryland Axisymmetric Waverider Program) was used to generate the waverider configuration for cruise conditions, while still allowing adequate room for the cabin, fuel, avionics, etc. The final configuration proposed by this report was almost completely driven by the output design of MAXWARP.

Three turbofanramjets were chosen as the propulsion of the aircraft due to the combination of good subsonic performance along with high speed propulsive capabilities. In order to utilize the relatively small volume within a waverider, a dual fuel scheme was chosen. The turbofans were fueled by a high grade jet fuel, and the ramjets by liquid hydrogen. This combination allowed for a smaller volume of fuel due to the use of the denser jet fuel during the subsonic and low supersonic portion of the mission, while

utilizing the propulsive efficiency of liquid hydrogen during cruise.

The liquid hydrogen, being a cryogenic fuel, needed some type of insulation to minimize boil-off and eliminate ice formation. The tanks were designed for minimum thickness, while still allowing for weight considerations. A carbon-dioxide frost system was chosen because only 1" of insulation was needed to keep the hydrogen below freezing and prohibit the formation of ice on the outside of the tanks.

Due to the harsh environment at Mach 6 and 100,000 ft, very high skin temperatures were predicted, especially on the nose cap and leading edges (2400 F - 1750 F). These high temperatures demand the use of an active cooling system used at the high heating areas of the aircraft. A combination of liquid silicon convective cooling for the leading edges with a highly radiative outer skin material wase chosen to reduce the skin temperatures to acceptable levels.

The cabin was designed to be more comfortable and spacious than even today's first class accommodations, with swivel chairs, a 6.5 ft ceiling, and full lavatory facilities.

Most of all, the range of 6500 nm encompasses all transatlantic, transamerican, transpacific, European, and most intercontinental flight routes. The range of 6500 nm is completed in 2 hrs 10 min, which allows for a 30 min loiter or divert to another airport.

Table 1 shows the specifications and Figure 1 shows the configuration for the proposed aircraft. The next section shows the positioning of the major components of the aircraft within the airframe.

Table 1 - Specifications

Length	115	ft
Span	90	ft
Planform Area	5661	sq ft
Aspect Ratio	1.41	
Leading Edge Sweep	70	deg
Take-Off Weight	171,379	lbs
Empty Weight	90,661	lbs
Cruise Mach Number	6	
Cruise Altitude	100,000	ft
Range	6500	nm
Endurance	2 hr 40	min
Take-Off:		
Lift Coefficient	0.296	
Velocity	291	ft/s
Distance	6930	ft
Wing Loading	29.8	lb/sq ft
Thrust Loading	0.440	
Landing:		
Lift Coefficient	0.6	
Velocity	145	ft/s
Distance	4152	ft
Wing Loading	16.0	lb/sq ft
Thrust Loading	0.712	

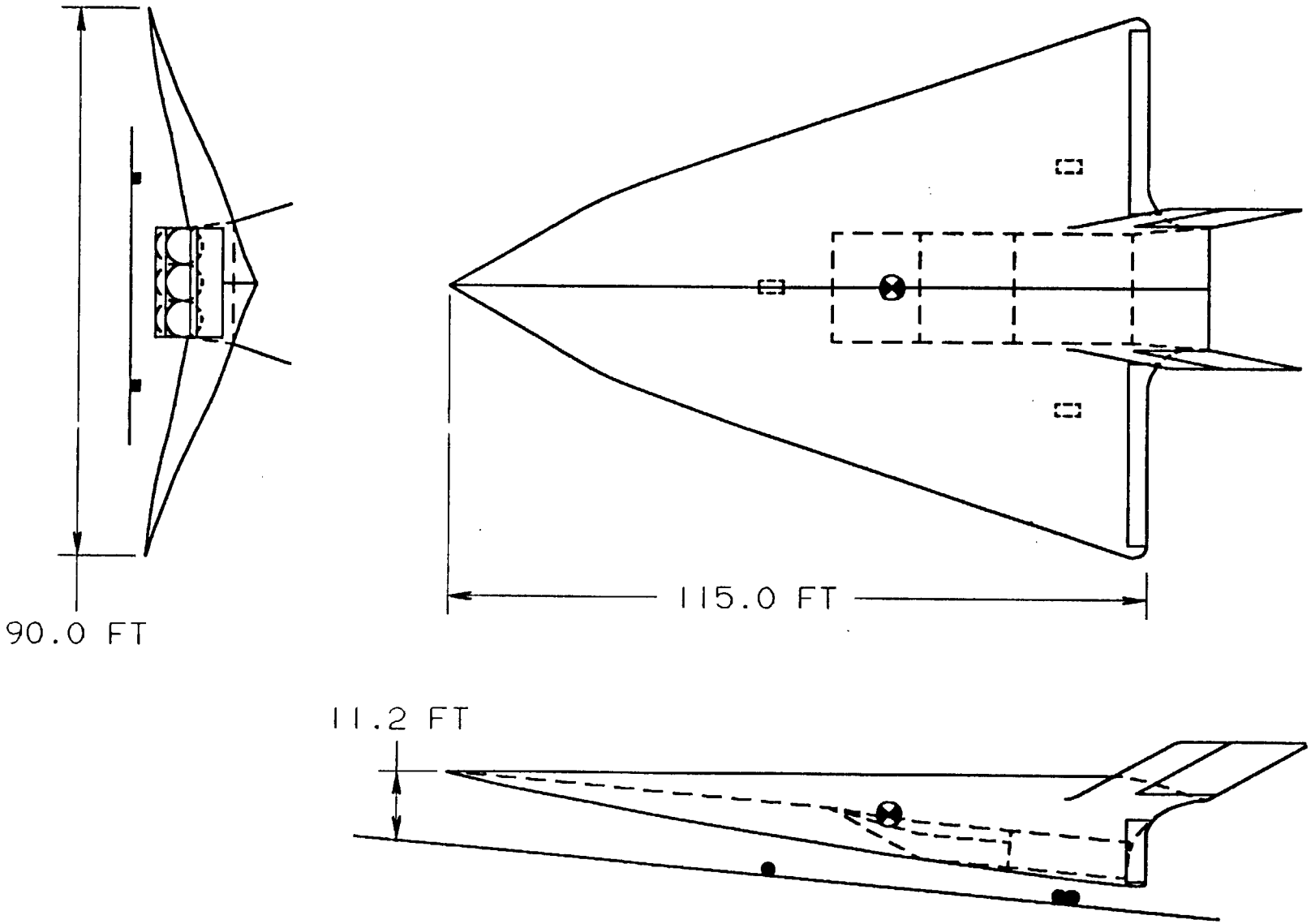

Figure 1 - Proposed Configuration

3. INBOARD POSITIONS

The position of the major internal components of the aircraft are shown in Figure 2. The isometric shown was generated using solid modelling techniques. The inboard isometric is a full scale solid model of the aircraft produced on a CAD system. This allowed the position of each component to be placed accurately and when combined with component weights, the center of gravity, moments and products of inertia were calculated by the CAD system for a full scale model of the aircraft. This allowed for a more accurate center of gravity and stability & control analyses. See Figure 1 for the center of gravity position.

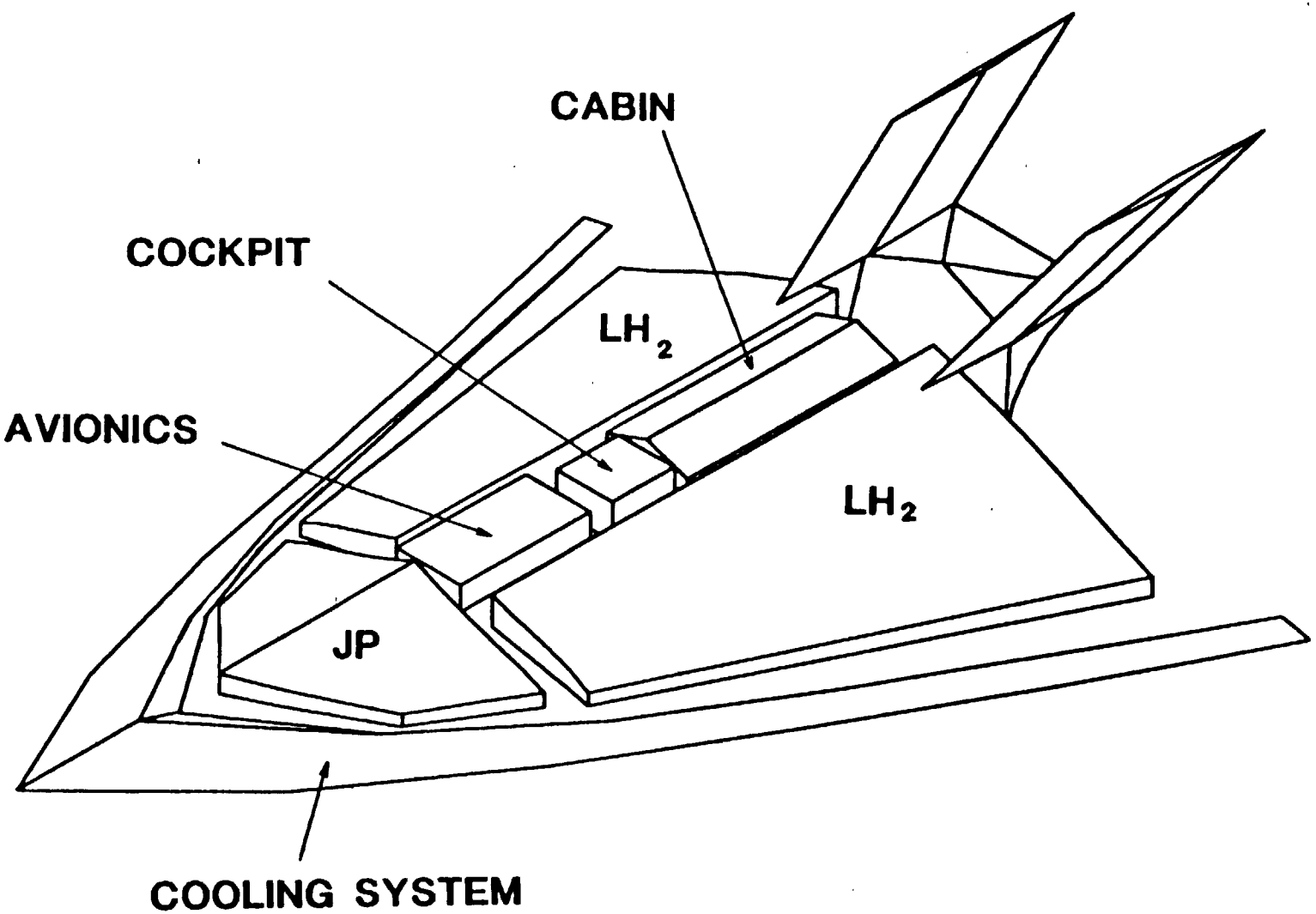

Figure 2 - Inboard Isometric

4. MISSION PROFILE

The mission profile is based on keeping the dynamic pressure constant at 1000 psf in the crucial climb phase, as shown in the Mission Acceleration graph. Should this trajectory be followed up to 100,000 ft., the terminal Mach number would be about 8, so a linear approximation dictates the trajectory for the last 20,000 ft. of climb. The same holds true for acceleration up to Mach 1. By using this kind of trajectory, there is significant fuel savings over a linear trajectory (Refefence 11).

Given the Mach numbers at each altitude (from the mission trajectory), a computer program computed the maximum angles of ascent, fuel burned, and aircraft weight at each step in the mission. The aircraft weight is shown throughout the mission in Figure 4. All along the mission profile, the aircraft never experiences more than 1/6 g acceleration, although acceleration will be lowered to 1/10 g to break through Mach 1. If the thrust required at any point along the flight profile turns out to be too high, the acceleration can be lowered as the aircraft passes through those points. Figure 8 shows the thrust required and available for the climb phase.

The nominal cruise altitude is 100,000 ft., but the aircraft never remains at that altitude for more than a brief time. To maintain optimum aerodynamic efficiency, a constant lift coefficient has to be maintained. Therefore, as weight is being burned off in the form of fuel, the lift keeps the aircraft ascending on a very gradual trajectory. Moreover, the altitude

must be increased to maintain the maximum engine efficiencies. As a result, the cruise leg is begun at 98,800 ft. and ended at 104,300 ft.

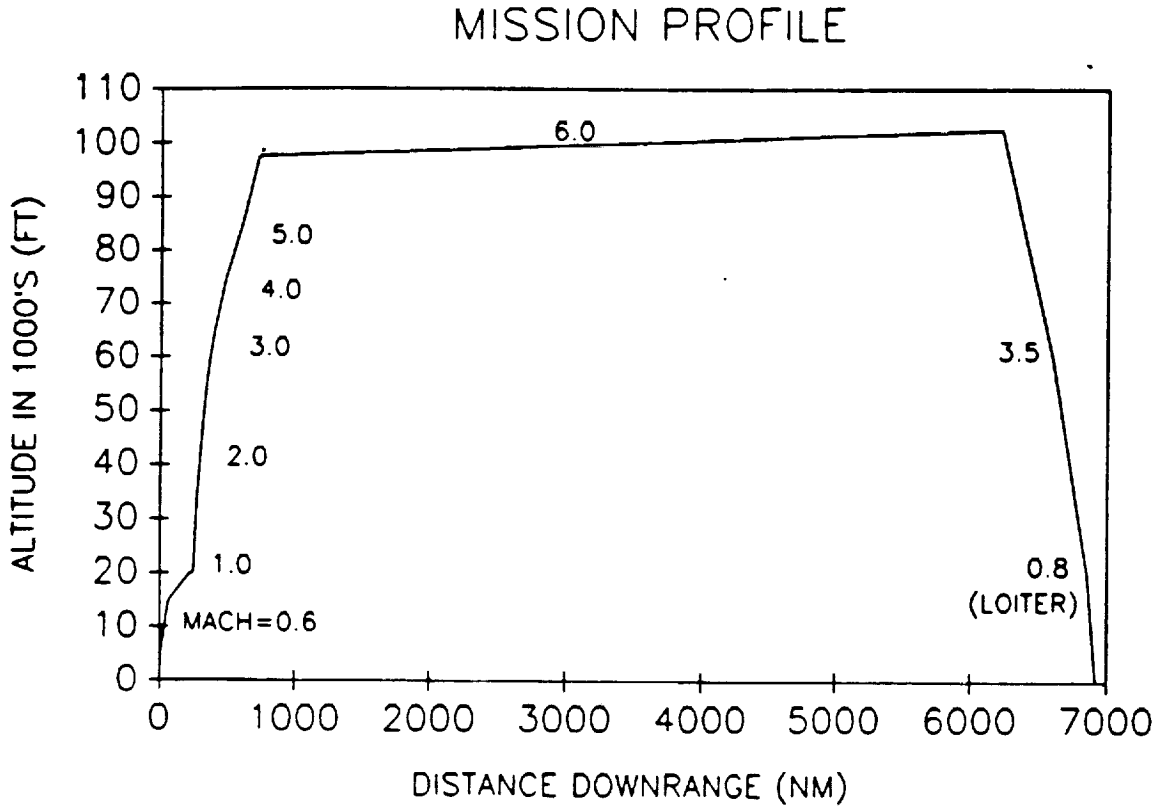

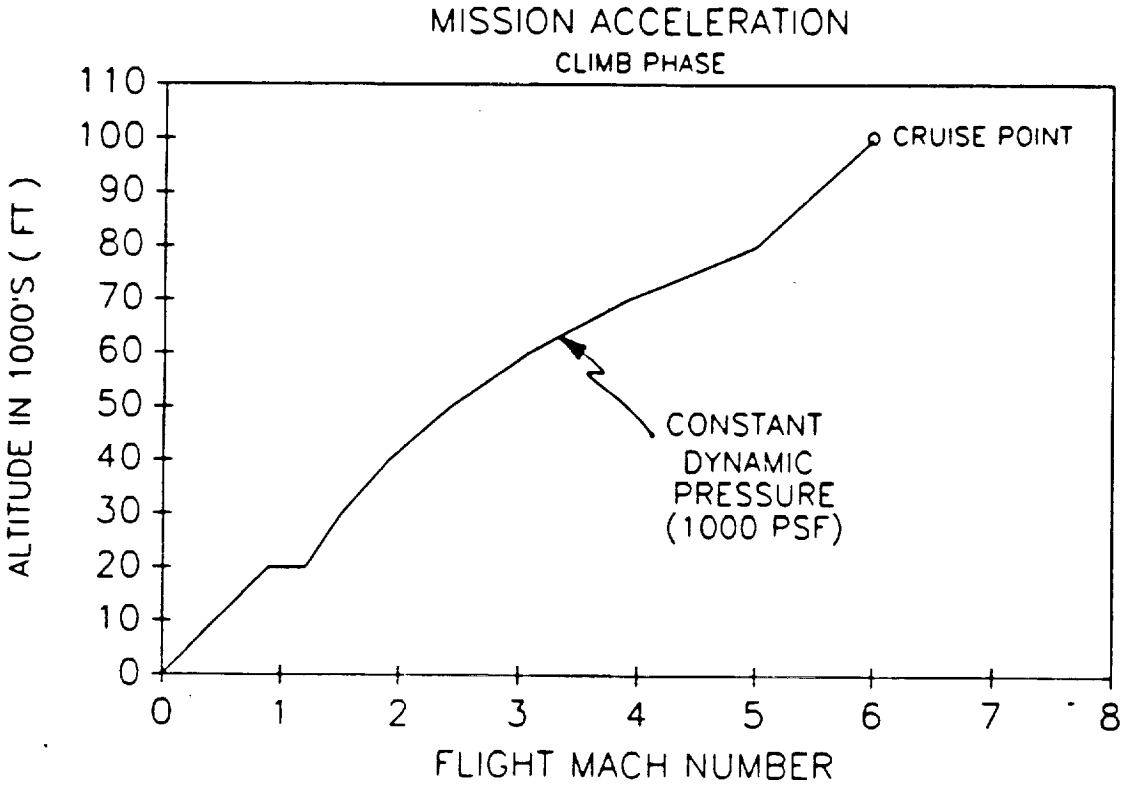

Figure 3 - Mission Profile and Acceleration

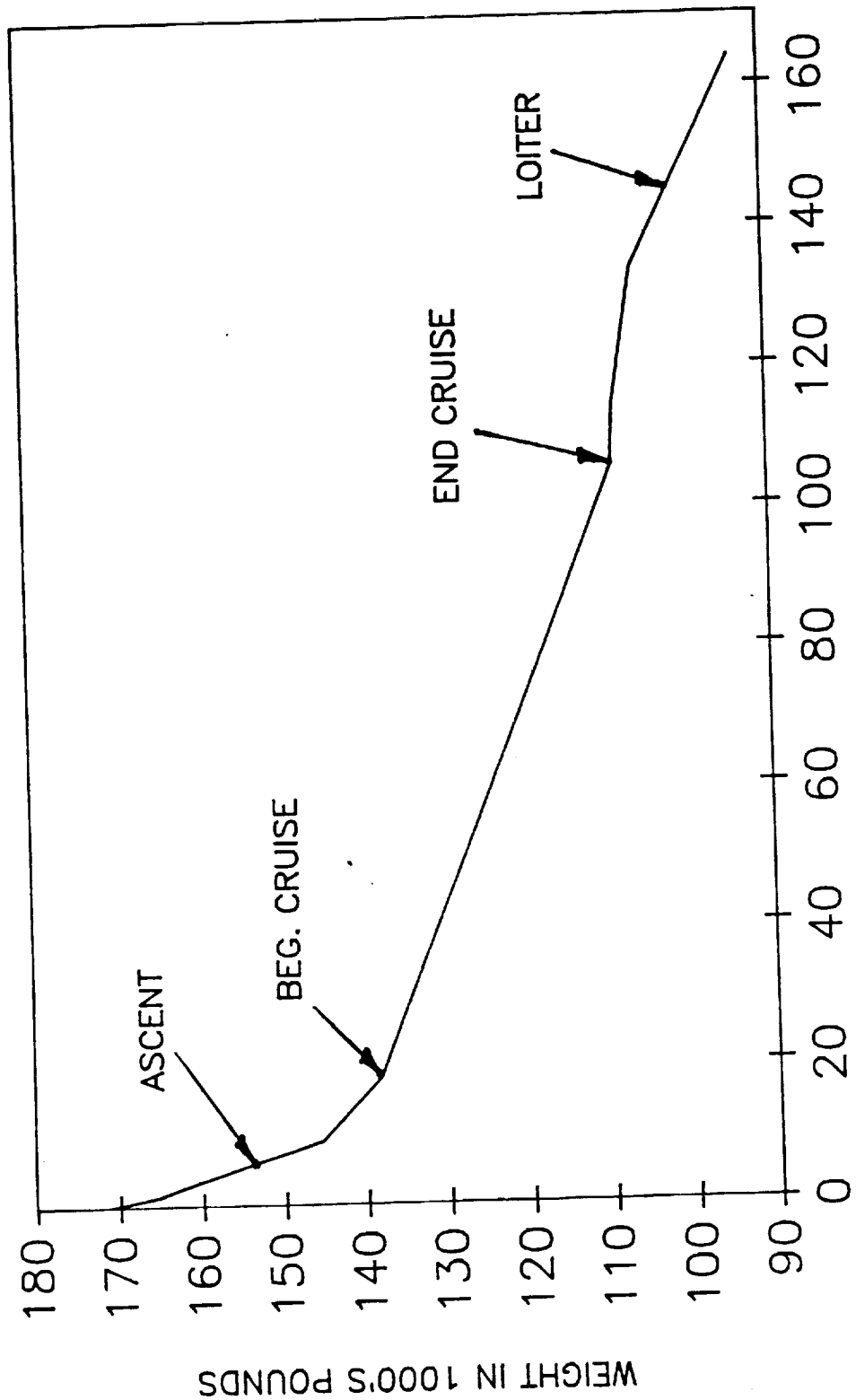

Figure 4 - Mission Weight Profile

5. PROPULSION SYSTEM

5.1 PROPULSION SYSTEM CONFIGURATION

5.1.1 ENGINE SELECTION

To satisfy the condition of continuous operation through the subsonic/supersonic/hypersonic regimes, a hybrid engine system is required. At Mach 6 cruise, anything more exotic than a ramjet is unnecessary, but the need to accelerate to ram ignition speeds is essential. Typically, a dual-mode system is needed for such an application, with the first mode (usually a turbo engine) handling subsonic/low supersonic speeds, and the second mode (a ramjet), high supersonic/hypersonic speeds. Various ramjet/ accelerator configurations are summarized:

Turboramjet:

This engine combines a turbojet accelerator which operates up to Mach 2.5-3, at which point a ramjet takes over and accelerates up to Mach 6 or so. Turboramjets may consist of two separate engines--turbojets and ramjets in an over/under configuration--or may be combined into one engine package in a wrap-around or in-line configuration. The maximum speed attainable by these engines is governed by that of a ramjet, which is about Mach 6.

Turbofanramjet:

Much like the turboramjet, the turbofanramjet boasts the improved subsonic and low supersonic performance characteristics of the turbofan.

Ejector Ramjet:

By introducing a high velocity combustion stream into a modified ramjet, significant static thrust can be achieved. Such ejectors may consist of a turbojet or rocket supercharger. The speed regime is about the same as the turboramjet.

Airturboramjet (ATR):

The ATR accelerates up to ram ignition speeds by LOX and hydrogen combustion, much like an augmented rocket engine. Variations of this engine may take a vehicle all the way into orbit.

Scramjet:

Scramjets are very efficient at hypersonic speeds, without the need for long compression inlets and are relatively simple compared to subsonic combustion ramjets. However, to take advantage of the supersonic combustion, the engine must operate in the Mach 6-12 regime.

The most feasible of these concepts is the turbofanramjet. Technologically, the turboramjet is already available to the U.S. aerospace industry, with a first-generation production model flying

on the Lockheed SR-71. Although billed as turbojets, the SR-71 engines essentially operate as ramjets at cruise speeds, burning just enough fuel to keep the machinery operating and the massflow up, all of the compression comes from the deceleration of the high speed flow. Most of the thrust in this regime comes from the inlet compression/nozzle expansion cycle. Therefore, a pure turboramjet/turbofanramjet is probably the next viable step, and General Electric suggests that their turbofanramjet concept engines may be available as early as 2005.

Three such engines are required to power the aircraft through the mission profile. Original preliminary work was based on a two-engine aircraft because of weight considerations. The prime mover behind changing the number of engines was how to package two very large engines (7.3 ft. diameter). By downsizing and using three engines, only 4% was added to the bare engine weight and this reduced the maximum diameters to 6.0 ft. If four engines could be used, it would entail a 7% increase in bare engine weight and maximum diameters of 5.2 ft. Ideally, four engines would have been the best compromise, but the engine scaling factors would have been beyond GE's prescribed scaling limits. Therefore, three engines were used. Not only did the available interior volume increase by mounting three smaller engines under the aircraft, but the transpacific requirement of three engines was met.

5.1.2 DESCRIPTION

A GE turbofanramjet is shown in Figure 5. At its core, the engine has a conventional low bypass turbofan, which is fueled by a next-generation aviation fuel, JP-X. In this mode, the annular duct around the core accommodates bypass air (less than 10% BPR) and injects it back into the flow ahead of the primary nozzle for cooling purposes. In the ramjet mode, all air is diverted around the core and the bypass duct becomes the ram duct, with all air passing through the windmilling fan. The ram burners, distinctly separate structures from the JP-X combustors, are fed with hydrogen fuel and are located toward the rear of the ram duct.

5.1.5 SPECIAL CONSIDERATIONS

Acoustic Constraining:

Should the design incorporate a standard turbofanramjet engine system, it would exceed FAR 36 stage 3 noise limits by a considerable margin. Since the aircraft is not a pure military type, and it will be operating from population centers (rather than remote airfields), acoustic constraining of some type is necessary. Therefore, the engines must be oversized to reduce takeoff and climb exhaust jet velocities. This results in increasing the inlet mass flows 64%, and thus the nozzle weights 50%. These nozzle weights are included in the bare engine weight figures in Table 2.

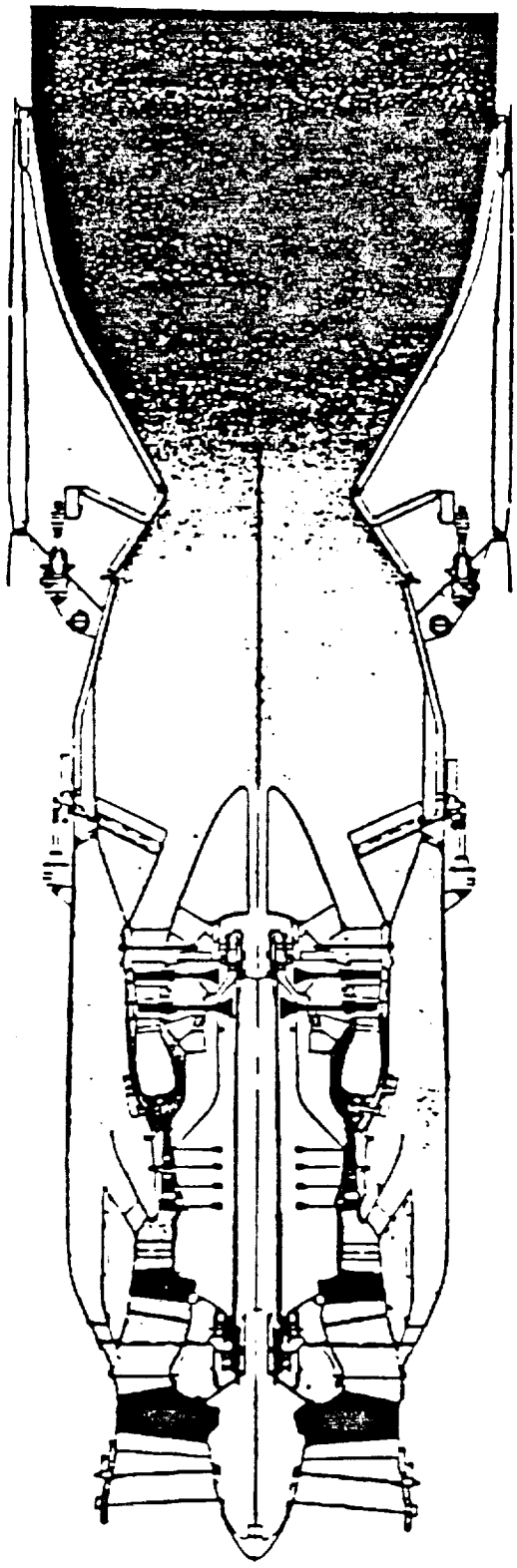

Figure 5 - Turbofanramjet

Table 2 - Engine Specifications

	GE Turbofanramjet	P & W F-100
Date of entry	2005-2010	In service
Sea level static thrust, lbs.	32,950	23,000
Sea level static TSFC, lb/lb/hr.	1.864	2.480
Sea level static airflow, lbs/sec.	441	217
Bare engine weight, lbs.	6304	2737
Engine length, ft.	19.9	15.8
Maximum diameter, ft.	6.1	3.7
Compressor face diameter, ft.	5.0	3.3

Air Precooling:

Several studies have shown that by cooling the air prior to compression, significant performance benefits can be realized. In running liquid hydrogen directly through a heat exchanger ahead of the compressor inlet, the following can be achieved:

1. For equal pressure ratios, less compression work is done, and specific thrust and fuel consumption improve.
2. By reducing the temperature at the compressor inlet, the mass flow rate can be increased, yielding higher thrust or smaller engines for similar thrust.
3. Also, temperatures are reduced at the compressor outlet, and the upper end the engine's speed regime can be extended.

The last point is of particular interest because it allows for a wider application of an engine design. Kunkler explains in Reference 27 that a standard subsonic-combustion ramjet can be pushed to upwards of Mach 7 flight. In fact, he describes a method for turbojets where the precooler is regulated to keep the hydrogen fuel from exceeding 1430°F. This allows for additional cooling capacity in the afterburner and thrust nozzle, where wall temperatures can be kept below 1700°F. The resulting turbine inlet temperatures are on the order of 2800°F and the afterburner, 3900°F.

Precooling has its limitations, however. The cooling rate of the heat exchanger is limited by the fuel rate through it. As a result, by running a stoichiometric fuel mixture, the cooling rate can only achieve so much success. In the case that the engine runs at a rich mixture, the cooling rate goes up, and the operating envelope can be pushed to even higher limits. Kunkler contends that by running a rich mixture on the system described above, a standard turbojet can be pushed to Mach 6.5 flight. A significant fuel consumption penalty must be paid, however.

5.2 SYSTEM PERFORMANCE

Engine specifications of the GE turbofanramjets are summarized in Table 2. Compared to the PW F-100, there are some significant differences. For one thing, the size and weight of the engines are at least twice that of the F-100. This is so because of the nature of the hybrid design, which is essentially two engines combined in one package, so it is reasonable to have significantly higher weight. Moreover, the acoustic suppressor nozzles weigh much more than the F-100's short nozzle. The higher massflows are justified by the same reasons. The significant specific fuel consumption improvements are the result of anticipated technological advances by the year 2005, as well as the benefits from the air precooling system.

Plots of maximum net thrust at given altitude and Mach number are shown for both engine modes in Figures 6 and 7.

5.2.1 ENGINE SIZING

In Figure 8, it is apparent that a narrow margin between available and required thrust occurs between an altitude of 30,000 and 40,000 feet (Mach 1.5-2.0). This becomes the sizing criterion for the engine system. The result was to size the JP-burning turbofans down to 70% of GE's data, allowing for at least 1500 lbs of excess thrust with the ramjets running at 10% power. Some other ways to clear the pinch by a greater margin could be to slow down to less than 1/10 g acceleration, or to throttle up the

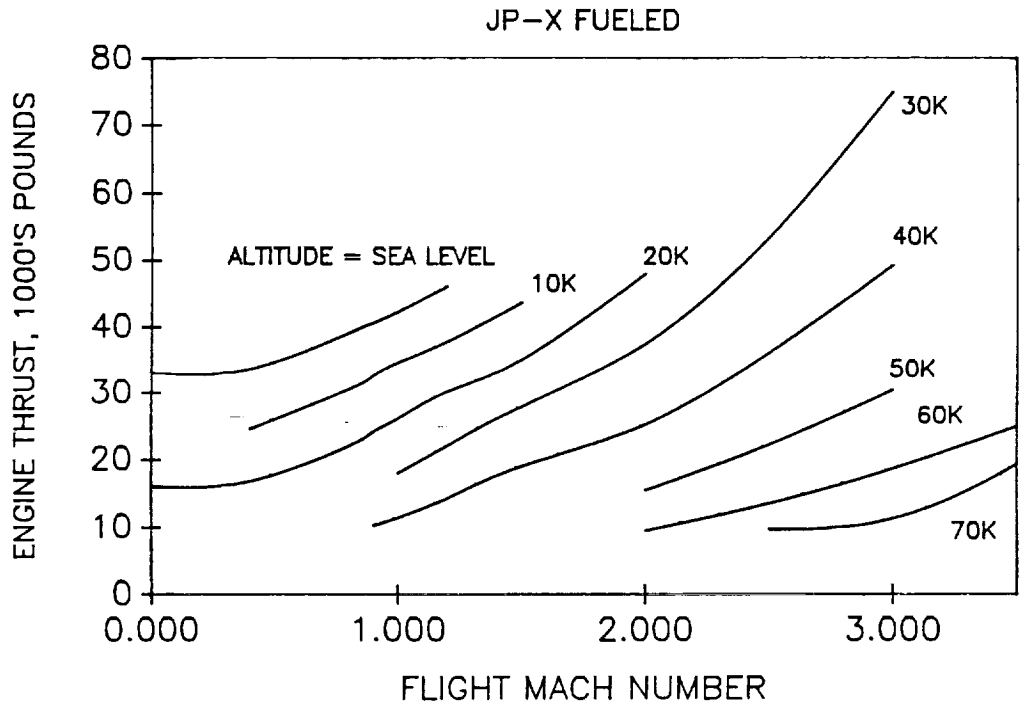

Figure 6 - Turbofan Thrust vs Mach Number

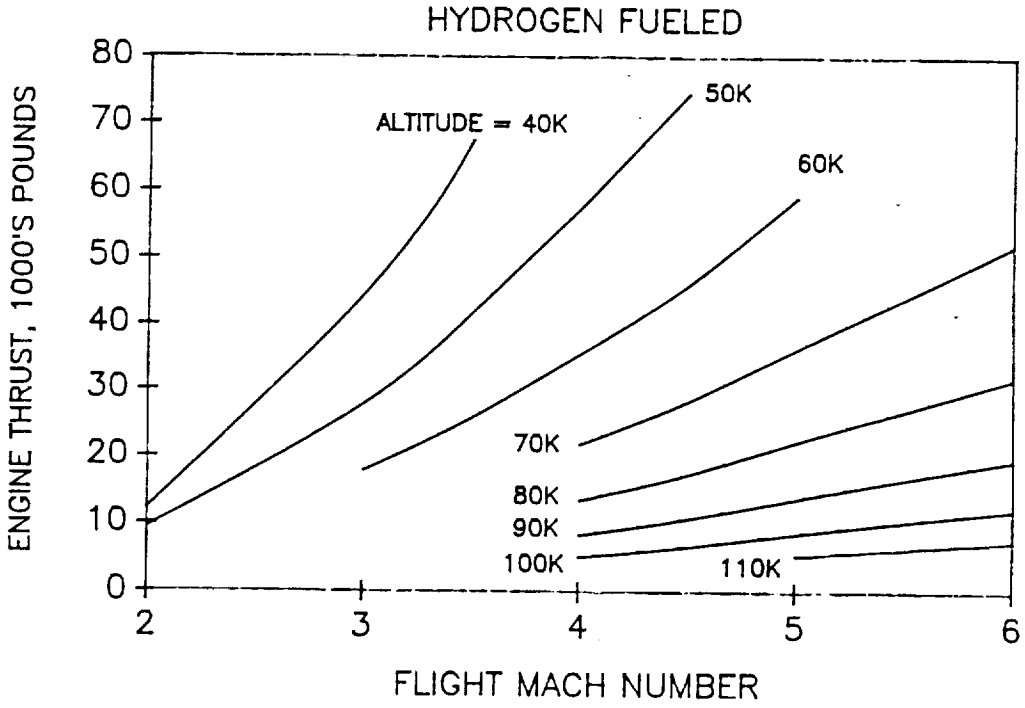

Figure 7 - Ramjet Thrust vs Mach Number

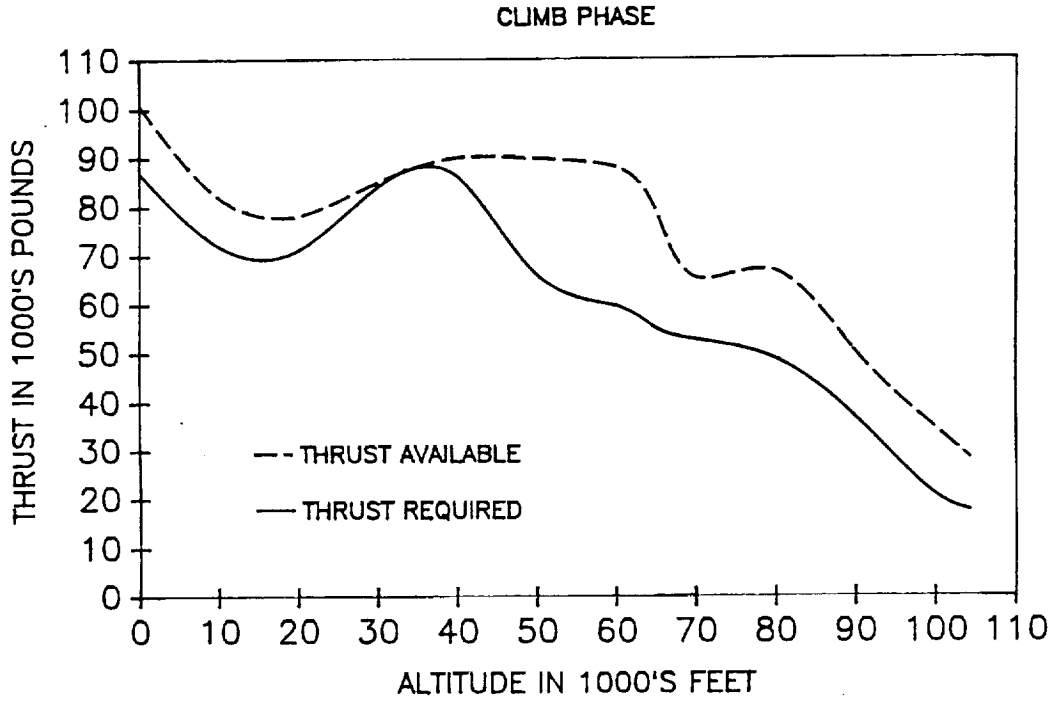

Figure 8 - Available and Required Thrust

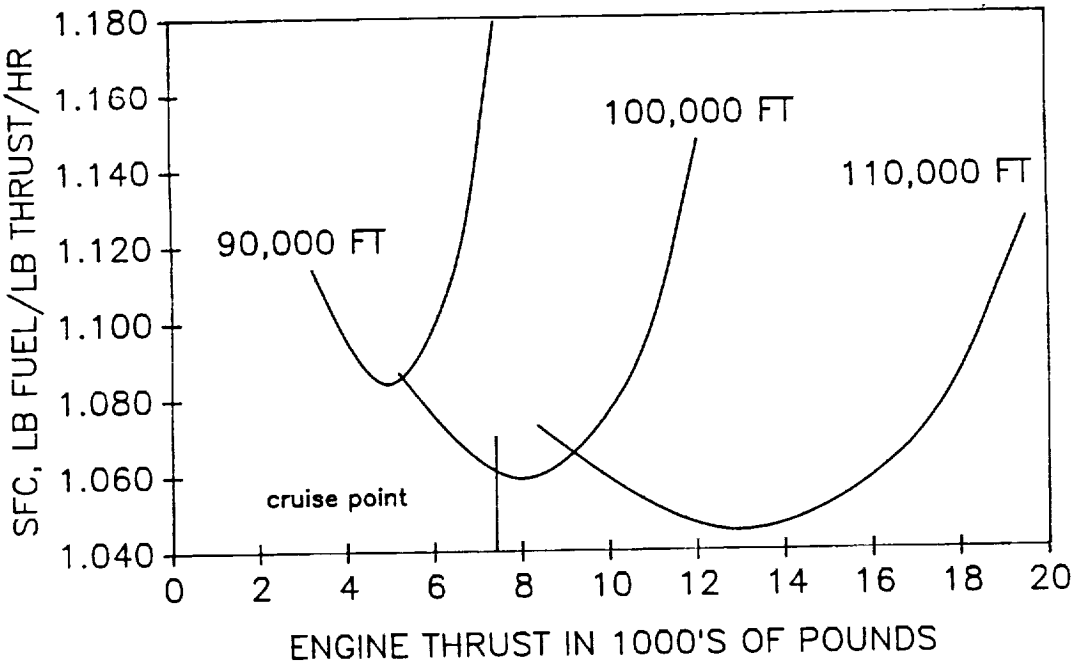

Figure 9 - SFC vs Thrust at Mach 6

ramjets. To size the hydrogen-burning ramjet data, all that was necessary was to match base corrected airflows with the turbofan data, which translated into a scaling factor of 0.57. In so doing, it gave near-optimum fuel consumption at cruise with the engines running at only 66% maximum rated thrust. This allows the pilot to maneuver without specifically changing his angle of attack and spoiling the waverider qualities. Since weight is being burned off and thus less thrust is needed, the aircraft must climb slightly throughout the cruise leg to maintain its optimum performance. At the beginning of cruise, 22,195 lbs total thrust is required (at an SFC of 1.057 lb/lb/hr), which puts the aircraft at an altitude of 98,800 ft. By the end of cruise, the aircraft has risen up to 104,300 ft. and requires 17,475 lbs thrust. Specific fuel consumption at the end of cruise has risen to 1.070 lb/lb/hr.

Engine scaling had a profound effect on aircraft performance. Obviously, the aircraft had to break through Mach 2 at 40,000 ft. to get to cruise, and having done so didn't guarantee an efficient cruise. As shown in Figure 9, the most efficient cruise at 100,000 ft. is at a required thrust of about 8000 lbs per engine. If the engines were to attain this, they would actually have to be scaled down further and risk not making it through the thrust pinch. On the other hand, if too much excess thrust was generated through the thrust pinch, the curves in Figure 9 will shift farther to the right, and the cruise fuel consumption will suffer dramatically.

This unique scaling problem also justifies the cruise altitude of the aircraft. Cruising at a nominal altitude of 110,000 ft. necessitates a large down-scaling of the engines and, just as

described above, the thrust pinch will never be surmounted. A 90,000 ft. cruise altitude requires a scaling up of the data, which would result in too much excess power in all other regimes.

5.2.2 TAKE-OFF PERFORMANCE

Engine sizing also had interesting effects on the takeoff performance. Figure 6 shows the augmented thrust at sea level. If the aircraft were to takeoff with full afterburners (T/W=0.59), the passengers would experience accelerations more like a fighter aircraft than a commercial transport (1/2-1/3 g). Conversely, if the takeoff roll were to be performed on dry thrust, passengers would experience only 1/8 g, but 11,253 ft. of runway would be needed. To compromise, the two outboard engines are run dry and the centerline engine is augmented, giving a T/W of 0.44. The passengers and crew only experience 1/6 g, which is the maximum acceleration in the climb phase, and the plane lifts off in 9258 ft. runway. What happens if an engine goes out? By augmenting the two operating engines, a T/W of 0.39 can be achieved and the plane lifts off in 10,038 ft. However, throughout the climb phase, all engines must be augmented to follow the mission profile.

5.2.3 ENGINE CYCLING

One crucial leg of the climb phase is where the turbojet mode is cycled out and the ramjet mode is cycled in. Figure 10 shows that turbofan output drops off sharply after 60,000 ft. altitude (Mach 3 in the mission profile). At this point, the ramjets must be running at maximum power to prevent a thrust deficiency. Although it doesn't peak until 70,000 or 80,000 ft., the ramjet thrust is sufficient below 60,000 ft. to keep a steady combined thrust level as the turbofan spools down. At 30,000 ft., there is 10% output from the ramjets, as compared to 80% at 65,000 ft. Between 50,000 and 65,000 ft., maximum ramjet thrust is impossible due to massflow constraints through the inlet.

5.3 FUEL SELECTION

In selecting a fuel to power the aircraft, weight soon became a prime consideration, and ultimately decided the fuel. JP fuels are simply out of the question for high Mach applications. The highest temperature JP fuels can withstand is about 4000 deg R, after which point significant dissociation occurs. Even with precooling, JP just cannot handle the temperatures characteristic of high Mach missions, and shows a marked decrease in specific impulse after Mach 2.5 or 3. Additionally, JP is a heavy fuel, weighing 47 lbs/cu.ft.

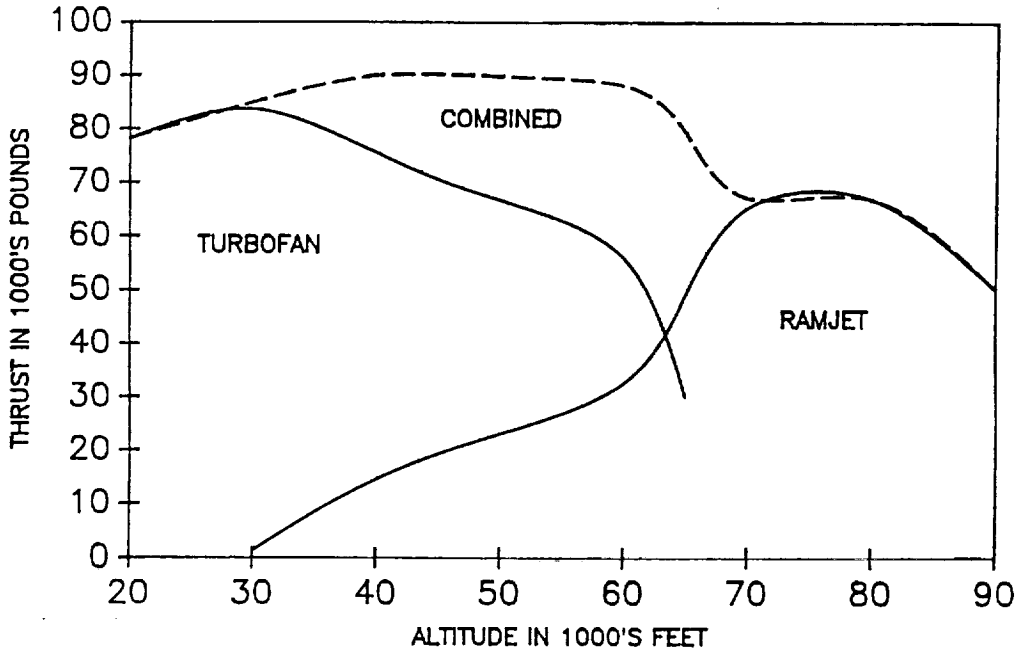

Figure 10 - Combined Thrust Avaiable

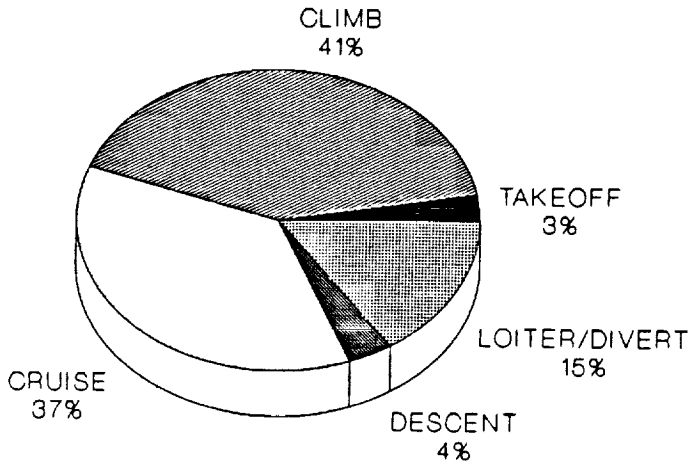

Figure 11 - Fuel Weight

In the preliminary layout phase, hydrogen was discussed, and questions arose about its density and handling qualities. At the onset, hydrogen appeared to be too voluminous to store in the aircraft, and too cold (37 deg R) to allow for feasible storage on board. As it turns out, hydrogen is 91% less dense than JP, but contains 180% more energy per unit weight. Ultimately, hydrogen requires 4 times the tankage volume for an equal amount of energy and its capacity as a heat sink cannot be ignored (Table 3).

Table 3 - Fuel Comparisons

	JP FUELS	METHANE	HYDROGEN
Heat of combustion, BTU/lb	18,400	21,120	51,590
Liquid density, lb/ft.^{3}	47.0	26.5	4.43
Boiling Point, $^\circ$F	400-500	-258	-423
Freezing Point, $^\circ$F	-58	-296	-434
Specific heat, BTU/lb $^\circ$F	0.48	0.822	2.22
Heat of vaporization, BTU/lb	105-110	250	193

Methane proves an attractive alternative in its own right. This fuel is 44% less dense than JP, but only 15% more energy content per weight. However, methane isn't as cold as hydrogen (202 deg R) and has less than one-third the heat capacity.

To reap the benefits of hydrogen fuel, while minimizing the volume, a dual fuel system seems the best alternative. By using dense JP-X for the turbofan regimes and hydrogen for the ramjet

regimes, the best of both worlds can be realized. JP fuels in general have excellent subsonic performance by comparison. In fact, at subsonic speeds, JP-fueled turbofans produce just as much thrust as hydrogen-fueled engines of the same type. Methane actually produces 6% less thrust in the same regime. Hydrogen, in turn, keeps the gross weight down and gives the aircraft hypersonic capabilities.

In this manner, the aircraft consumes a total of 40,920 lbs JP (6485 gal) and 36,850 lbs of hydrogen (61,960 gal), giving a gross takeoff weight of 171,400 lbs. Table 4 compares the dual fuel system with other schemes.

Table 4 - Fueling Schemes

FUELS	TOT. FUEL WT.	FUEL VOLUME	GROSS TAKEOFF WT.
JP/HYDROGEN	77,780 LBS	68,450 GAL.	171,400 LBS
ALL HYDROGEN	50,900	86,020	135,000
ALL METHANE	157,200	44,132	260,000

In general, by using hydrogen the gross weight drops significantly, lowering the thrust requirements, and lowering the fuel consumption. The fuel weight breakdown in Figure 11 justifies the dual-fuel system. Obviously, almost half the fuel weight is consumed in the climb phase, so by burning dense JP-X, the greater volume can be reserved for the hydrogen needed to cruise. By exclusively using hydrogen, the total fuel weight drops 34%, but the volume required increases 26%.

5.3.1 THE POTENTIAL OF HYDROGEN FUEL

The quest for incorporating liquid hydrogen as an aviation fuel is justified by the following four considerations:

1. Depleting resources and increasing costs of hydrocarbons
2. The need for environmentally clean fuels
3. Anticipating a nuclear energy economy that will replace the current fossil-fuel economy.
4. The need for high energy fuels for hypersonic applications.

The combustion properties of hydrogen make it ideal for high altitude, high Mach missions. Environmentally, hydrogen is noted for being one of the cleanest-burning fuels available; there are no carbon monoxide or unburned hydrocarbons present in the combustion products, and NOX production can be kept at very low levels with properly-designed combustors. In addition, Pratt and Whitney have demonstrated that combustion efficiencies of over 99% can be obtained with one-fourth the mixing length of hydrocarbon fuels (Reference 10). With respect to the current design, the environmental benefits apply only above 65,000 ft., where the JP-burning turbofans are no longer operating.

One problem with the use of hydrogen is a need for an expanded infrastructure for the production and storage of liquid hydrogen. Indeed, hydrogen has a history of use in the U.S. space program and industrial applications. Moreover, several large electrolyzer

plants exist today to supply the ammonia and fertilizer industries, and hydrogen supply pipelines extend for 50 miles in the Houston area and up to 72 miles in the Ruhr. Granted, a hydrogen production facility may cost up to $200 million to build, but storage facilities are much cheaper and many more could be built using current techniques. As for its comparison to JP-X fuel, Reference 10 suggests that by the time a commercial hypersonic fleet becomes operational, the cost of hydrogen will be slightly more than twice the cost of
JP-X ($2.85/million BTU as compared to $1.37/million BTU).

SAFETY OF HYDROGEN

The safety of hydrogen becomes a primary concern if the fuel is to be used in a transport aircraft. Certainly, catastrophes such as the Hindenburg and Challenger accidents raise doubts about using hydrogen, but such instances are rare. In fact, the various properties of hydrogen make it no more dangerous than gasoline (Reference 9). These properties of hydrogen emphasize that hydrogen may be used in civil aviation safely:

1. Hydrogen has a higher ignition temperature than methane (1544 deg R vs. 1460 deg R), making it safer.
2. Hydrogen produces no toxic combustion products.
3. Hydrogen flames radiate little heat compared to JP.
4. Despite its wide flammability limits, hydrogen is not explosive under unconfined conditions.
5. Hydrogen vaporizes and dissipates quickly when spilled, unlike JP fuel.

5.4 INLET CONFIGURATION

5.4.1 EXTERNAL VERSUS INTERNAL COMPRESSION

In order to supply air to both the turbofan and ramjet cycles, the flow has to be decelerated to about Mach 0.4 before it can be compressed. To accomplish this, different types of inlet configurations were examined for optimum performance in all regimes. External compression was the first type examined. Much like the name, an external compression inlet gets all of its compression from surfaces external to the inlet ducting, as shown in Figure 12. The most primitive example of this is the single normal shock on the pitot inlet of the F-86 Sabre. An attached normal shock inlet gets good efficiency only up to Mach 1.5, where it has a pressure recovery of 93%. Beyond that, the total pressure recovered behind the shock drops off rapidly (by Mach 2, it is down to 72%). Other inlet designs incorporate a series of ramps to set up an oblique shock system, which shocks down the flow in

many, more efficient steps rather than one big, inefficient step. Just as in the pitot inlet, the terminal normal shock lies at or near the cowl lip. By increasing the number of shocks to approach infinity, a smooth isentropic compression contour results.

Isentropic compression can be very efficient, with pressure recoveries in excess of 90% maintained out to Mach 2.7. One reason for this is because optimum isentropic compression involves no terminal normal shock, and thus the losses associated with it.

Pure external compression loses its appeal as the flight Mach number reaches the high supersonic regime. Compression at these speeds needs more oblique shocks, and thus more ramps to keep the pressure recovery high. The result is higher total turning angles for higher Mach numbers. As an example, an isentropic compression inlet at Mach 6 would dictate a total turning angle of about 43°. Wave drag also goes up, since the external cowl angles increase as well. Furthermore, if the inlet turns the massflow 43° away from the aircraft centerline, then the subsonic diffuser must turn it back 43°.

Internal compression inlets were also investigated. As illustrated by Figure 13, all compression takes place within the inlet ducting. In contrast to external compression, the throat is inside the duct, rather than at the cowl lip, and internal compression involves a decreasing flow area before the subsonic diffuser. Typically, there is a succession of flow stages that an internal compression inlet may encounter. These stages refer to parts A, B, C, and D of Figure 13.

A. Shock attached with $M_t < 1$: when the throat is opened enough to pass the required massflow, a normal shock attaches at the lip, and the inlet is running "full" ($A_{inf} / A_c^* = 1$).

B. By lowering the back pressure from case A, the normal shock moves inside the duct and past the throat, giving a supersonic throat Mach number. In this case, the inlet is "started" in the supersonic sense.

C. Shock detached with $M_t = 1$. If the throat chokes before the bowshock attaches at the lip, the inlet is prevented from passing the required massflow.

D. By lowering the back pressure from case C, a second shock forms and stabilizes in the diverging section. In this case, the inlet is "unstarted," and most of the flow is subsonic. This hardly makes for an efficient supersonic inlet (from reference 37).

External compression inlets do not have such a sensitivity to unstarting. Simply by lowering the back pressure in these inlets, the shock-on-lip condition can be attained because the geometric throat is at or near the cowl lip. Internal compression inlets, on the other hand, require extensive variable geometry to reach the same condition. Before such inlets can be started, the throat must be opened up enough to pass the massflow and swallow the shock, and then closed back down to the needed dimensions. On the ground, an unstarted inlet can be easily remedied, but flight conditions

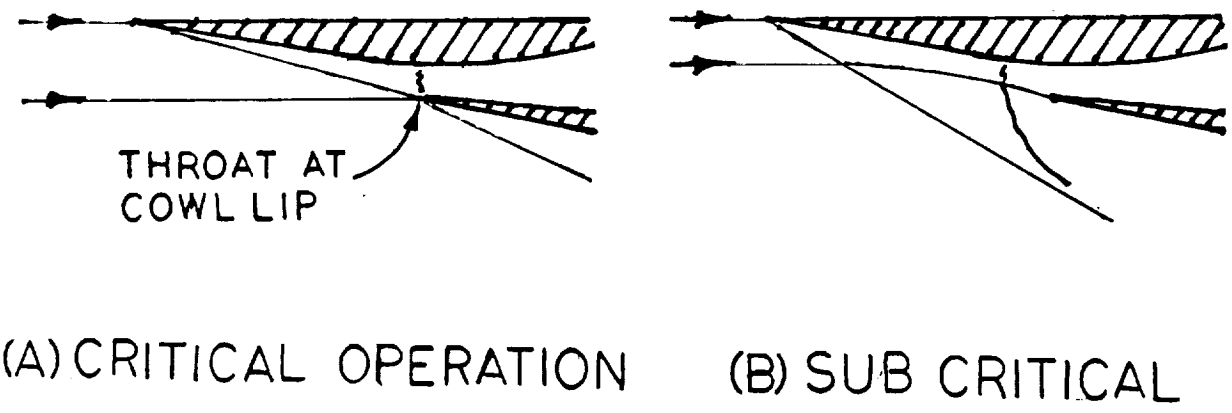

Figure 12 - External Compression Inlet

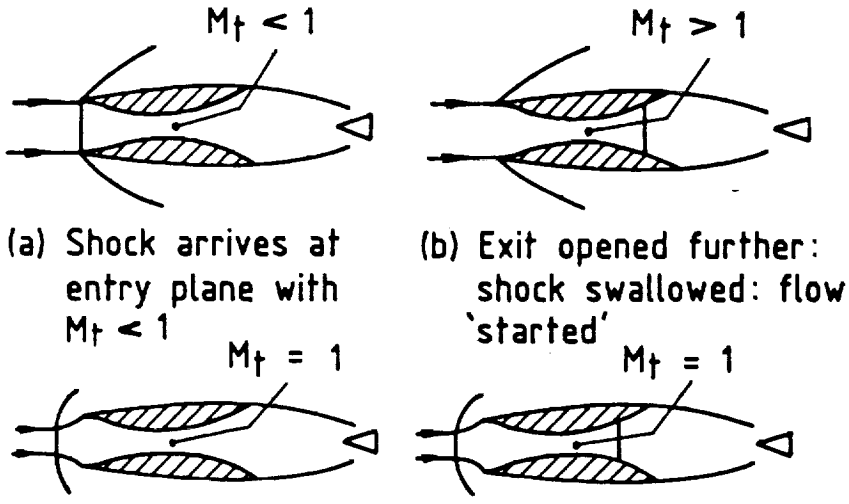

Figure 13 - Internal Compression Inlet

complicate matters. Extensive flight-control equipment must accompany the inlet configuration.

In addition to the unstart problems, boundary layer effects play a major role in pressure losses for internal compression. In such inlets, the flow is constrained on all sides by ducting surfaces, making a greater area for the boundary layer forces than external compression inlets. Multiple shock interactions at the endwalls further complicate matters.

5.4.2 INLET CONFIGURATION AND PERFORMANCE

To obtain the best compromise, a two-dimensional mixed compression inlet was developed, as shown in Figures 14 and 15. This inlet scheme is similar to that of the XB-70 Mach 3+ research aircraft and involves a 30/70 ratio of external/internal compression at the hypersonic design point. At Mach numbers below 2, the normal shock pops out of the duct because the maximum angle for shock attachment has been exceeded; it then settles ahead of the cowl lip. This geometry produces good pressure recovery (see Figure 16), but pays the price of spillage drag. Even with the cowl in its closed position, the inlet spills approximately 30% of the massflow. By the time Mach 2 is reached, the first shock impinges on the cowl lip, drastically reducing spillage to less than 20%. As the normal shock moves inside the duct, its position can be stabilized by adjusting the bleed flow rate.

Higher Mach numbers bring about two shocks on the lip and

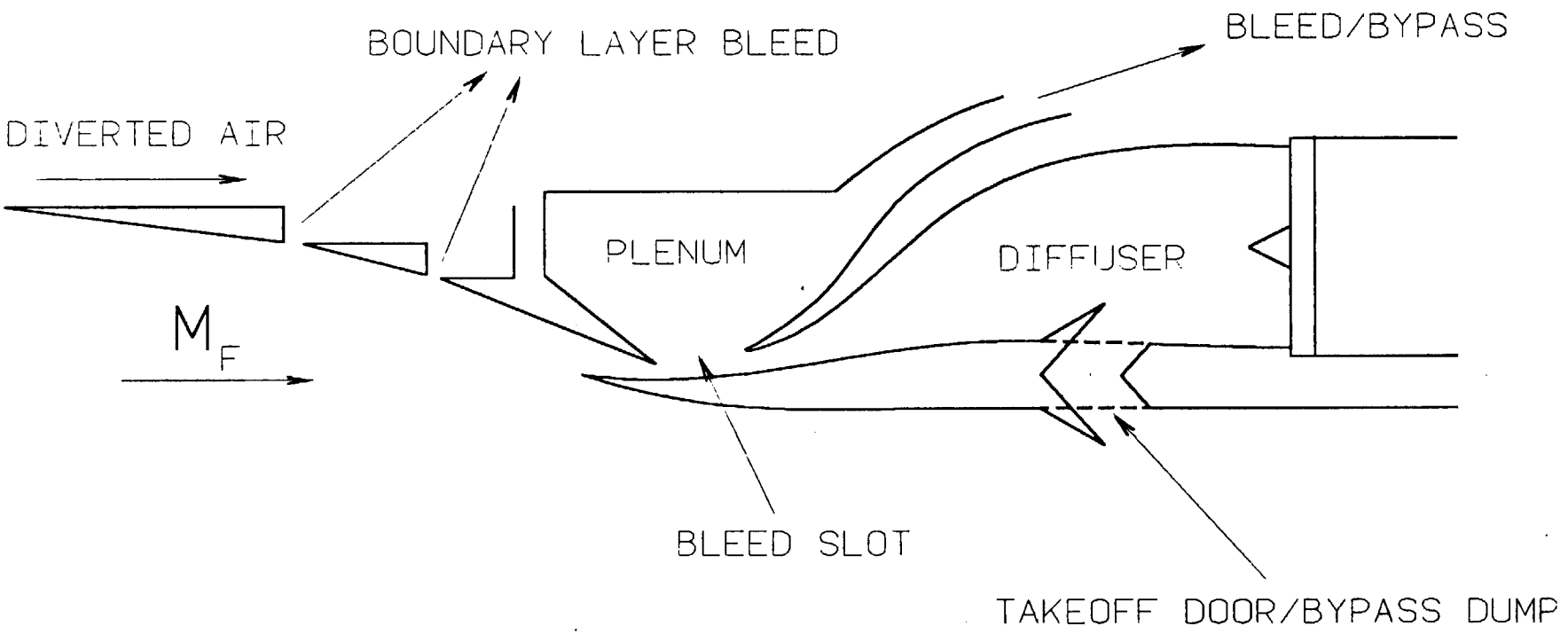

Figure 14 - Inlet Configuration

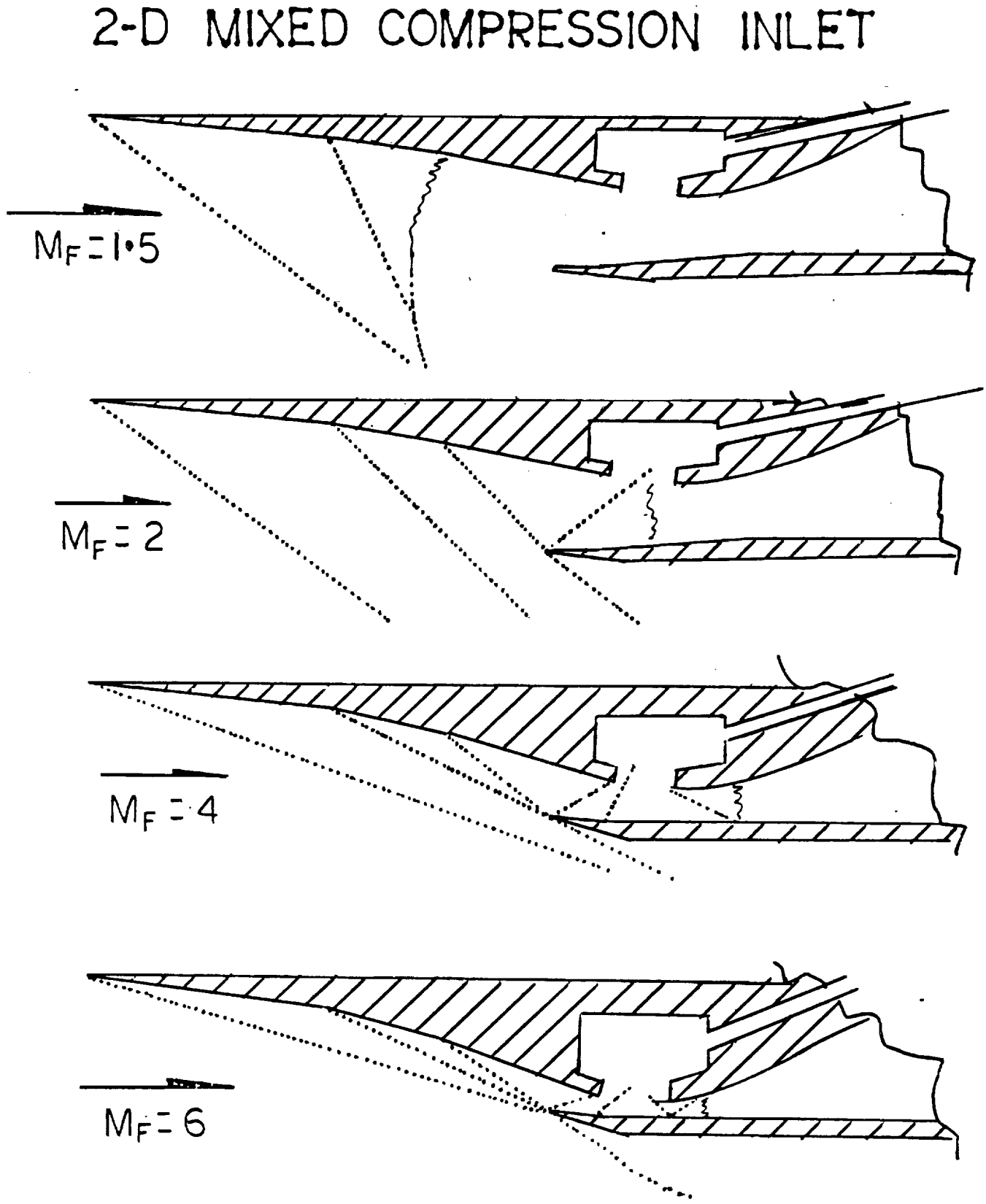

Figure 15 - Inlet Shock System Schematic

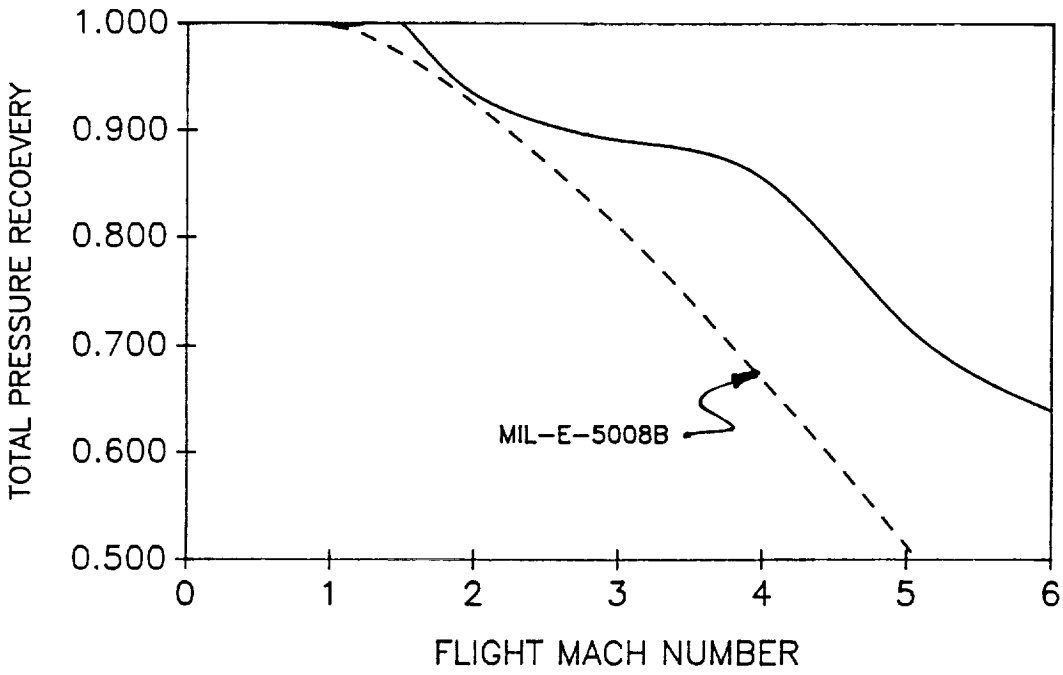

Figure 16 - Inlet Pressure Recovery

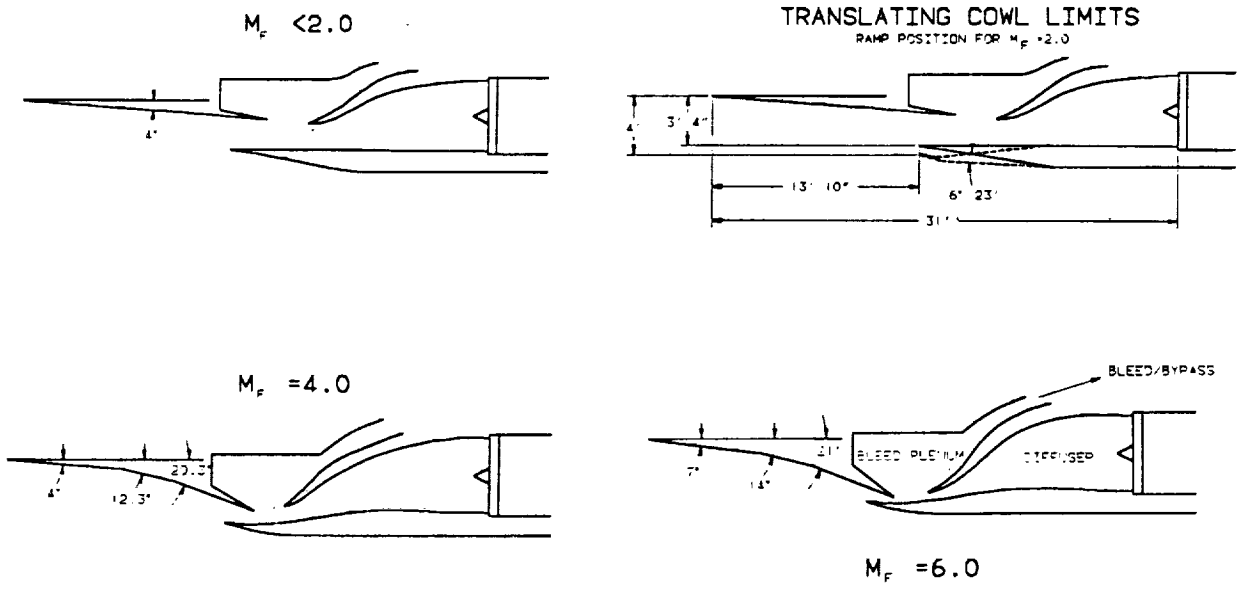

Figure 17 - Inlet Geometries

minimizes spillage. As Mach 4 is reached, the cowl lip has been extended to its open position. More importantly, however, is the location of the normal shock, which is now downstream of the bleed slot and the geometric throat. In these regimes, the bleed slot is solely responsible for boundary layer bleed and no longer regulates the back pressure. This job is handled by poppet valves and bypass dump doors in the subsonic diffuser. Finally, by the time cruise is reached, all three external shocks are focused (actually, very nearly focused) on the cowl lip and the inlet is running at a massflow ratio of unity (i.e. no spillage). In its extended position, the external cowl angle remains less than 10° to keep the wave drag down. Ramp geometries are shown in Figure 17.

During the inlet analysis, a computer program calculated the temperatures and pressures throughout an oblique shock system. No pressure losses due to friction, boundary layer interactions, or heat extraction (precooler) were compensated for.

5.4.3 INLET SIZING

Before inlet sizing could take place, required massflows had to be determined. Table 5 summarizes these requirements.

Table 5 - Inlet Massflows Required

ALT(/1000 ft)	MACH	AIRFLOW (lb/s)	FREESTREAM AREA (sq ft)
0	0.1	491	57.7
0	0.4	491	15.4
10	0.6	423	11.6
20	1.0	419	9.9
30	1.5	504	11.8
40	2.0	550	14.9
50	2.5	511	18.1
60	3.0	461	21.8
70	4.0	329	18.8
80	5.0	319	23.5
90	5.5	250	27.4
100	6.0	190	32.1

Engine massflows came right from the GE data, where is was corrected by the total conditions at the compressor face (based on the milspec recoveries of Figure 16). To this figure was added the bleed requirements as shown in Figure 18 (taken from Nicolai for mixed compression inlets). At cruise, as much as 18% of the massflow is bled off, while less is required at lower Mach numbers. Finally, the supporting system requirements are accounted for (see Table 6) in the engine requirements.

Table 6 - Support System Requirements

SYSTEM	REQUIRED ENGINE AIRFLOW
ENGINE OIL COOLING	1%
ENGINE NACELLE COOLING	4%
HYDRAULIC SYSTEM COOLING	1%
ENVIRONMENT CONTROL	5%

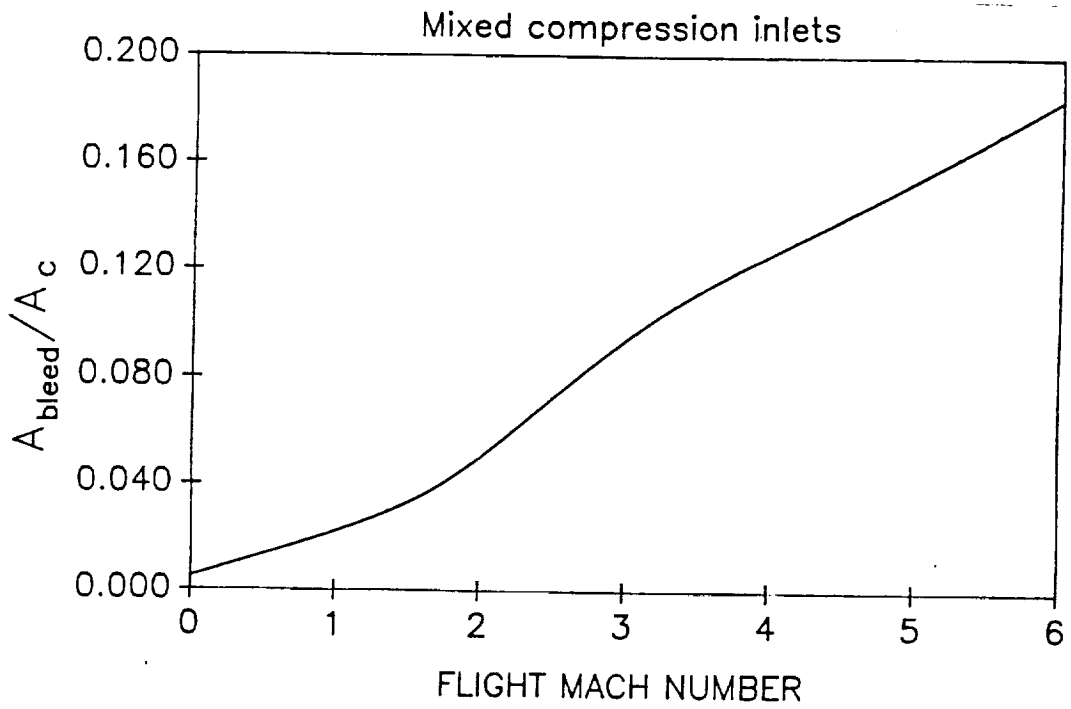

Figure 18 - Required Bleed Flow

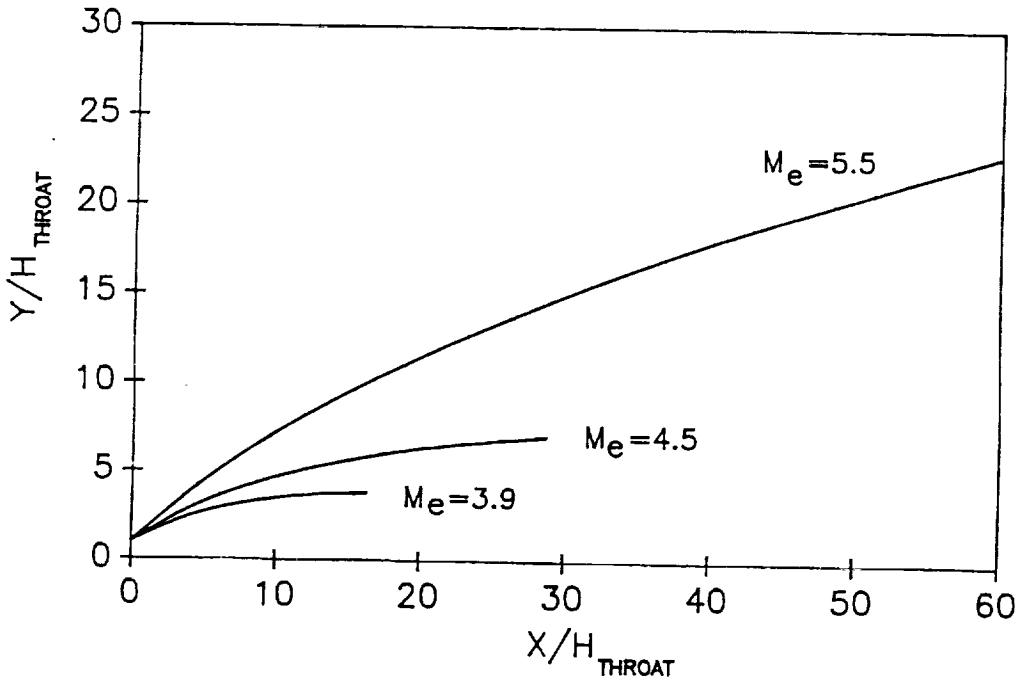

Figure 19 - MOC Boattail Contours

The total massflows per engine shown in Table 5 indicate a peak at Mach 2. This is the point where the ramjets are being cycled in while the turbofans are still at full throttle, so higher massflows are to be expected.

By far, the largest area requirement in flight is at cruise, which is where the inlet capture area was sized. If the streamlines enter the inlet in a parallel fashion, which is the case in sizing at cruise, the pre-entry pressure rise is eliminated along with its associated drag penalty. Total capture area with the cowl in its open position is 96 $ft.^2$ (24 x 4 ft.) as opposed to 80 $ft.^2$ in its closed position (24 x 3.3 ft.). During cruise, the throat area was sized to 8.8 $ft.^2$ by using the sonic massflow parameter ($MFP^* = 0.1270$). Takeoff is achieved by blow-in doors in the diffuser to augment the inlet airflow. At off-design, the inlets supply more massflow than the engines need, so the takeoff doors reverse to become bypass dump doors to expel the unused massflow.

5.5 NOZZLE CONFIGURATION

5.5.1 CONSIDERATIONS

The design of an exhaust nozzle involves many different factors. Such considerations as cooling, acoustic noise, off-design performance, and airframe integration need to be considered to realize the full potential of the propulsion system. Examples of some the more important factors influencing design are shown as

follows:

REQUIREMENT	EFFECT ON NOZZLE
Sustained supersonic/ subsonic operation	High area ratios, variable geometry, ejector nozzles
Propulsion system integration	Drag and propulsion system, installed performance
Community noise regulations	Jet noise suppression
Dual mode cycle	Bypass ducts/valves and secondary air systems
High exhaust temperatures	Cooling/materials

5.4.2 GEOMETRY

The nozzle configuration is shown in Figure 20. A two-dimensional primary nozzle with a boattail expansion has been the accepted arrangement for high Mach flight. Designed using a Method of Characteristics program for a minimum length nozzle, the primary nozzle expands the 4000° R combustion flow to Mach 1.9, which sets the exit area at 21 ft.^{2} (and a throat height of 7 in.). By expanding to Mach 2.5, the exit area rises to 36 ft.^{2}. All analyses of the nozzle configuration were taken at cruise and assumed a gamma of 1.33 ($MFP^* = 0.1277$).

To design the boattail contour, an MOC model of an expansion surface above and a slipline below was developed. Conditions at the slipline were based on the shocks from the aircraft forebody, inlet cowl lip, and the slipline itself, giving a slipline pressure of 800 lbs/ft.^{2}. This pressure is a function of the different

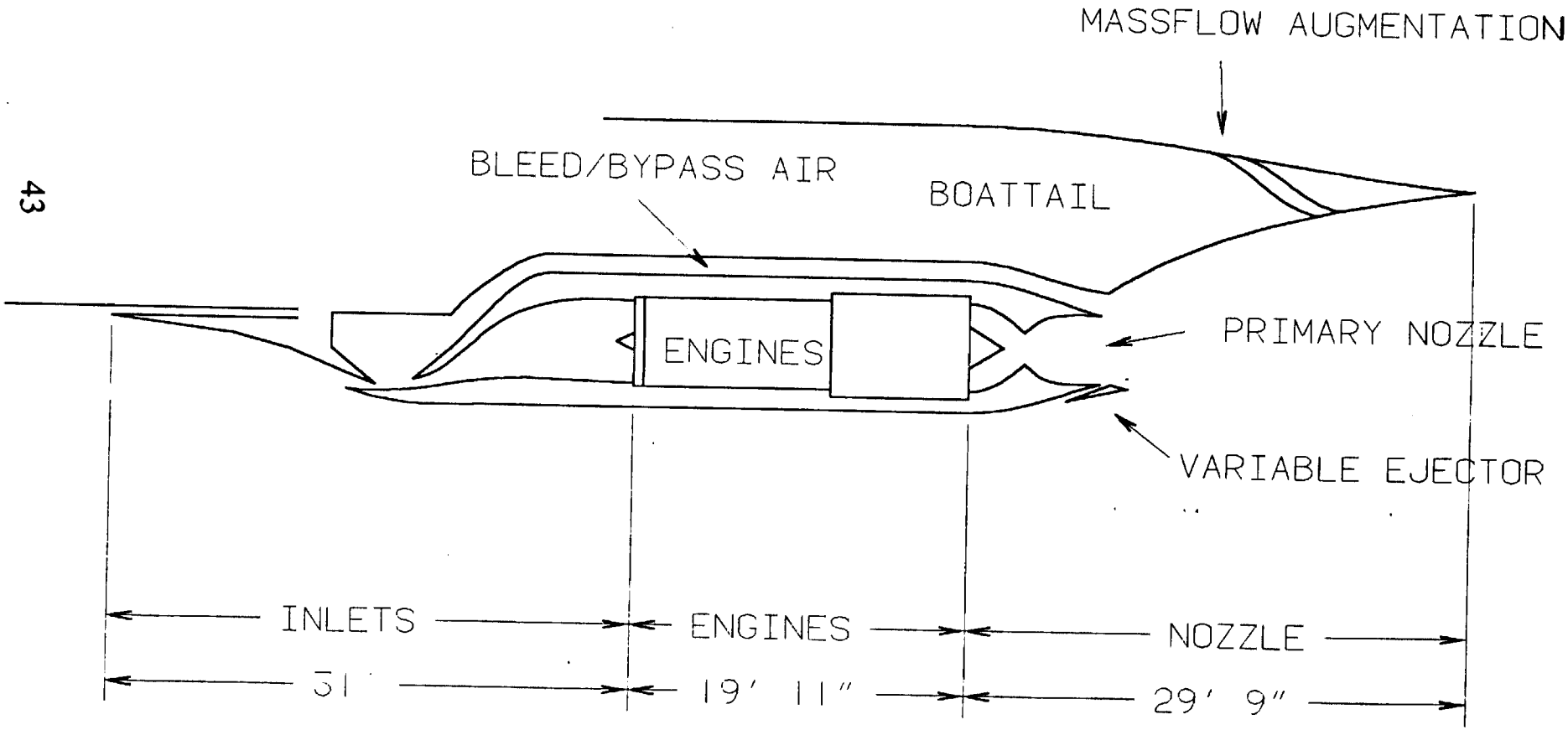

Figure 20 - Turbofanramjet System Configuration

total pressures on either side of the slipline, and remained constant regardless of the exit Mach number.

The boattail expansion had to be carefully decided. The exhaust gas had to be expanded to at least Mach 3.91, where the exhaust velocity equals the flight velocity. Above Mach 5.5, the flow is overexpanded. Both expansion limits had to be observed to keep the exhaust plume from causing further drag on the aircraft in flight. The MOC contours of Figure 19 show that at $M_e = 5.5$, the non-dimensionalized height is in excess of 25, not practical for an aircraft that is 11 ft. high at the rear. An M_e of 3.9 gives a contour that produces too much base drag from the faired upper surface. In the end, expansion to Mach 4.5 was chosen based on the geometrical considerations.

5.4.3 SPECIAL FEATURES

If the aircraft could maintain the cruise condition from start to finish of the mission, then the baseline nozzle configuration would be perfect. However, all speed regimes are experienced on a given mission, so the nozzle configuration must perform at least nominally well at off-design conditions. When descending from cruise, the aircraft slows down, and the atmosphere becomes more dense. The net result is that the massflow exit Mach number drops off, making the exhaust plume smaller, and increasing the area of base drag. Several fixes have been devised to deal with this problem, two of which are implemented here. At small off-design deviations, such as at Mach 5, the variable area ejector on the

bottom lip of the nozzle can pivot up into the exhaust stream and generate a shock. This shock travels up to the boattail contour and reflects, effectively turning the exit flow toward the boattail to keep it attached and minimize the base drag. In the case of extreme off-design conditions, such as the subsonic regime, more drastic measures are needed. Subsonic operation produces an exhaust flowfield that is almost parallel to the freestream, requiring either a variable geometry boattail or large amounts of massflow to augment the exhaust stream. With the immense complexities of a 25 ft. movable boattail in mind, the latter of the suggestions was chosen. The required massflow could be added from below through the variable geometry ejector, which is standard equipment for a hypersonic applications (see Figure 20). However, most of the massflow must come from above, where the drag-inducing pressure void will be. By using a ram scoop on the upper surface of the wing, additional massflow could be drawn down through the boattail structure and fill the void left by the exhaust plume.

One problem that cannot be ignored in a nozzle design is the heating of the supporting structures, such as afterburners, nozzle walls, and ejector doors. At full afterburner, some of the aft surfaces reach temperatures approaching 4000° F. Not only is fuel circulation around the hot spots effective in cooling the nozzle, but implementation of cooler bleed/bypass air works as well. These layers of air are kept next to the nozzle walls, where they can help insulate against excessive heat.

5.4.4 ENGINE-EXHAUST-AIRFRAME INTERFERENCE

Reference 26 has shown that significant aerodynamic benefits can be gained from an expansion surface. The results indicate that the normal force generated by the nozzle expansion actually increases an aircraft's L/D and help to offset the nose-up moment created by the engine thrust. Improvements in L/D on a flat plate model were approximately 7% for axisymmetric nozzles, and 15% for two-dimensional nozzles for comparable exit pressure ratios (for the current design with $M_e = 4.5$, $p_e / p_{inf} = 3.4$). On the aircraft configuration tested in Reference 26, the L/D was about 7% higher. Similar improvements were assumed for the current design.

6. AERODYNAMICS

6.1 INTRODUCTION TO AERODYNAMIC DESIGN

The main goal of the entire aerodynamic design section was threefold:

1) Understand the flowfields around the aircraft at all flight regimes.
2) Prove the feasibility of operating the aircraft at all flight regimes.
3) Provide necessary data for the design of other systems dependent on aerodynamics.

At the start of the design phase, it became clear that the aerodynamics would drive the design of the entire aircraft. During the very demanding cruise regime of Mach 6 at 100,000 feet, aerodynamics would be of utmost importance. For the reasons that the most time is spent at cruise, it is the most hostile environment, and the fact that the very voluminous fuel hydrogen is burned at cruise, it was necessary to optimize the design for cruise.

At first, when the concept of a waverider was not adequately understood, a waverider-like body was drawn up. With the acquisition of the MAXWARP waverider program, exact waverider shapes as well as performance could be determined. This program proved an invaluable tool in the determination of aerodynamics in

the hypersonic regime.

Next, thoughts turned to subsonic performance. Since the waverider was basically a flying delta wing, approximations to a flat plate delta wing were made. From this data it was shown that the aircraft could indeed fly satisfactorily at subsonic speeds. Later experimental data on an actual waverider proved very similar to the flat plate data. Because of the optimization for hypersonic flight, the efficiencies at subsonic speeds were very poor when compared to actual subsonic transport aircraft.

When it was decided to use liquid hydrogen as a fuel, internal volume also became a concern. The MAXWARP program calculates the internal volume of the waverider. Approximately 1/3 (7500 ft^3) of the internal volume of the aircraft is taken up by the hydrogen fuel. Another consideration was the fact that so much of the volume (therefore weight) was at the rear of the plane. This caused problems in the area of stability and control because the center of gravity was pushed so far back. By moving as much weight as possible to the nose, a stable aircraft was finally designed.

Since the lowest and highest speed regimes were taken care of, the regimes in between had to be researched. The transonic performance of the waverider was by far the most difficult to predict. Most of the transonic regime data was adapted from experimental data. A program was written using shock expansion theory to predict the supersonic performance of the aircraft.

Waverider configurations are also very helpful in the area of engine airframe integration. Since the waverider sets up a shock surface underneath the body, the flow is slowed to a lower Mach

number than freestream therefore increasing the efficiency of the actual engine inlets. The flow after the underbody shock is Mach 5.3.

6.2 SUBSONIC AERODYNAMICS

When the all wing waverider configuration was first considered, thought also went into the off-design performance. There has been much research in the area of sharp leading edge delta wings (with some projects being conducted at OSU) mostly for use in delta winged fighter aircraft from Reference 17. This method models a delta wing aircraft as finite thickness flat plate delta wing with a sharp leading edge. Since the waverider has a very sharp leading edge and is relatively flat, a flat plate delta wing is a reasonable approximation. The waverider is basically a delta wing of 115 ft length and 90 ft span. This corresponds to an aspect ratio of 1.41. This data showed that an adequate L/D could be obtained with C_L's in the range needed by our aircraft. Figure 21 shows the data for C_L vs angle of attack. The lift curve slope $C_{L\alpha}$ = .045 per degree with a stall angle of 33°. The aerodynamic efficiency is very low in comparison with conventional aircraft that fly in the subsonic regime, but this was a small price to pay for the much improved hypersonic efficiency.

Since the waverider is basically a sharp leading-edge delta wing, vortex lift will be produced. Vortex lift is the saving grace of highly swept wings at subsonic speeds. Lift produced normally is by the 2-D motion of air over a wing, this lift is

called potential lift. In a highly swept delta wing, 3-D vortices are formed along the sharp leading edge of the wing as shown in Figure 22. This main vortex creates a secondary vortex along the surface of the wing. Because of the high velocity of the secondary vortex along the leading portion of the wing, a lower Cp thus higher lift is produced. This lift accounts for approximately 50% of the lift at angles of attack over 10 degrees. The data was originally taken from Reference 17 for a sharp leading edge 70 degree delta wing with a conical body.

This data proved useful for preliminary design of the aircraft but did not take into account the thickness near the base nor the anhedral of the waverider. Late in the design phase, data for a 3/4 power law body waverider in subsonic flow was acquired. This configuration was very similar to our waverider with a comparable anhedral and thickness but with a more blunted nose. This data was very similar to the other subsonic data except for the C_M vs. alpha curve as seen in Figure 23. The change in C_M is probably due to the fact that the waverider does not have an exact delta planform, but in fact has more area towards the nose of the aircraft.

The line chosen to represent alpha equal zero degrees is defined as when the top surface of the waverider is parallel to the flow. For this reason, at zero angle of attack, there is some lift as can be seen in Figure 21. The nose must be set at an angle of attack of -2.5 degrees to obtain zero lift at subsonic speeds.

Take-off is a very important part of the flight regime and enough lift must be generated at take-off in order to clear the runway. Other problems also exist such as pitching moment at take-

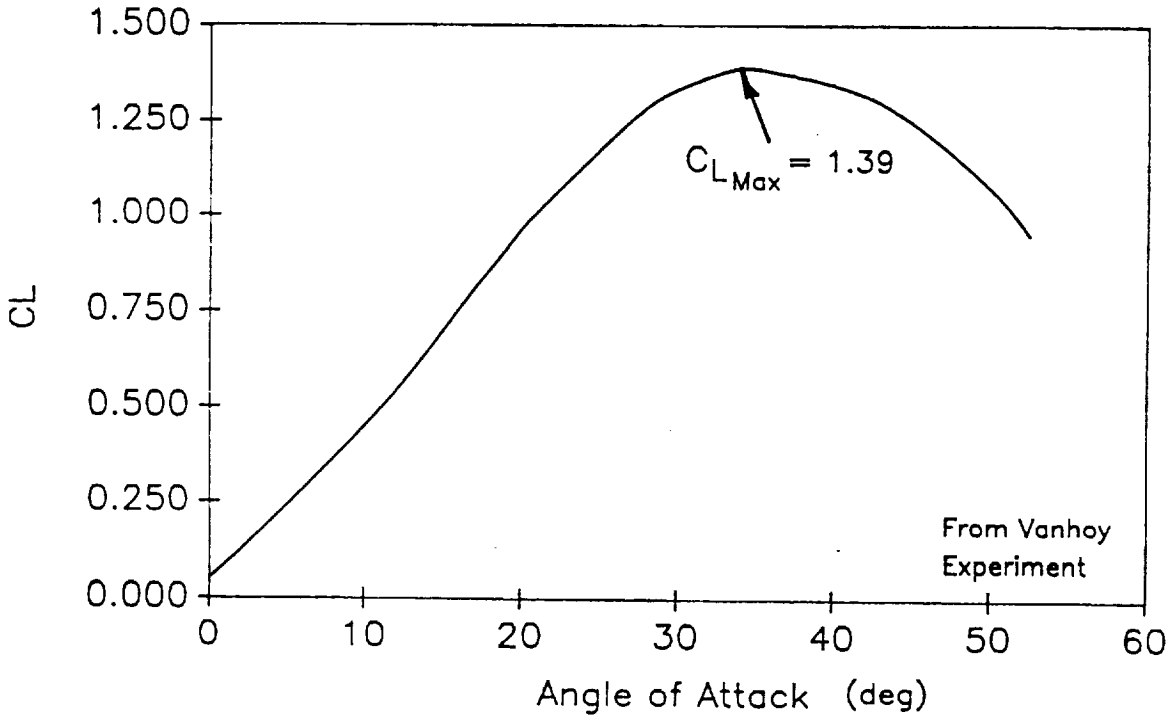

Figure 21 - C_L vs Alpha for Subsonic Flow

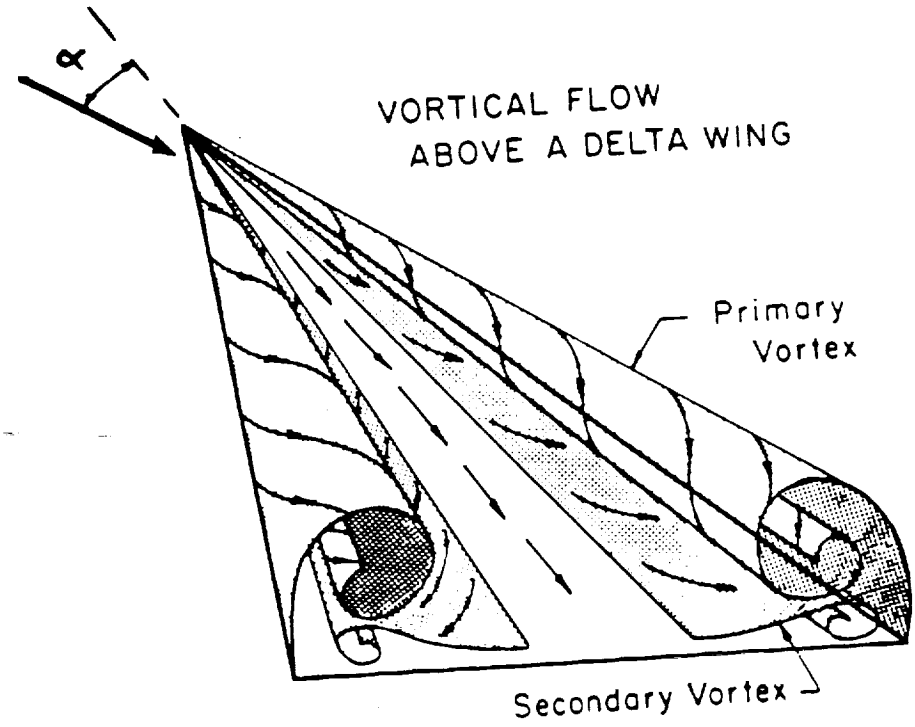

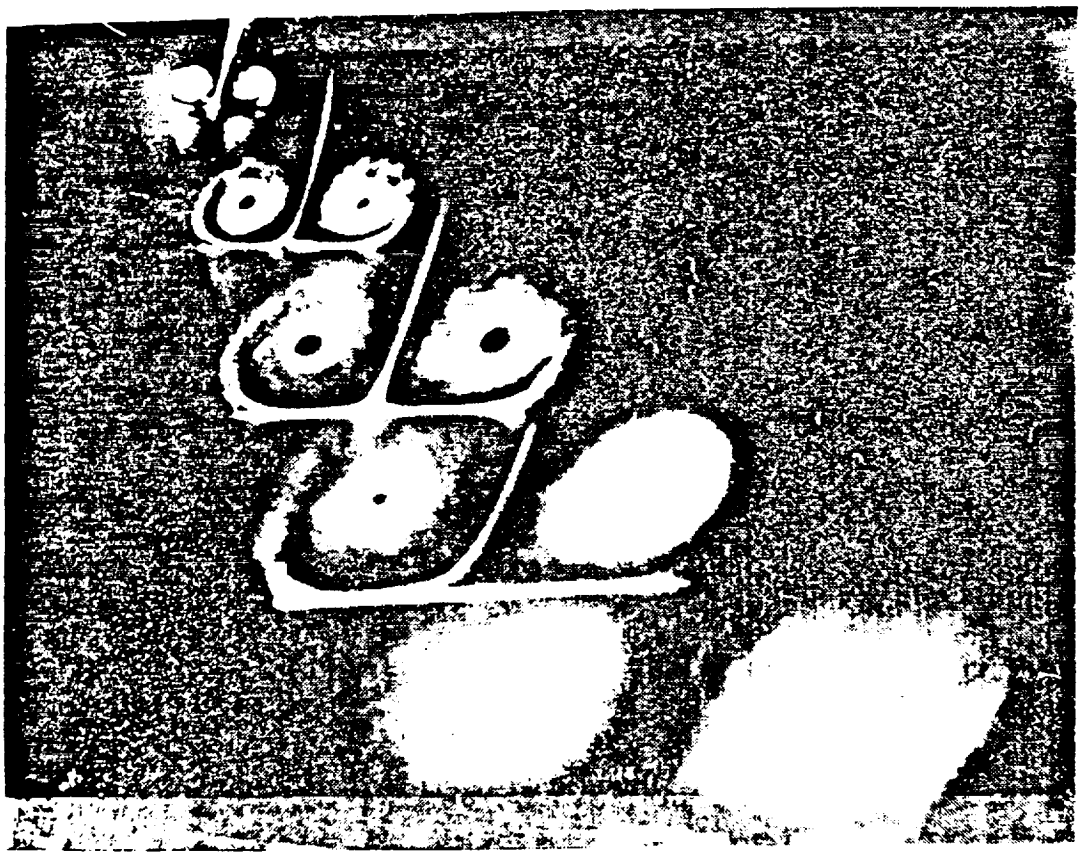

Figure 22 - Vortex Lift for a 70° Delta Wing

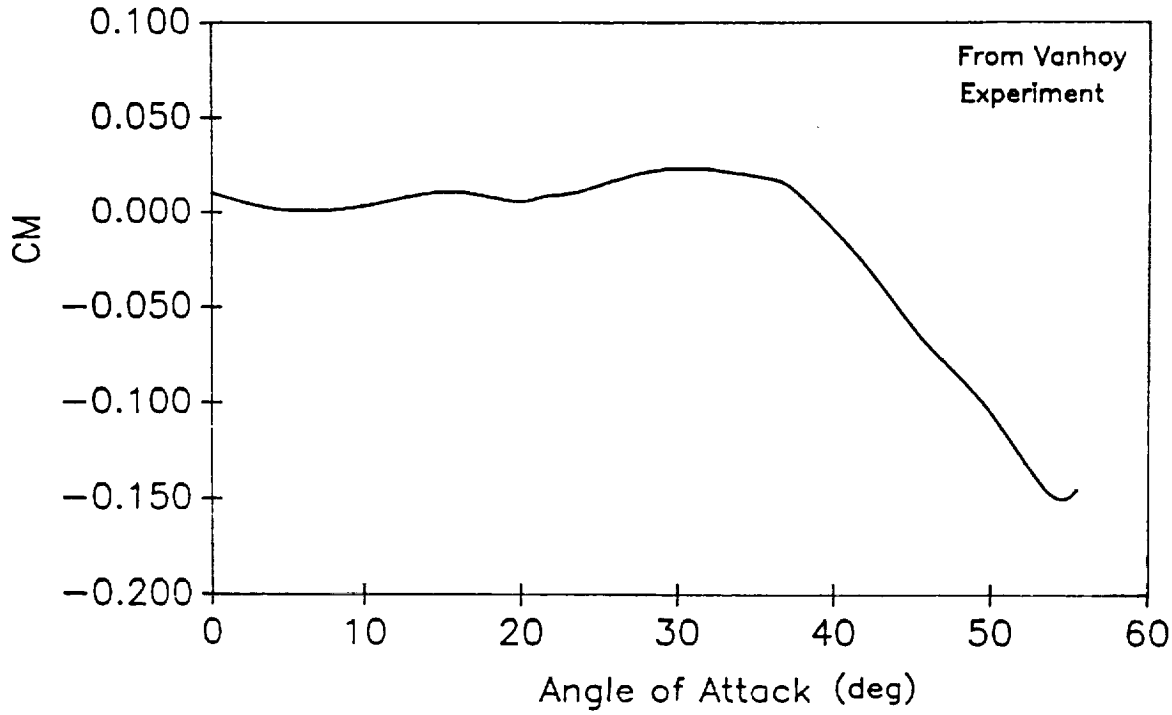

Figure 23 - C_M vs Alpha for Subsonic Flow

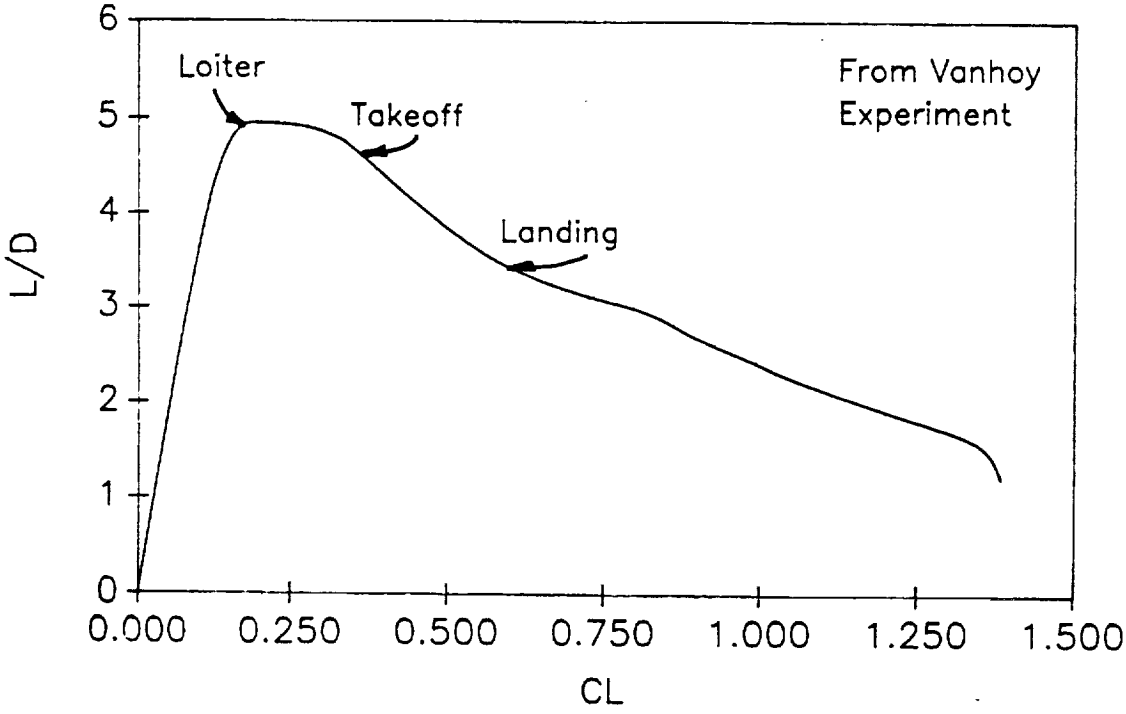

Figure 24 - L/D vs C_L for Subsonic Flow

off and stall speeds. At take-off, a C_L of .3 is necessary with a speed 291 feet per second. This will produce enough lift at the end of the take-off roll. The delta wing can create a large C_{Lmax} at very high angles of attack (33°). This corresponds to a stall speed of only 141 ft/sec. There is a small positive C_m at takeoff which helps to rotate the aircraft to a small extent. Because of the large moment needed to pull the nose up while rotating about the main landing gear, it is necessary to use a hydraulic lifting nose gear to rotate the nose upward for takeoff.

The aircraft is required to loiter for 30 minutes before landing in order to divert to a secondary airport in case of emergency. To make this operation most efficient, it is necessary to fly at the highest L/D possible. The maximum L/D occurs at a Cl of .2, giving a loiter speed of Mach .35 at 20,000 feet. This L/D is shown in Figure 24. In order to keep the aircraft as stable as possible throughout the flight regime, this last used fuel is stored as far foreword as possible.

When the aircraft vertical surfaces were designed, the dead air accompanied with the boundary layer had to be taken into effect. With a Reynolds number based on aircraft length of 220×10^6, the boundary layer along a flat plate using the Prandtl's formula for a turbulent boundary layer (incompressible flow) is only 1.5 inches thick (Reference 38). The actual number should be close to this approximation. At angle of attack, the vortices generated by the leading edge will also contribute to the boundary layer near the vertical stabilizers. The effectiveness of the portion of the vertical stabilizer within the boundary layer is

very low. The boundary layer at angle of attack of 20^{o} was assumed to be one foot for the purpose of designing the vertical stabilizers.

The wing loading of an aircraft is often used as a reference to deduce some of it's characteristics. Wing loading values of todays modern aircraft such as the B-1 Bomber have wing loadings are as high as 150-200 psf. These high wing loadings provide a very stable ride in the subsonic regime as well as a need for a very solid structural design. The wing loading on a waverider type aircraft is extremely low in comparison. Wing loading on takeoff is only 30 psf with a continual decrease proportional to the loss in weight to an even smaller 16 psf at landing. Since the entire aircraft is considered to be a wing, the planform area (5661 ft^2) term in the calculation of wing loading (weight/wing area) will be very high resulting in a very low wing loading. Problems involved with such a low wing loading include buffeting and stability problems at low speeds. These problems may not be as large as some may suspect because it is actually an apples and oranges comparison. One large advantage of such a low wing loading is the drastic reduction in the takeoff distance. The aircraft will also need less structure to support the forces generated by lower wing loading. The values of wing loading that experts are used to are for conventional wing-body-tail configurations. The waverider is far from conventional and will need a different set of acceptable wing loading values.

6.3 TRANSONIC AERODYNAMICS

The transonic regime was by far the most difficult to analyze. Little experimental and even less theoretical work with applications to waveriders in transonic flow has been done. It was very difficult to find information relating to waveriders. Much of the data used was from finite thickness delta wing experiments. Reference 15 and Reference 20 provided some information about the high subsonic and transonic regimes.

There is one main problem with waveriders in transonic flow, the poor distribution of the area and the inability to area rule this aircraft to much extent because one must keep the integrity of the waverider shape intact. In transonic theory, there would be two critical Mach numbers for the aircraft, one when the Mach angle is parallel to the sweep angle of the trailing edge (Mach 1) and the second when the Mach angle is parallel to the leading edge sweep (Mach 3) from Reference 15. The drag near Mach 1 increases rapidly, therefore a large dip in the L/D in Figure 33 near Mach 1. This drag will stay reasonably high until after Mach 2 when the volume distribution at this Mach number become more like the Sears-Haack volume distribution. The second critical Mach number at Mach 3 is much less critical as shown in Figure 33. A C_L vs C_D curve is shown in Figure 25 for Mach 1.2 flight.

Since the waverider upper surface will be designed as an expansion surface, it may be possible to incorporate some type of area ruling into the basic design. Even a small change in the area distribution should have a favorable effect on the transonic drag.

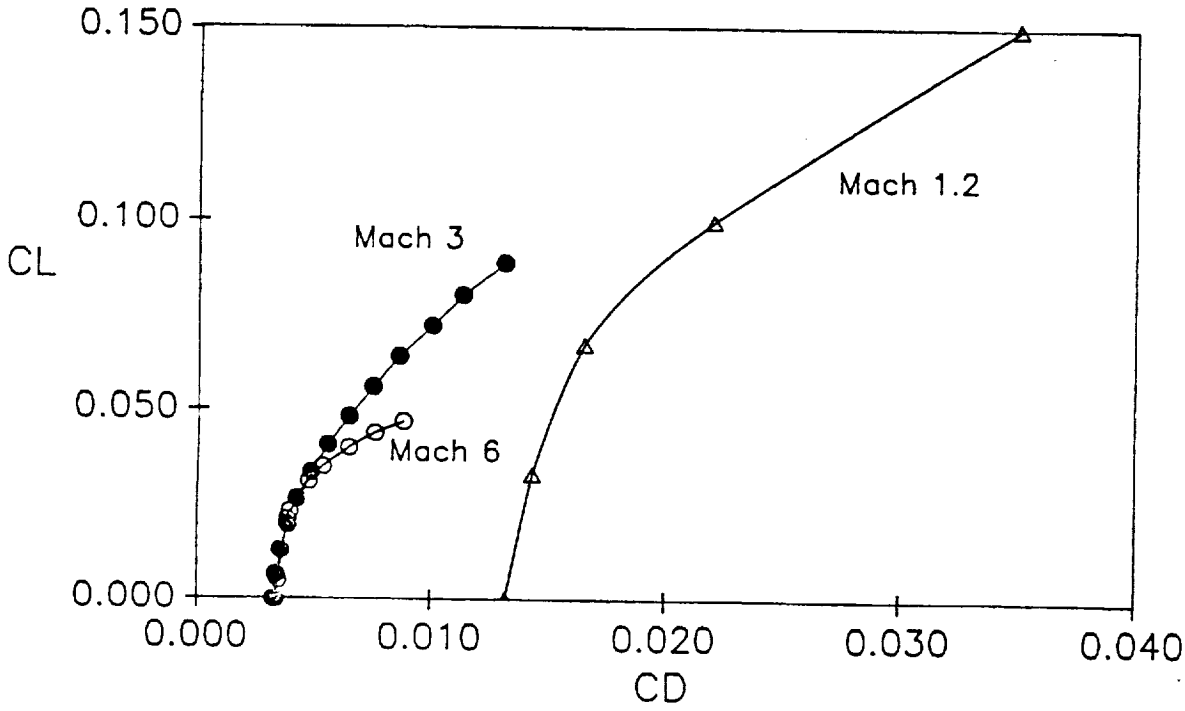

Figure 25 - C_L vs C_D at M = 1.2, 3, 6

6.4 SUPERSONIC AERODYNAMICS

The aircraft was modelled as a wedge in a computer program written to calculate supersonic drag. Shock expansion theory, skin friction drag, and base drag were used to assess supersonic performance. Oblique shock relations were used to determine the pressure behind the shock wave. The pressure difference between the lower and upper surface determined the lift. Friction drag was calculated from equations in Reference 2. The base drag was calculated using local freestream conditions to determine the pressure forces on the aircraft. The results of these calculations are shown in Figures 25 and 33.

6.5 WAVE DRAG

A wave rider can be described essentially as a large flying wing. The modelling for the Wave Drag program was in large part a wing. Also included in this modelling were fins and nacelles. Since the program only allows for circular nacelles, the square engine box of this design was modelled using three circular nacelles having equivalent cross-sectional area.

The wave drag coefficient is shown in Table 6. Drag values shown were found by multiplying the drag divided by dynamic pressure by the dynamic pressure the aircraft is expected to experience at the corresponding Mach Number.

Table 7 - Wave Drag Results

M	C_{D_W}	D/Q	D (lbs)
1	0.5507	3117.327	857,838
2	0.0500	283.173	193,154
3	0.0297	168.116	159,960
4	0.0212	119.775	77,973
5	0.0182	101.838	64,678
6	0.0153	86.692	50,432

The drag results are large for low Mach numbers resulting in lift to drag ratios of less than one and are at least two times greater than originally predicted values.

Although the Wave Drag results are widely excepted by industry, for a non-traditional wingbody configuration the drag results are higher then expected. Emperical transonic data from a 70 degree, 7% thick delta wing with vortex flaps gives a drag coefficient of approximatly 0.023 in the transonic region where Wave Drag predicts a wave drag coefficient of 0.55. Even though the empirical data was not for an exact wave rider configuration these results are more realistic.

At higher Mach Numbers (i.e. greater than 3) the Wave Drag results are unreliable. The drag at these Mach numbers were taken as the originally calculated values as described earlier.

6.6 HYPERSONIC AERODYNAMICS

A waverider is basically a reverse engineered aircraft. Instead of taking and aircraft design and then by various means, calculating the flowfield about this body, the waverider concept takes a known flowfield and superimposes a body upon the flowfield. The flowfields usually used are those of a simple $y=x^n$ with $0<n<1$ shape rotated about the x-axis to form a power law body of revolution. The shock generated by this body when it is introduced into the flowfield is used to calculate the waverider.

The idea of waveriders is not a new one. Nonweiler first proposed an inviscid caret wing waverider in the 1950's. This concept was recently tackled using modern computer methods when Bowcutt calculated a viscous solution of an optimum waverider on a shock wave formed by a cone. This program also optimized the upper surface as an expansion surface to further enhance the aerodynamic efficiency. Corda then included waveriders derived from axisymmetric power law bodies. A view of the waverider used as a base for this aircraft is shown in Figure 26.

Figure 27 shows the cone and resulting conical shock surface flowfield about a cone flow waverider. In part a of Figure 27, the cone is shown with an axisymmetric cone shock surface around the cone. On top of this shock surface is then superimposed a leading edge shape used to define the waverider itself. In the MAXWARP program, five points are plotted on the leading edge of the waverider. From these five points, the entire flowfield is traced back on streamlines resulting from the cone shock wave. By

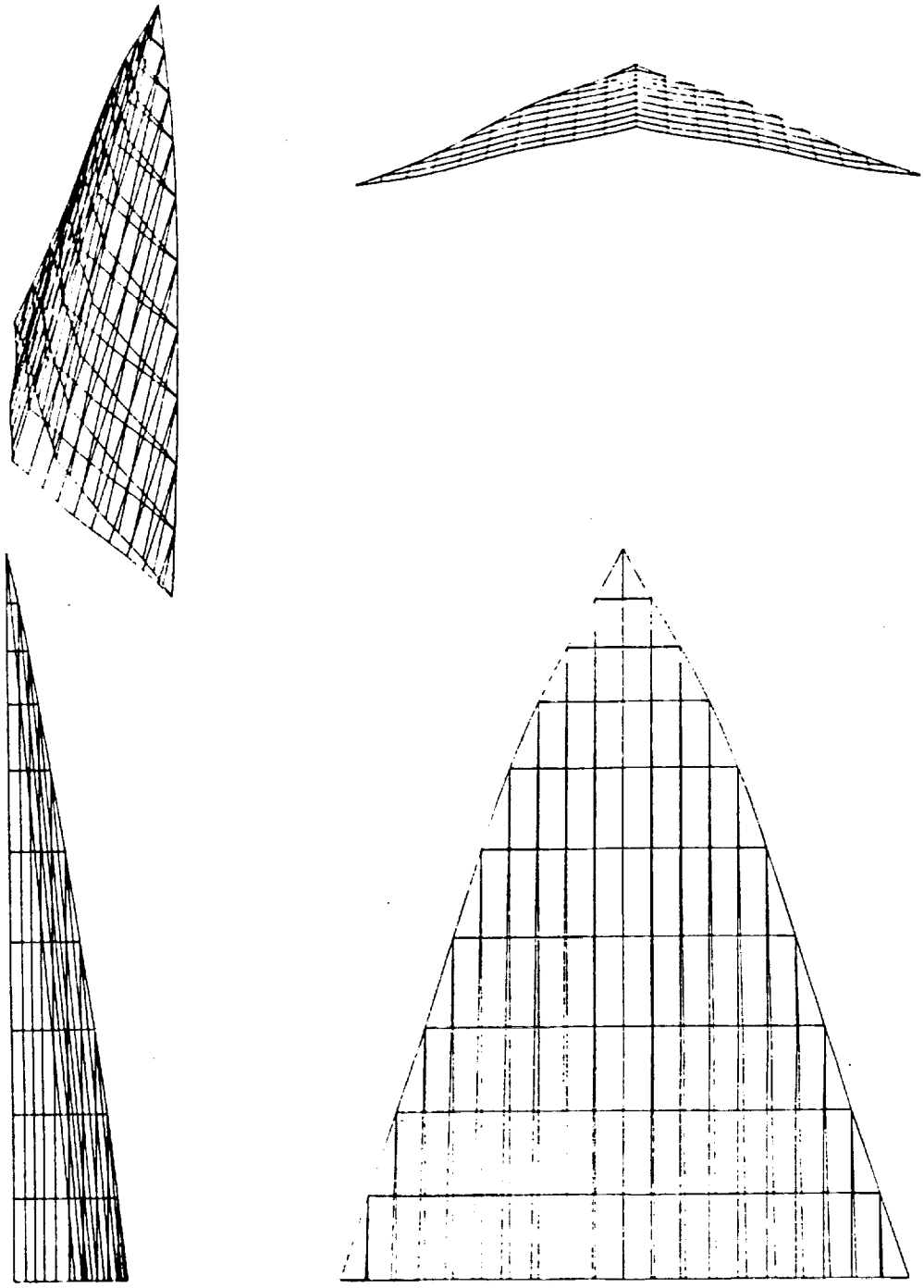

Figure 26 - Waverider 3 View

varying these five leading edge points, different waverider shapes will be generated. An optimization process is accomplished by making very small changes in the leading edge shape. The upper surface of the waverider for Corda's MAXWARP program is defined as a freestream surface, therefore no lift is produced. Once the leading edge is chosen, and the streamlines used to define the upper and lower surface of the waverider are traced back, the pressures on the waverider can be determined. From these pressures along with skin friction drag calculations, the lift, drag, and pitching moment can be calculated. Part b of Figure 27 shows the waverider shape riding on the attached conical shock wave (from Reference 22).

Appendix B shows the MAXWARP input and output data use to calculate the waverider shapes. Some of the important input parameters include:

1) Power of the power law body.
2) Slenderness ratio of the power law body.
3) Length of the aircraft.
4) Freestream Mach number.
5) Freestream pressure and density.
6) Average aircraft wall temperature.
7) Minimum slenderness ratio of aircraft.
8) Box size (semi-span/length).

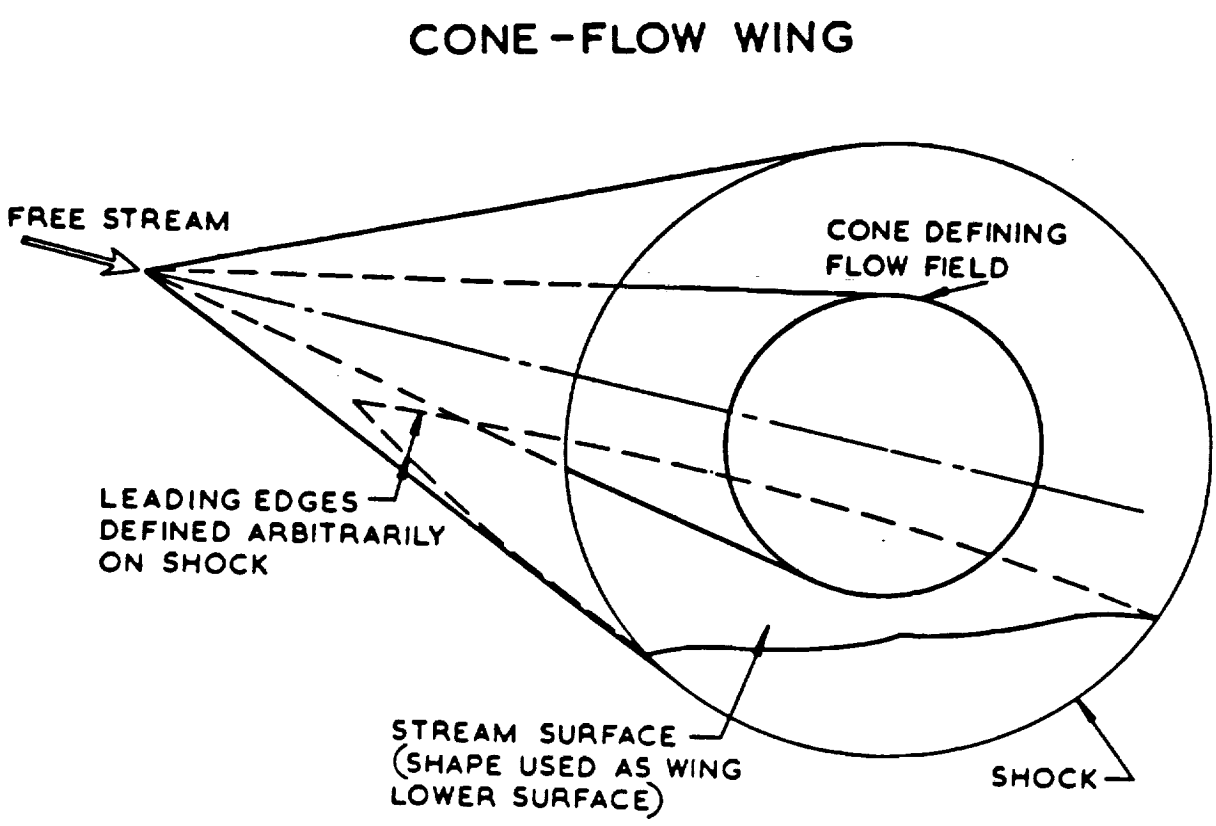

Figure 27 - Pictorial Definition of Waveriders

The important values of the output data include:

1) Base height/length and semi-span/length.
2) Planform area.
3) Aircraft Volume.
4) Inviscid and viscous values of C_L, C_D, and C_M For the upper and lower surfaces as well as the base.
5) L/D ratio

Because of the high altitudes (low pressure) compression lift (lift produced by generating a shock wave under the aircraft) is an efficient way to generate enough lift at such low pressures. Since the air is at such a low pressure, the lift generated by an upper surface pressure differential (suction) is almost negligible. The much more violent underbody shock compression produces much more lift than could be obtained otherwise.

The associated Reynolds number for the aircraft at cruise is 69×10^6. This means that the flow over the waverider is almost entirely turbulent. The transition from laminar to turbulent flow occurs approximately five feet from the leading edge. The MAXWARP program allows the user to use either a completely laminar or turbulent flowfield or one in which MAXWARP calculates the transition point. The latter flowfield being the one used for this design.

It is also interesting to note that laminar flow control seems to be ideal for the lower surface of waveriders, because of the conventional hypersonic aircraft because of the high pressure under the body and freestream upper surface. This large pressure differential could be used in passive laminar flow control, where the lower surface boundary layer is sucked off by the low pressure, freestream upper surface. This means no heavy machinery, only

airflow passages would be needed. If it were possible to create a completely laminar flow field, an L/D of 9.49 could be achieved for the base waverider, which is a 33% increase over the current design. Therefore, even with a modest amount of laminar flow control, large benefits could be accrued.

In order to obtain an attached shock wave on the leading edge of the airfoil, the leading edge must be "aerodynamically sharp" or else aerodynamic losses will occur. This definition of sharpness is quite vague and the losses associated with having a non-zero leading edge radius are not exactly known. The ratio of leading edge radius to the length of our aircraft (the usual measure of sharpness) is 9.06×10^{-5} which should be small enough to make any of these inefficiencies negligible.

The MAXWARP program calculates the coordinates in three dimensions of all the points on the waverider. A graphic of the MAXWARP output is shown in Figure 26 with a three-view drawing and an isometric. These wire frame pictures show only one-sixth of the actual points that MAXWARP uses to calculate the flowfield. A total of 8,500 points on the waverider are used to calculate the aerodynamic forces on the waverider.

6.7 CHANGES TO THE MAXWARP WAVERIDER

Since MAXWARP constructs only a basic waverider, which is not a feasible aircraft bt itself, some design changes must be made. Much thought went into the benefits and drawbacks that the changes will incur. The main points that needed to be studied were: addition of vertical fins, engine box, expansion nozzle boattail, inclusion of aerodynamic control surfaces, and a non-freestream upper surface.

As a baseline estimate, averaging over the cruise leg, the lift will need to be 123,000 pounds and the corresponding drag will be 17,600 pounds for a waverider with no modifications. This corresponds to an L/D of 6.984 as specified by the MAXWARP output. The lift needed to supported our aircraft will demand a Cl of .039. This Cl is a little above the optimum Cl of .0366 as defined by the MAXWARP program in Appendix M. The boattail produces 8,000 pounds of additional lift a cruise. This lift corresponds to an increase in C_L of .002. With this small increase, the waverider will be operating at a maximum L/D as shown in Figure 28. The baseline drag of 17,600 pounds was calculated directly from the MAXWARP output, additional areas of drag and lift increases were either calculated or estimated to obtain a final L/D estimate.

6.7.1 VERTICAL FINS

The vertical fins can be aligned with the streamlines originating from the leading edge of the waverider in order to minimize drag. In actuality, they will need to be "toed-out" a few degrees in order to make sure that at least one surface is wetted at all times, making the aircraft more controlable at the higher Mach numbers. A very thin supersonic airfoil section of about 4% thickness was chosen as a trade-off between least drag and an adequate structural integrity. The sweep of the vertical tail was also made as large as possible to decrease the wave drag. The drag of the two vertical tails was estimated as adding 3% to the baseline drag (Reference 20).

6.7.2 ENGINE BOX

The engine box and inlet was a major addition to the drag of the baseline waverider. The engine box will also be designed to conform to the streamlines created by the leading edge of the waverider. This will reduce the wave drag substantially. Drag of the engine box itself will only need to be calculated because the ram drag of the engines is already included in the data for the engine thrust. Also the friction drag does not need to be taken into account since it only moves the surface of the waverider away from the baseline (basically the engine box covers up part of the waverider for which a skin friction was already calculated). There were no exact methods found for calculating the actual wave drag

on an engine enclosure so with some creative thought an addition of 7% to the total drag was estimated.

6.7.3 EXPANSION BOATTAIL

This aerodynamic device is discussed in detail in the propulsion section. Basically, the boattail serves two purposes, to adequately expand the exhaust of the engine to produce thrust and if a properly under-expanded nozzle is created it will add lift. This lift produced is equal to 5% of the total lift produced by the aircraft. This lift also produces a nose-down moment which helps to alleviate the nose-up moment created by the engines which makes it easier to trim in the cruise regime. The only drag added at cruise, is the small skin friction on the upper surface of the boattail.

6.7.4 AERODYNAMIC CONTROL SURFACES

These control surfaces also include provisions for gracefully ending the base of the aircraft. MAXWARP assumes a flat base and does not calculate the base drag. Base drag at this altitude is very low because of the very low density (75 times less dense than sea level) and the small interaction of the air behind the aircraft with the aircraft itself because of the high speeds involved. This drag was estimated to be an additional 7% of the baseline drag (Reference 2).

6.7.5 NON-FREESTREAM UPPER SURFACE

The upper surface of the waverider generated by MAXWARP is a freestream upper surface thus no lift is produced, only drag is produced. The reason for this is that the upper surface design is very difficult and demands more CPU time than it is worth in the eyes of the programmer Dr. Corda. By optimizing the upper surface as an expansion surface an additional 5% increase in lift can be produced (Reference 39).

6.7.6 TOTAL HYPERSONIC AERODYNAMIC FORCES

The MAXWARP output L/D is 6.984 for the base waverider. This means every 6.984 pounds of lift, 1.0 pounds of drag will be produced. From the past calculations on additional lift and drag, lift will be increased by 10% and drag increased by 17%. Taking these additional forces into account,and an L/D of 6.5 is the result, which isthe L/D used for the hypersonic cruise regime for the proposed configuration.

Since this waverider is optimized for a certain C_L, it is desired to always operate at this C_L. The weight of the aircraft is higher at the beginning of cruise, thus a higher C_L will be needed. In order to alleviate this problem, the airplane operates at a slightly lower altitude at the beginning of cruise in order to increase the dynamic pressure, and therefore increase the lift for the same value of C_L. The altitude at the beginning of cruise is 98,800 and then a climb to an altitude at the end of cruise of

104,300 gives the right amount of lift at each point in the mission profile.

The boundary layer at hypersonic speeds will also be a consideration both in the design of the vertical control surfaces and the engine inlet. The boundary layer on the lower surface of the aircraft will be thinner than that of the upper surface because of the interaction between the boundary layer and the shock waves formed by the leading edge. The boundary layer on the upper surface at the trailing edge of the wing will be approximately ten inches thick. The corresponding boundary layer on the lower surface will be between six and eight inches thick. In order to divert the boundary layer air from the engine inlets, a maximum thickness of six inches was chosen at the lip of inlet.

6.8 HYPERSONIC TRADE STUDIES

Since the aircraft is designed to be a hypersonic cruise vehicle, it is most advantageous to have a maximum lift to drag ratio (L/D). The aircraft will be spending the most time at cruise, and equally as important, it will be burning the voluminous fuel hydrogen in this regime. In order to cruise efficiently and burn the least hydrogen, it is advantageous to create the most lift with the least amount of drag which means maximize the L/D. Of course, the C_L's at which the maximum L/D's occur must provide enough lift at the given flight condition. Many parameters were studied in order to define an optimum design. Effects of temperature, exponent of the power law body, slenderness ratio, and

altitude of cruise were investigated. All throughout the tests, only one parameter was changed with the others staying the same as the baseline.

6.8.1 TEMPERATURE

The MAXWARP program calculates both skin friction and wave drag. This temperature is the average temperature over the entire aircraft. The wave drag stays relatively constant at all temperatures while the skin friction drag decreases as the temperature increases. As temperature increases, the boundary layer becomes fuller, creating a lower velocity gradient and therefore a lower skin friction drag. This trend is shown in Figure 29. Although it was desired to have the highest acceptable skin temperature over the surface, the average value of 1100°R was computed using the method from Appendix D. The L/D for this temperature is that of the baseline waverider, 6.984.

6.8.2 EXPONENT OF THE POWER LAW BODY

The flowfield is generated by inserting an axisymetric body into the flowfield. The shock generated by this body defines the flowfield that is used to construct the waverider. This concept is shown in Figure 27 for a cone flow body. The power law body is defined as $y=x^n$ rotated about the x-axis where n is the power of the flow generating body. The higher the defining power is, the more rounded the nose of the aircraft will be. All of the

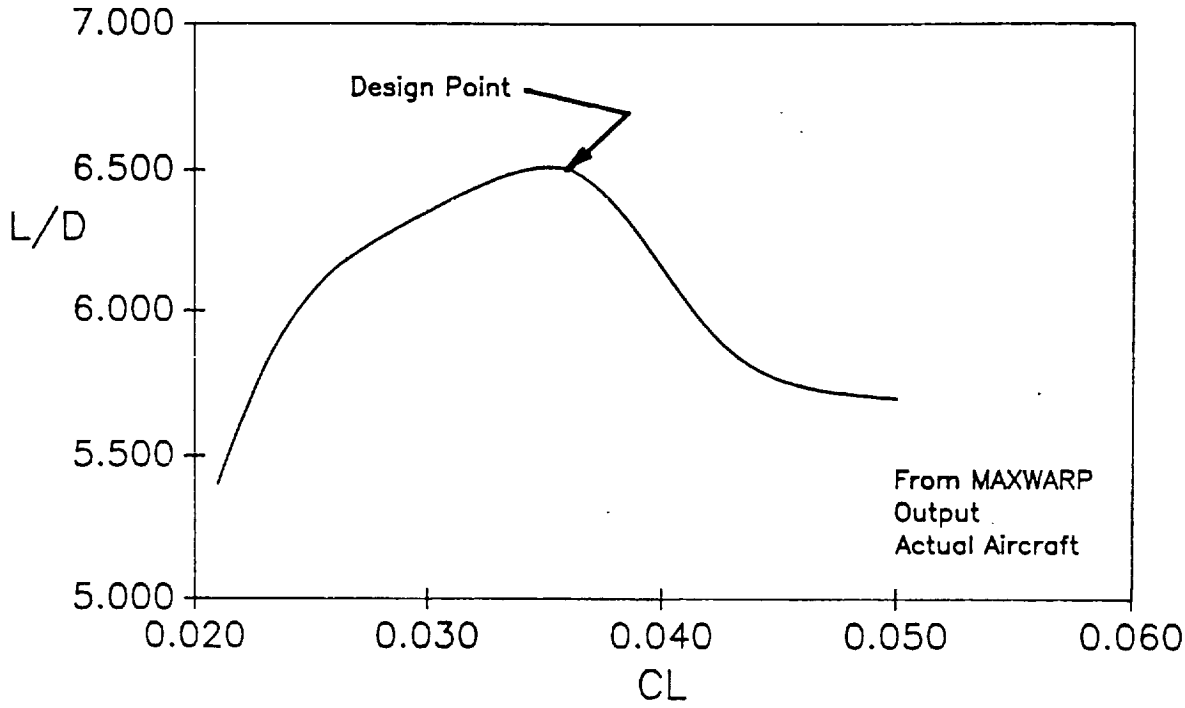

Figure 28 - L/D vs C_L at M = 6

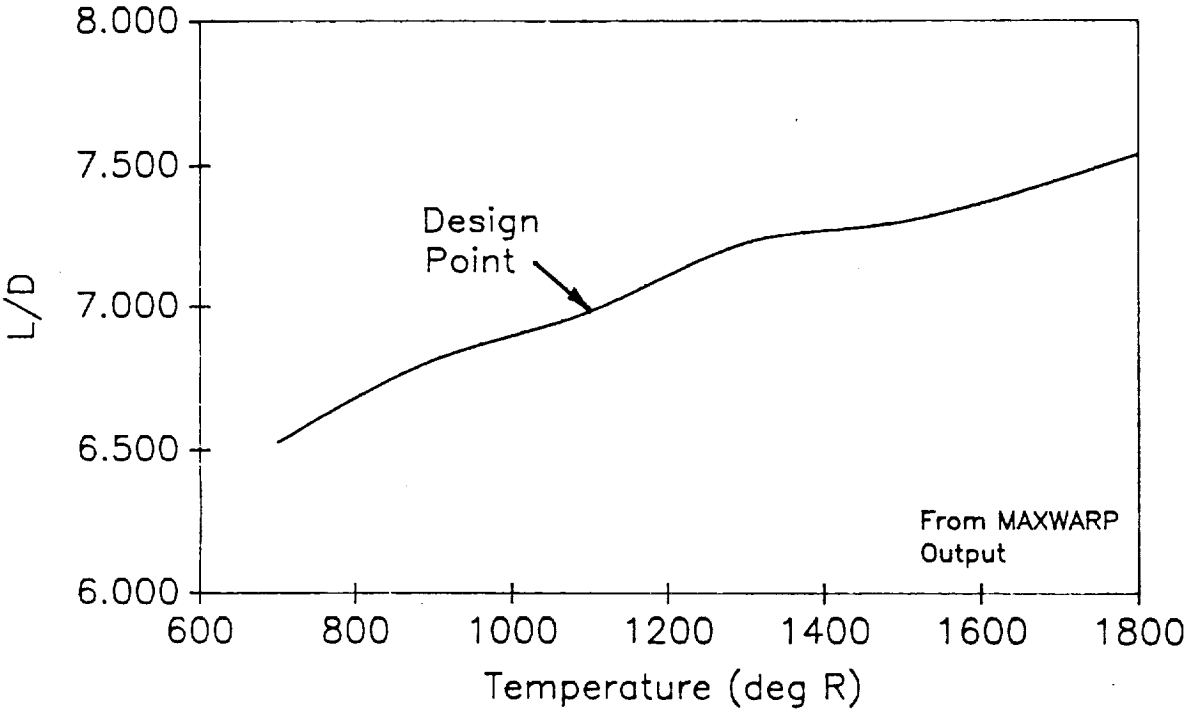

Figure 29 - L/D vs Temperature at M = 6

waveriders generated in the figure represent feasible aircraft. A maximum L/D occurred at a power of 1/2 which is the defining power of the waverider chosen for this project. Because of the complicated optimization processes of MAXWARP, Figure 30 is not a linear relationship of the exponent.

6.8.3 BODY SLENDERNESS RATIO

This is the ratio of the maximum thickness of the flow defining body to the length of the body. This has a direct correlation to the thickness ratio of the waverider itself. A very thin waverider will not create enough lift while still having a reasonably large skin friction drag and lower wave drag. A thicker waverider will create too much lift therefore a higher wave drag with approximately the same skin friction drag. There will be an optimum point between the two extremes where the lift and drag combine to form a maximum L/D. The optimum slenderness ratio occurred at .16 with and L/D of 6.984 as shown in Figure 31. The resulting waverider generated had a thickness ratio (base height/length) of .085.

6.8.4 ALTITUDE OF CRUISE

At differing altitudes, the pressure and density of the air change drastically. If the pressure of the air is higher, a less violent shock will produce the same pressure under the aircraft. In contrast, a lower pressure will correspond to a more violent

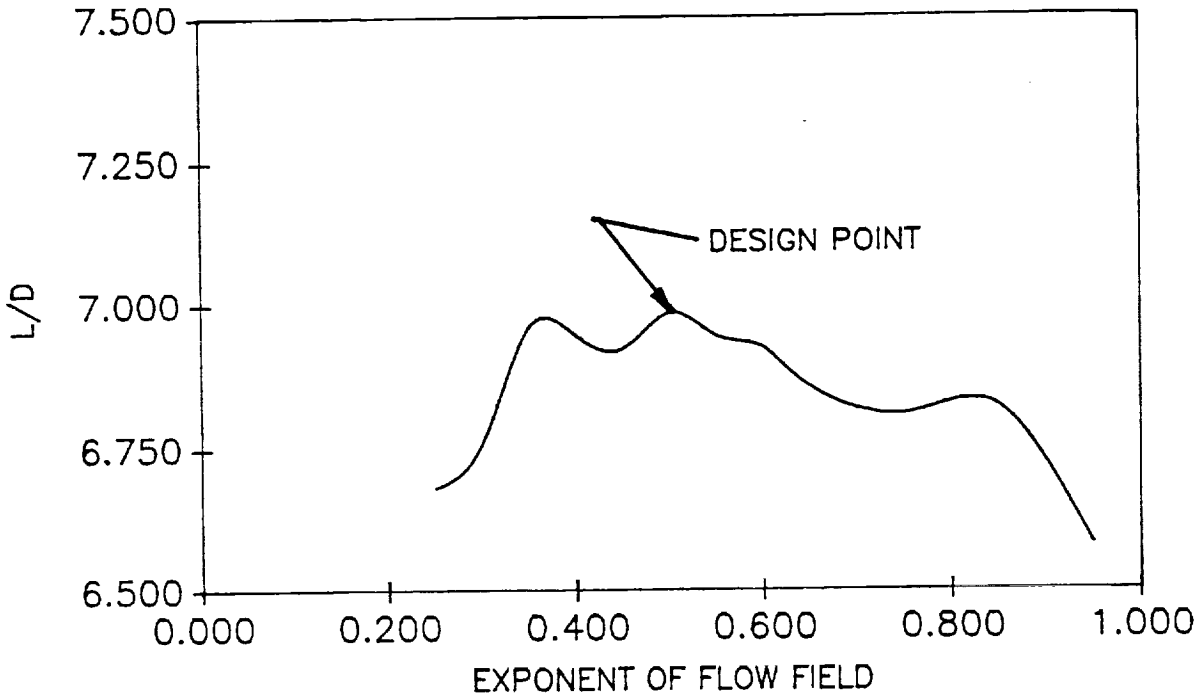

Figure 30 - L/D vs Exponent of Power Law Body at M = 6

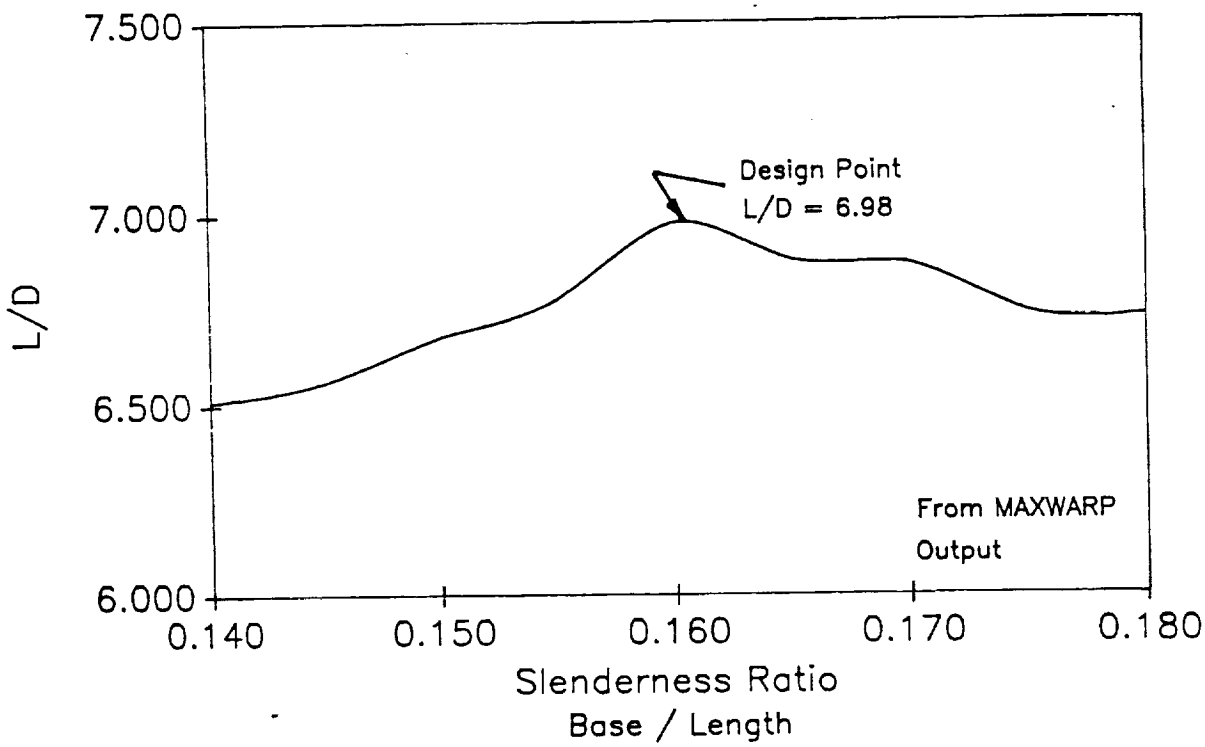

Figure 31 - L/D vs Slenderness Ratio at M = 6

shock in order to produce the same lift. This of course assumes that the planform areas of the aircraft stay constant. For this reason, it is best to fly at the lowest possible altitude. This is really the only reason to fly at a lower altitude. At a lower altitude, the shock overpressure on the ground will be higher, the ramjet engine efficiency will be lower, and the aerodynamic heating will be higher. For these reasons, an altitude of 100,000 feet was chosen as a tradeoff between these four driving factors. The change in L/D with respect to altitude is shown in Figure 32.

Since one of the main objectives was to produce data useable by other sections of the report, an all encompassing graph of aerodynamic efficiency was produced. Figure 33 shows L/D vs Mach number. The altitude of cruise as calculated by the mission profile was taken into account in this figure. This also gives a good overall view of the efficiency through each flight regime.

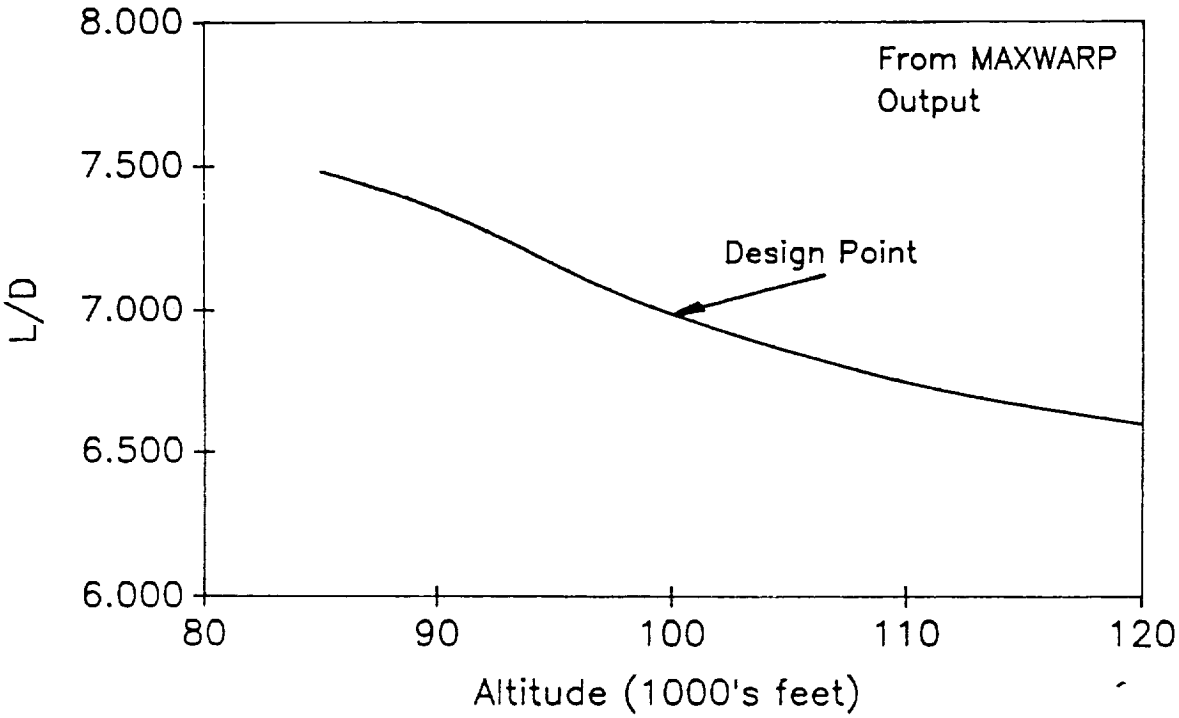

Figure 32 - L/D vs Altitude at M = 6

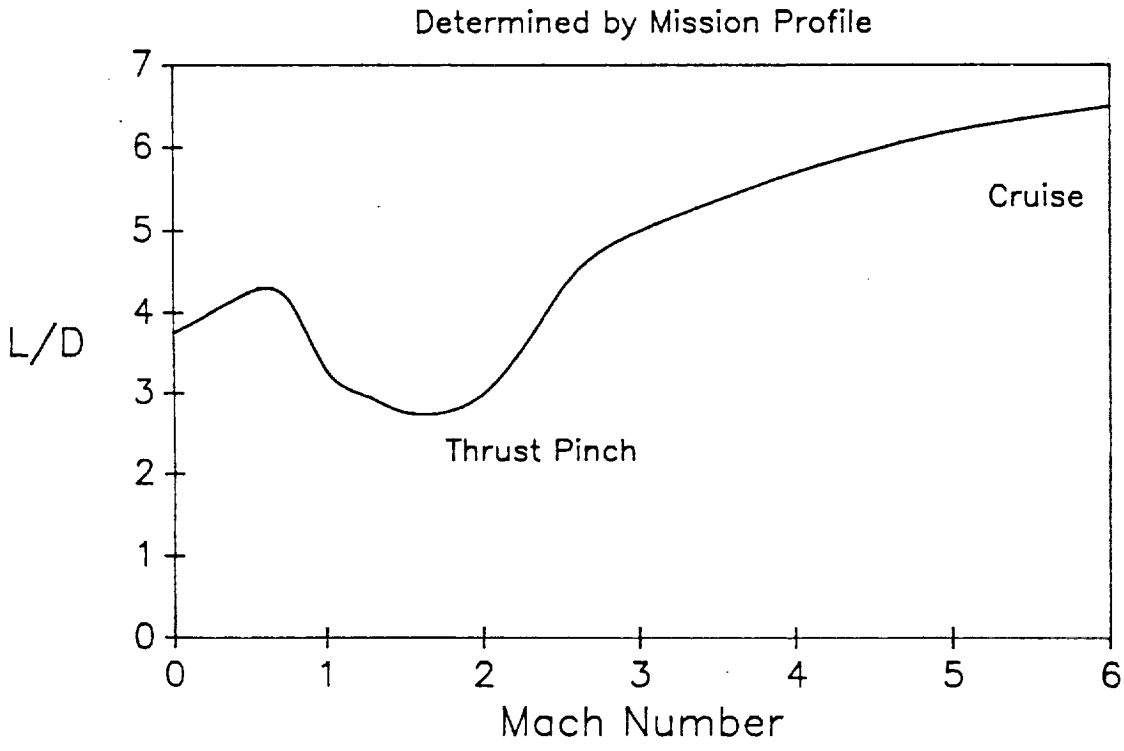

Figure 33 - L/D vs Mach Number

6.9 SHOCK OVERPRESSURES

Since this aircraft will be travelling at speeds greater than the speed of sound, it will produce a sonic boom (shock overpressure). This sonic boom is annoying to the general population. The only supersonic aircraft currently operating in a non-military mode is the Concorde. This aircraft produces shock overpressures at cruise on the order of 2.5 psf. This overpressure is very loud, and this along with its very loud take-off and landing noise is why the Concorde must take-off toward, and land from the ocean.

In order to be able to fly as many routes as possible, it is vital that this aircraft be able to fly over land. Current political views point to an acceptable shock overpressure below 1 psf may be permissible for overland flight. Equations for shock overpressures relate the overall sonic boom as functions of altitude, Mach number, atmospheric pressure, length of vehicle, and weight of vehicle. A number of factors provide for a relatively low overpressure for this waverider aircraft: the low weight, high altitude, and long length. These three factors provide for a shock overpressure at cruise of .77 psf. This will allow the aircraft to cruise over land (allowing that below 1 psf is acceptable). Of course when the altitude is lower, a higher shock overpressure is created as shown in Figure 34. This will mean that the aircraft will be limited to landing at coastal airports in order to ascend or descend over water when the shock overpressures are unacceptably high.

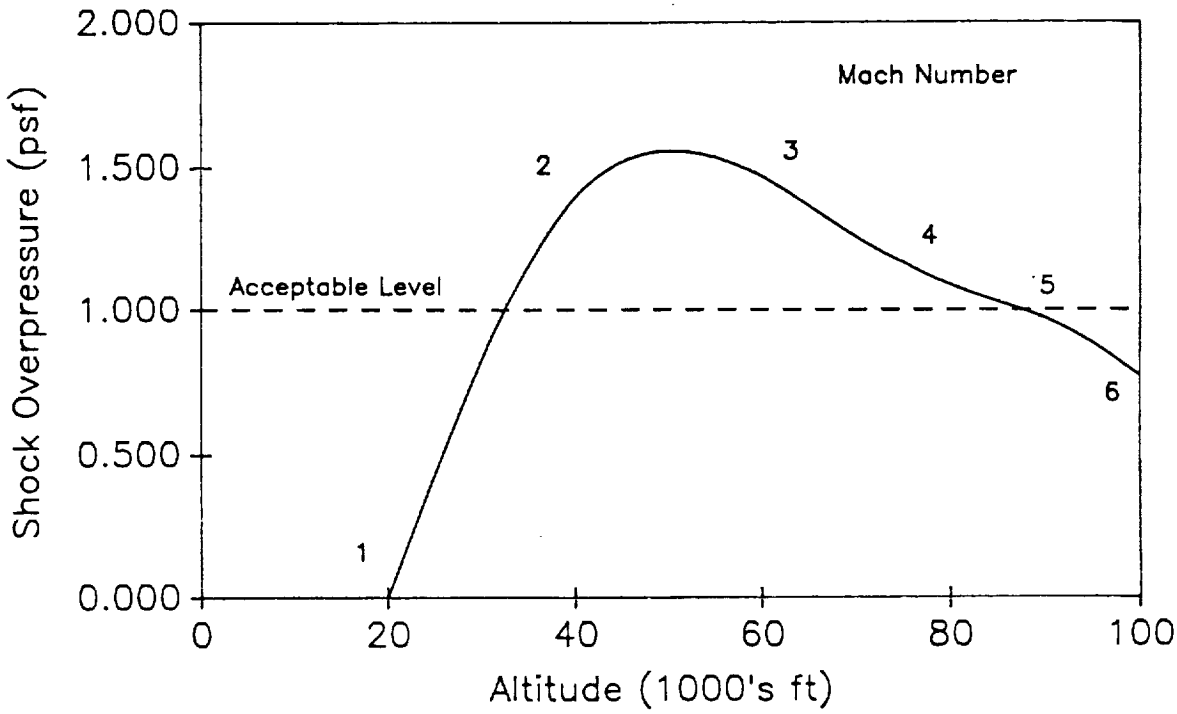

Figure 34 - Shock Overpressure vs Altitude

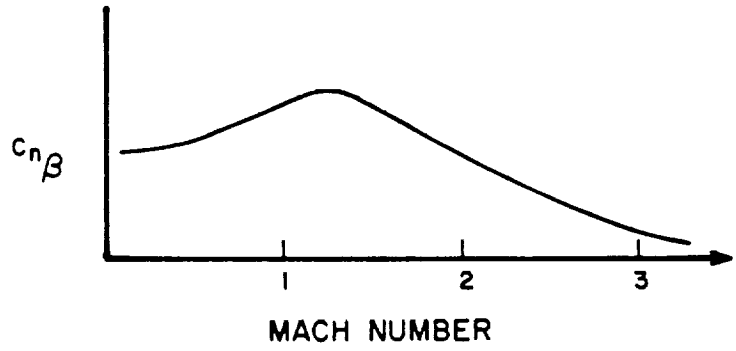

Figure 35 - Typical C_{n_β} Variation with Mach Number

7. STABILITY AND CONTROL

Since the most demanding portion of control for this aircraft takes place at subsonic speeds, the stability and control analysis concentrated on that regime.

7.1 STATIC MARGIN

The analysis began with the determination of the static margin (SM), which is the difference between the aircraft center of gravity (CG) and aerodynamic center (AC), nondimensionalized by the mean aerodynamic chord (MAC). The CG at takeoff is located at x = 73.39 feet from the nose, y = 0.0 feet from the centerline, and z = 6.59 feet from the upper surface. The internal layout was driven by accomodation of the large volumes of both JP and hydrogen fuels, along with locating the passenger cabin to allow for 6.5 feet of height at its centerline while leaving 6 inches between the skin and cabin walls for insulation. The CG was therefore determined from the internal layout, instead of vice versa. The CG travels 7.6 feet aft from fully fueled to dry. Appendix C gives tables for component weights and component CG locations for important points in the mission profile. Next, the subsonic center of pressure (C_p) was assumed to be that of a Delta wing: 2/3 of the maximum chord, or 76.67 feet from the nose. The aerodynamic center was then determined from Vanhoy's results (Reference 35), where a similar configuration yielded a c_{mo} (equal to c_{mac} for a wing alone) of 0.012. That puts the aerodynamic center at 77.03 feet from the

nose, assuming that the C_p location is correct. The hypersonic AC came from the output of the MAXWARP program, and is 78.67 feet from the nose. A summary the CG and AC locations are presented with their resulting static margins in Table 8 for important points in the mission profile. A positve SM (CG forward of the AC) means the aircraft is longitudinally statically stable. When the aircraft is out of fuel, it is unstable. This means that the aircraft can become unstable during a long loiter. When this happens, a stability augmentation system will be required to fly the aircraft. To delay (and prevent for a short loiter) the instability, a fuel management system use the fuel in the JP tank from aft to forward, keeping the fuel moment arm as long as possible.

Table 8 - Static Margins

	AC (ft from nose)	CG (ft from nose)	SM
Fuelly Fueled	77.03	72.77	5.55 %
At Takeoff	77.03	73.39	4.74 %
Start of Cruise	78.67	77.92	0.98 %
End of Cruise	78.67	75.20	4.53 %
Dry	77.03	80.36	-4.81 %

7.2 CONTROL SURFACE SIZING

The waverider configuration alone is statically stable with respect to all three axes at subsonic speeds, but by very small margins. Each derivative is also sensitive to Mach number, especially $c_{n\beta}$ (see Figure 35). In order to insure directional and lateral stability in high angle of attack and hypersonic

flight, the vertical stabilizers were oversized for the subsonic regime. The elevons, however, will need to provide little pitch and roll authority at Mach 6 and were designed for subsonic flight.

7.2.1 VERTICAL STABILIZERS

The vertical stabilizers were designed to give a subsonic C_n of 0.2000 using the method given in Nicolai (Reference 2) See the stability and control appendix for the calculations. An augmentation system will be necessary to improve the handling qualities resulting from a large C_{n_β}. The hypersonic value will be on the order of 10 % of the subsonic value. Instead of one centrally located fin, the 440 ft^2 of area was divided into 2 stabilizers, each placed 11 feet outboard of the centerline, perpendicular to the 20 degree anhedral upper surface. This will lessen the effects of washout due to the large boundary layer at hypersonic speeds and flow separation during descent where the angle of attack is 20 degrees. The 70 degree leading edge sweep helps to reduce drag. In order to increase the high Mach number stability, the stabilizers were canted inward to increase their high speed effectiveness.

7.2.2 RUDDERS

FAR Part 23 gives the power requirements for the rudder as follows:

1. It must be able to hold $\beta = 0$ for a one engine out flight condition at 1.2 V_{TO}.
2. It must hold the aircraft on a straight ground path during takeoff and landing in a crosswind up to 20 % of V_{TO}.
3. It must overcome the adverse yaw associated with abrupt aileron rolls.

Nicolai's method was used to size the rudders. The crosswind condition was by far the worst case and required that 64 % of the vertical stabilizer area be a rudder, deflectable to 20 degrees.

7.2.3 ELEVONS

A tailless aircraft incorporates pitch and roll control into one surface called an Elevon (Elevator - Aileron). The sizing method came from Roskam (Reference 31) with inputs from Dr. Gerald Gregorek and Dr. Michael Bragg. The elevons meet the Class II roll rate requirement of 45 degrees in 1.4 seconds with a 20 degree deflection. Table 9 shows roll rates for different elevon deflections. Elevon deflection angle is defined as one-half the total angle between differentially deflected elevons.

Table 9 - Roll Rate Performance

Deflection Angle (deg)	Roll Rate (deg/s)
0	0
5	8.32
10	16.64
12	20.00
15	24.60
20	33.28

The shape of the aircraft and location of the hydrogen tanks left only 3 feet of chord that could be deflected. The boattail uses the center span 22 feet, and the cooling system in the leading edge requires the most outboard foot of span to be stationary. The elevons were designed around these geomertric parameters, resulting in each having a 3 foot chord and a 30 foot span (y = 12 to y = 32).

7.3 TRIMMING

The method for trimming ($c_{mcg} = 0$) was based on the method in Nicolai (Reference 2). However, Nicolai suggests neglecting the thrust and drag contributions to the moment, which is not valid for this aircrft. In addition to accounting for the thrust and drag moments, the moment from the additional lift on the boattail was also accounted for. Since c_m is nondimensionalized by qSc, a small c_{mcg} will still give a large pitching moment, and accuracy in c_{mcg} is important.

7.3.1 SUBSONIC TRIM

The aircraft was trimmed for the following flight conditions: c_L = 0.3, c_D = 0.075, M=0.4, α = 10 , h=5000 ft, a = 1097 ft/sec, ρ= 0.002048 sl/ft^3, Thrust= 76,296 lbs. These parameters resulted in c_{mcg} = -0.00058, or a nose down moment of 64,011 ft lbs. Deflection upwards of the inboard 11 feet of the elevons by 1.85 degrees results in no net moment about the CG.

7.3.2 TRIM AT CRUISE

The following parameters were used in the hypersonic analysis: c_L = 0.036, c_D = 0.00554, M=6, h=100,000 ft, ρ = 0.000032114 sl/ft3, a = 1003 ft/s, Thrust= 21,081 lbs, and the boattail adds 5 % to the lift. The center of pressure will move aft with the increase in Mach number, resulting in a different value for c_{mo}. Wind tunnel tests are necessary for accurate predictions for this configuration since an established airfoil is not used. The moment coefficient around the CG is equal to c_{mo} - 0.001005. Once c_{mo} is known, trimming without changing the optimized lift to drag ratio will be an even more difficult problem.

7.4 TAKEOFF ROTATION

Rotation around the main landing gear to takeoff angle of attack proved to be a difficult problem. The moment about the main gear at takeoff speed for ground roll angle of attack is over a million foot-pounds nose down. Neither trailing edge flaps or elevators could generate enough moment to lift the nose. Leading edge devices interfere with the cooling system and are not usable. Instead, the nose gear strut will telescope to lift the nose to 10 degrees as the aircraft reaches takeoff speed. See the Landing Gear section of this report for further information.

7.5 STABILITY DERIVATIVES

The subsonic stability derivatives were calculated from methods in Nicolai (Reference 2), USAF DATCOM (Reference 32), and Roskam (Reference 30). Parameters used in the calcuations are as follows: M=0.3, c_L=0.3, c_D = 0.075, leading edge sweep angle = 70°, anhedral angle = 20°, α = 10°, weight = 169,800 lbs, thrust = 76,296 lbs, engines canted at 5.56°. Table 10 gives the derivatives, their values, and when designated the required sign for stability.

Table 10 - Static Stability Derivatives

Derivative	Value (1/rad)	Stable Sign
$C_{m\alpha}$	-0.1104	-
$C_{m\dot{\alpha}}$	0.0831	
C_{mq}	-0.2240	
$C_{L\alpha}$	2.58	+
C_{Lq}	1.0591	
$C_{D\alpha}$	0.7371	
C_{Dq}	0.2167	
C_{Du}	0.0	
C_{xtu}	0.130	
$C_{L\delta e}$	0.394	
$C_{m\delta e}$	-0.161	
$C_{l\beta}$	-0.1004	-
C_{lp}	-0.1031	
$C_{l\delta a}$	0.0258	
$C_{n\beta}$	0.2003	+
C_{nr}	-0.1190	
$C_{n\delta r}$	0.1217	
$C_{y\beta}$	-0.0844	
C_{yp}	0.4781	
C_{yr}	0.0	

7.6 STATIC STABILITY

Static stability is defined by 3 derivatives: $c_{m\alpha} < 0$ (longitudinal), $c_{l\beta} < 0$ (lateral), and $c_{n\beta} > 0$ (directional). From the values in Table 9, these requirements are met; the aircraft is statically stable. While static stability is a necessary condition for dynamic stability, it does not insure dynamic stability or controllability.

7.7 DYNAMIC STABILITY

The dynamic stability analysis was limited to solving Roskam's approximations (Reference 30) of each mode to see if the aircraft is dynamically stable; that is, the real part of each root was negative. Table 11 shows the roots for each mode. The approximations assume steady, level, sticked fixed flight. No attempt was made to augment the handling qualities of this conceptual design.

Table 11 - Dynamic Sstability Roots

Mode	Root
Spiral	-0.00925
Roll	-0.02185
Dutch Roll	-0.01931 +/- i(0.2808)
Phugoid	-0.0367 +/- i(0.1061)
Short Period	-0.6573 +/- i(i(0.5014))

The short period mode should have complex roots. Since it does not, there must be a problem within the dynamic derivatives, probably caused by a disproportionally large values for the Z terms. While most of the dynamic derivatives are less than unity, $Z_{\delta e}$=83.414 and Z_{α} = -530.33.

The moments of inertia were found using full scale solid modelling on a CAD system, and are very large, as shown in Table 12.

Table 12 - Inertial Constants

Moment/Product	Value (x 10^6 sl/ft^2)
I_{xx}	38.79
I_{yy}	95.34
I_{zz}	129.81
I_{xy}	0.0
I_{xz}	6.98
I_{yz}	0.0

8. WEIGHT BREAKDOWN

The weight breakdown was obtained combining the output of the WAATS program and data obtained from in depth research into particular areas. Valid weights for the engines, inlet, environmental protection, and insulation were obtained by separate research other than the WAATS program. Since the aircraft did not have a conventional configuration, obtaining valid weights using the program was a challenge. The aircraft was modelled as a lifting body. In doing so, all the dimensions for the aircraft were entered as dimensions of the body. This modelling gave a structural body weight of 42,935 pounds. This value seemed reasonable given the size and configuration of the aircraft.

The aircraft also used a dual fuel combination of JP-X and liquid hydrogen. This made obtaining the weight of the fuel tanks using the WAATS program a challenge also. The aircraft was assumed to have only non-cryogenic fuel to obtain data on the JP-X fuel tank weight, and then assumed to only carry cryogenic liquid hydrogen to obtain the cryogenic tank weight. In doing this, a weight breakdown for the two different types of tanks were obtained. Once again, the insulation weight was obtained from previous research as described in this report.

The landing gear weight given by WAATS was simply a function of the gross takeoff weight. At no time was the gross takeoff weight determined by WAATS, in order to correctly design the landing gear, the program was run for the case of all cryogenic fuel and then all noncryogenic fuel. By assuming a dummy value of

JP-X fuel weight equal to the real value of the liquid hydrogen plus the JP-X, a proper gross takeoff weight was determined which in turn gave the proper landing gear weight.

The amount of fuel required is a function of the dry weight, and the dry weight is in turn a function of the fuel required. As the amount of fuel increases, the landing gear weight to support the extra weight increases as do the tank weights to carry the extra volume. To find the point where the dry weight and amount of fuel required match, a cross plot was constructed as in Figure 36. By varying the amount of fuel required in the WAATS output, the corresponding dry weights were obtained. This produced the line marked WAATS output on Figure 36. Then in the same manner, the fuel weight analysis program was run, varying the input dry weight of the aircraft determined the different fuel requirements. The line marked fuel weight analysis was obtained. Where these lines crossed gave the proper dry weight needed to carry the needed fuel and vice versa. A reduction for advances in composites and other materials was assumed at 15% of the dry weight. The results of the aircraft weight breakdown can be seen in Table 13 .

Table 13 - Breakdown of Aircraft Weights

System	Weight (lbs)	
Body Structure		42,935
Basic	31,626	
Secondary	11,096	
Trust Structure	214	
Environmental Protection		7,687
Landing Gear		3,977
Engines		19,233
Engine Mounts		9
JP-X Fuel Tanks		1,035
H2 Fuel Tanks & Insulation		11,109
Inlet System		12,000
Aero Control Surfaces		1,386
Power System	2,420	
Electrical	1,466	
Hydraulic/Pneumatic	955	
Avionics		4,869
TOTAL (minus 15% for advances)		90,661
Payload	2,500	
Crew	440	
JP-X Fuel	40,924	
LH_2 Fuel	36,854	
TOTAL GROSS WEIGHT		171,379

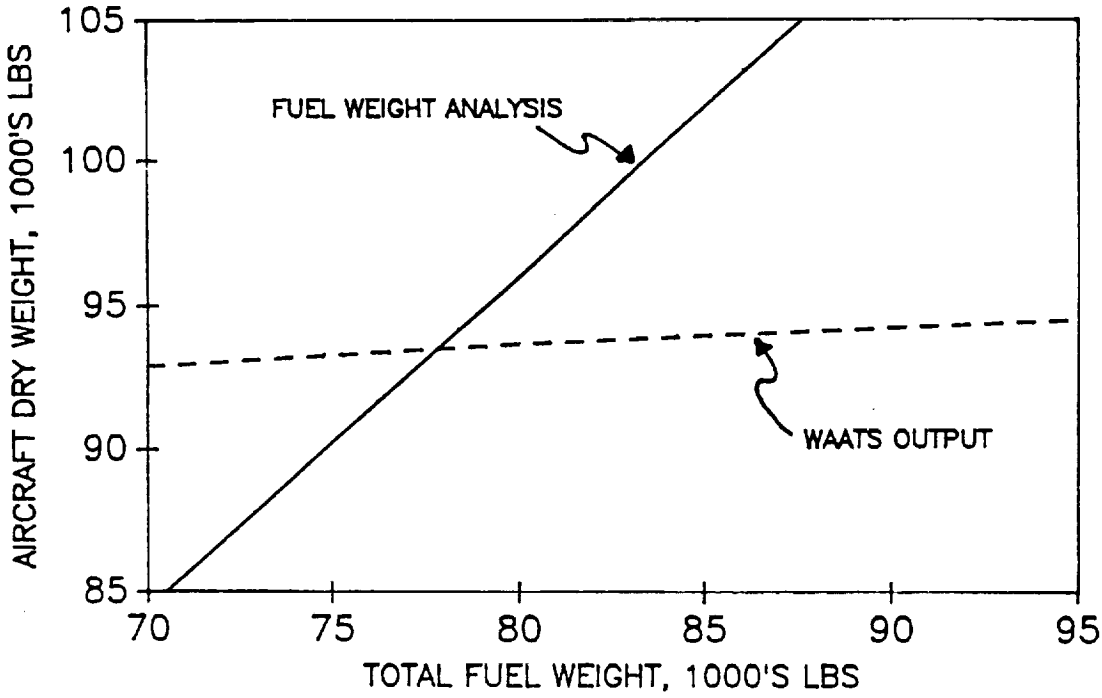

Figure 36 - Weight/Fuel Cross Plot

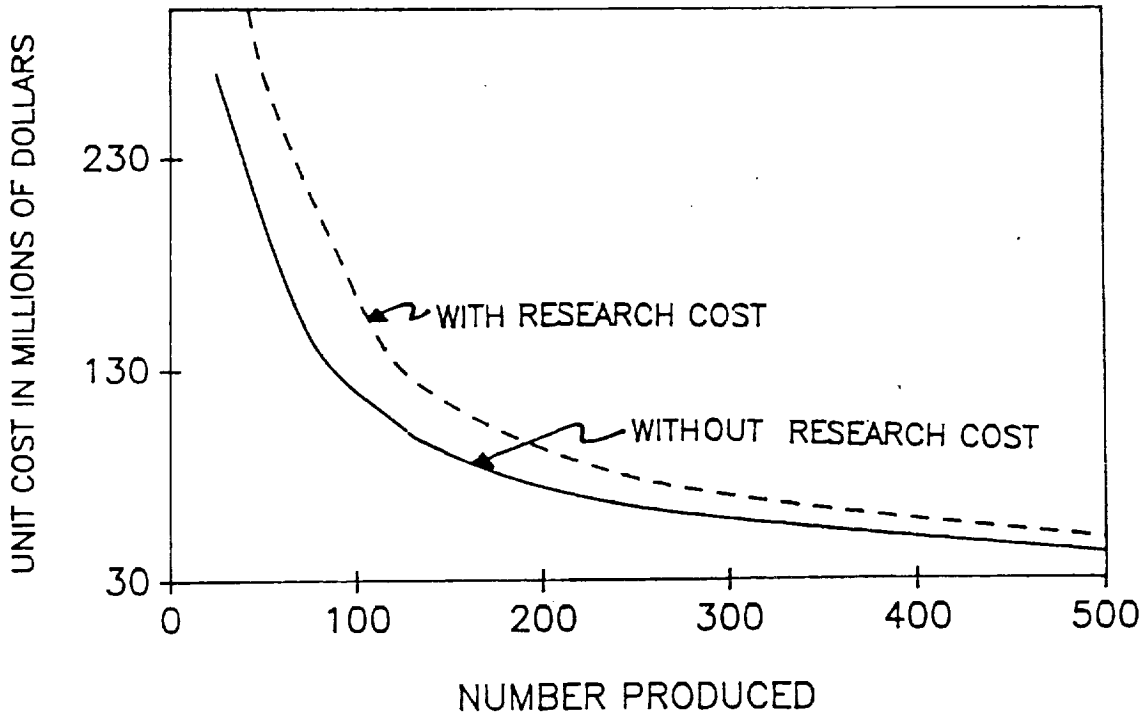

Figure 37 - Unit Cost vs Number Produced

9. AIRCRAFT COST AND D.O.C. ANALYSIS

The cost analysis was based on a method empirically derived from the costs of previously built aircraft. Since the method outlined in Reference 2 has no means of estimation of research costs, it was arbitrarily assumed to be 40% of the total development, testing, and evaluation cost of the aircraft. This cost of 3.5 billion dollars could go up or down according to the amount of prior research performed by private and governmental institutions.

One of the biggest questions is how many of the aircraft could be sold, and therefore built. By varying the number of aircraft produced, a cost versus number produced plot can be obtained as in Figure 37. The graph is plotted with and without the research costs added in. The cost is also based on the production of 4 test aircraft. The cost per aircraft reduces sharply for the first 100 or so aircraft, and then begins to taper off. If an average tangent line is drawn, it intersects the curve at 130 production aircraft. This is the point where a detailed breakdown in cost is presented in Table 14. It is interesting to note that the total cost of manpower and materials to build 130 production aircraft is less than a total cost of research, development, testing, and evaluation.

Table 14 - Breakdown of Aircraft Cost

RESEARCH & D T &$ E		COST ($x10^6$ $)
Research		3,500
D T & E Costs:		
Airframe Engineering		2,057
Development Support		2,371
Flight Test Aircraft		363
Engines & Avionics	37	
Manufacturing Labor	232	
Materials & Equip.	60	
Tooling	4	
Quality Control	30	
Flight Test Operations		406
Profit (10% of subtotal)		520
TOTAL		9,217
PRODUCTION		
Engines & Avionics		909
Manufacture & Labor		1,207
Materials & Equip.		941
Sustaining Engineering		1,833
Tooling		1,469
Quality Control		157
10% Profit		651
TOTAL		7,167
TOTAL COST		16,384
COST PER AIRCRAFT (130 produced)		126

In order to fly the aircraft in a commercial type environment an assessment of the direct operating costs of the aircraft is essential. The analysis is again based on a aircraft cost of 126 million dollars and a production run of 130 aircraft. Producing 130 aircraft was chosen because at that point, the curve in Figure 37 starts to level off, thereby maximizing marginal revenues for a minimum number of aircraft produced. A salvage value of 15% of the purchase price was used with a depreciation period of 14 years. These are standard values for today's subsonic commercial transport aircraft. The avionics and other highly technological devices used

on this aircraft could possibly increase the salvage value considerably.

The utilization of the aircraft is assumed to be 1500 hrs/yr or 2 flights a day 365 days per year. The price of hydrogen was assumed to be $3.00/gal. Currently, $3.00/gal is very optimistic. With increased usage in the future, the price will drop making this estimate more reasonable. A summary of the fixed parameters of the analysis is presented in Table 15.

Table 15 - Direct Operating Costs Fixed Parameters

Aircraft Purchase Price	$126 mil
Salvage Value	$18.9 mil
Depreciation Period	14 yr
Load Factor	100%
Number of Seats	10
Stage Length	5178 mi
Block Time	2.29 hr
Block Speed	2256 mph
Utilization	1500 hr
Fuel Price	
H2	$3.00/gal.
JP-X	$1.00/gal.

The direct operating costs breakdown is presented in Table 15. The cost per revenue-seat-mile is $4.00. This price is quite high as compared to subsonic widebody commercial jet in use today. The cost per revenue-seat-mile for subsonic aircraft is about 30 cents for first class seating. At $4.00, the cost per

revenue-seat-mile would put the price of a ticket out of reach of most middle class passengers. But, a corporation or governmental leaders may feel that their saved time in travel is worth the extra cost. This would make the cost of $4.00 per revenue-seat-mile not as unreasonable as first thought. Extensive use of liquid hydrogen as a fuel will eventually bring the cost below $3.00/gallon, this would reduce the cost per revenue-seat-mile below $4.00.

Table 16 - Direct Operating Costs

Fixed Costs	Cost (mil)
Insurance	2.25
Depreciation	7.65
TOTAL	10.17
Variable Costs	
Landing Fees	90
Maintenance	8,750
Crew	1,500
Fuel Cost	74,000
TOTAL	84,340
Total Cost of Operation($/hr)	91,120
Cost per Mile	$40.00
Cost per Available-Seat-Mile	$4.00
Cost per Revenue-Seat-Mile	$4.00

10. SYSTEMS

10.1 PASSENGER ACCOMMODATIONS

The layout of the pressurized passenger cabin is shown in Figure 38. Ten seats are spaced into five rows with a 3 ft. wide aisle in the center. Seats are comfortable and spacious, with 1.75 ft of leg room between rows. Each seat can pivot 90 degrees toward the centerline of the cabin, thus turning the cabin into a conference room. A 3.5 ft^3 refrigerator, a lavatory, and 2 storage areas for luggage are also provided. Since aerodynamic heating at Mach 6 makes cabin windows impossible, a view screen showing a fiber-optic display of the outside world will be installed at the front of the cabin so that the passengers can "see" their take-off and landing.

Each seat is designed to serve as both a comfortable place to relax during the trip and as an efficient work station. A lap desk can be pulled up from next to the right leg of the seat and folded over the occupant's lap. A 110 volt outlet is provided in the left armrest for those who wish to use their laptop computers. The right armrest holds a cassette tape recorder/player with headphones. The armrest away from the cabin aisle has a drink holder. Telephone service via satellite link will also be possible.

TOP VIEW

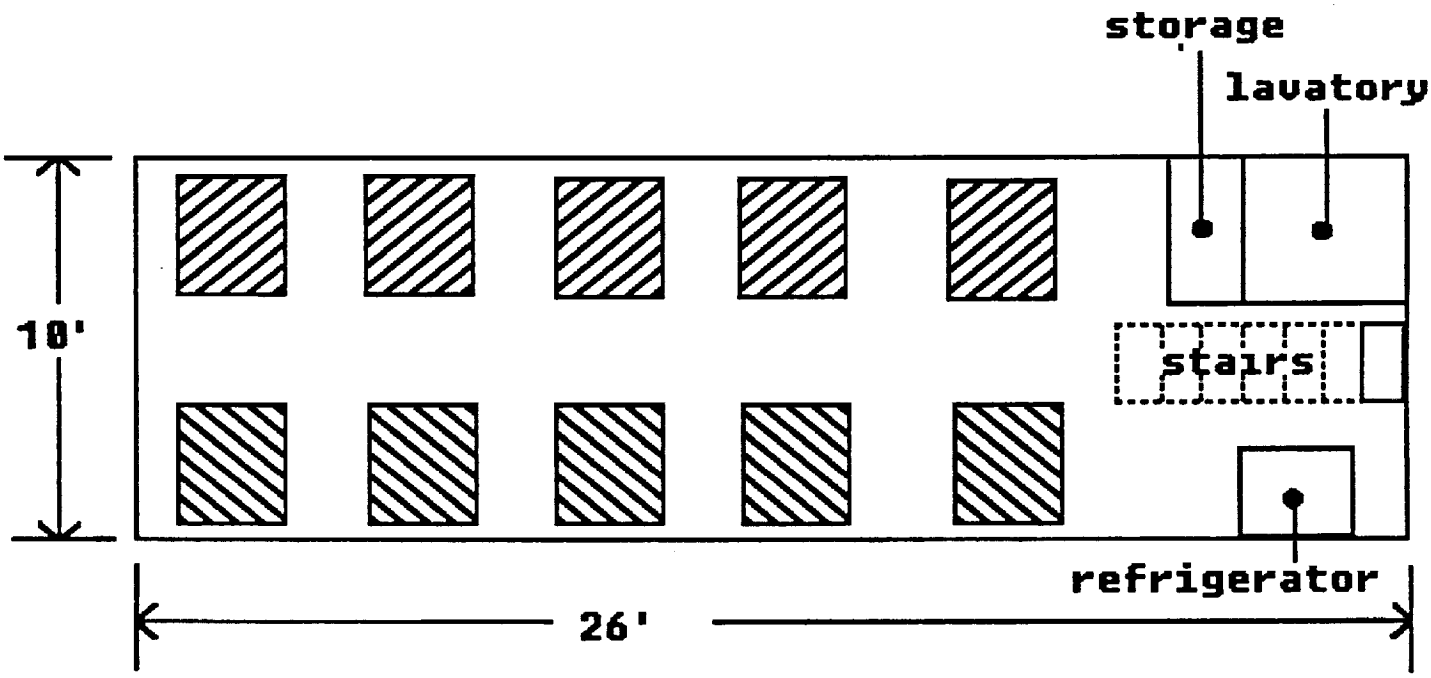

FRONT VIEW

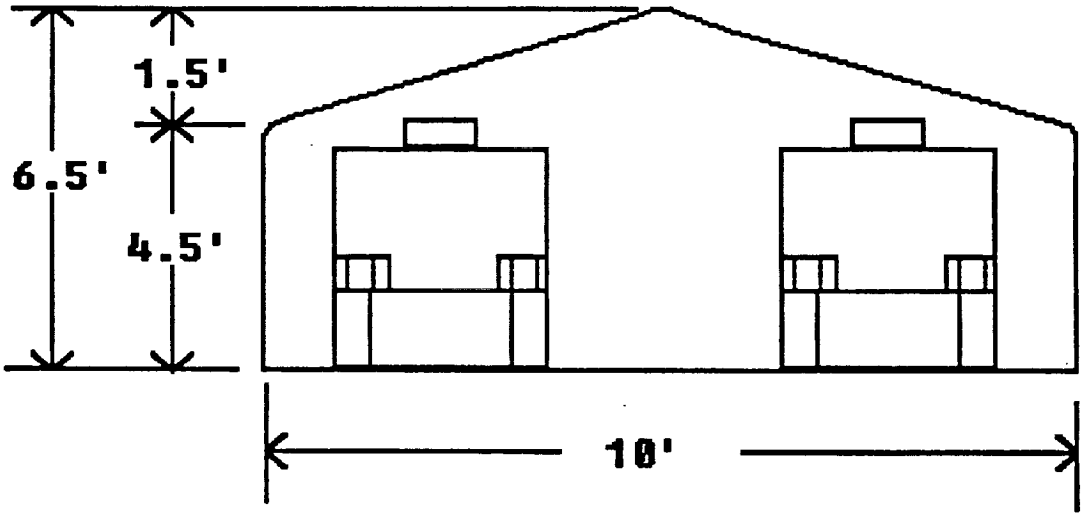

Figure 38 - Cabin Layout

10.2 LANDING GEAR

The landing gear assemblies consist of one single bogie nose gear and two double bogie main gears. The placement of the landing gear assemblies was done to ensure ground stability. The main gears were placed 14 feet from the rear of the aircraft to enable it to rotate up to 15 degrees on takeoff, before the trailing edge makes contact with the runway surface. The placement of the nose gear was originally determined by calculating the distance from the nose of the aircraft to the point where the body was large enough to house the retracted gear. Once these positions were determined, the ground stability criteria, in Reference 24, were used to calculate the lateral position of the two main gears. Having determined the positions of the landing gears, the forces acting on each gear was calculated and used to find the equivalent single wheel load (ESWL) for each gear. Then the pressure and approximate size of the tires were found, in Reference 24, and used to determine the spacing of the two dual wheels and the wheel base of the dual tandem undercarriage. The shock absorbers were then sized using the above information. The footprint and the dimensions of both the nose gear and the main gear can be found in Figure 39. The total length of each gear was determined by calculating the distance from the ground to the bottom of the aircraft and adding two feet. At this point it was determined that there was no way to rotate the aircraft by aerodynamic means for takeoff. Because the aircraft could not be rotated by aerodynamic means, a new system was devised. The system consists of a nose gear that

telescopes out to a length of 17 feet. With the nose gear extended to this length the aircraft is forced to a positive angle of attack. The nose gear retracts forward and the two main gears retract in toward the center line of the aircraft. Because of the length of the landing gears, ways to shorten them as they retracted were studied. The current system, for both the nose gear and the two main landing gears, consists of gears that telescope as they retract into the aircraft. The nose gear is normally 11 feet in length, it extends to 17 feet to force the aircraft to a positive angle of attack for takeoff, and collapses to a length of 7 feet for storage (Figure 40). The two main gears are 11 feet in length and collapse to a length of 7 feet for storage (Figure 41). All the information on the landing gears and the tires can be found in Table 17.

Table 17 - Landing Gear Systems

GEAR	MAIN	NOSE
Number	2	1
Type	twin tandem	tandem
Height (ft)	11	17.5
Distance to center of gravity (ft)	26	23
Distance to center-line (ft)	20	0
SHOCK ABSORBER		
Type	oleo-pneumatic	oleo-pneumatic
Static deflection (in)	5.4	4.5
Stroke (in)	17	12
Diameter (in)	8.5	6.5
TIRES		
Diameter (in)	40	40
Width (in)	14	14
Inflation pressure (psi)	175	180
Lateral spacing (in)	25	22.5
Longitudinal spacing (in)	48	0.0
Features	nitrogen filled	chine nitrogen filled

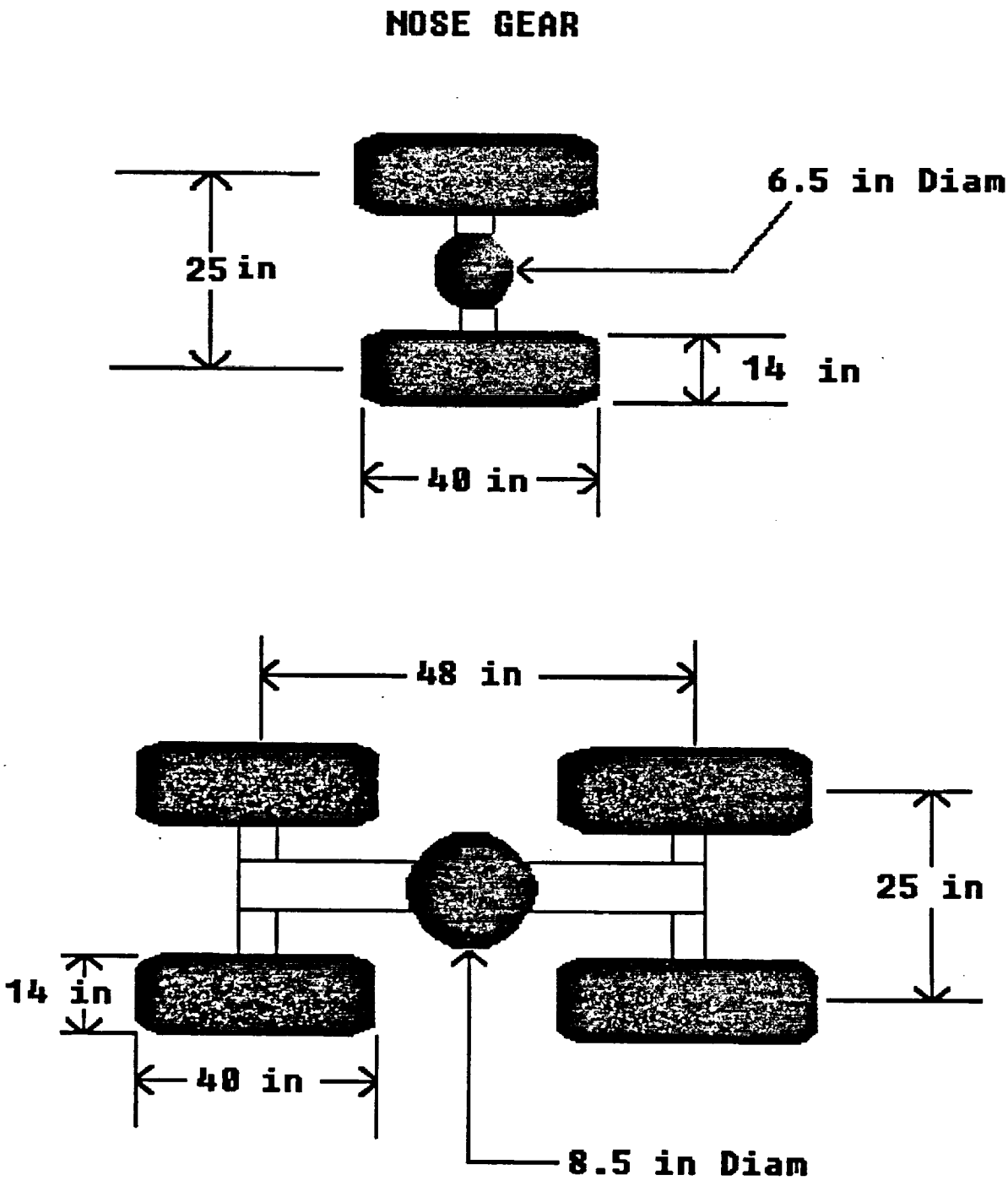

Figure 39 - Landing Gear Footprints

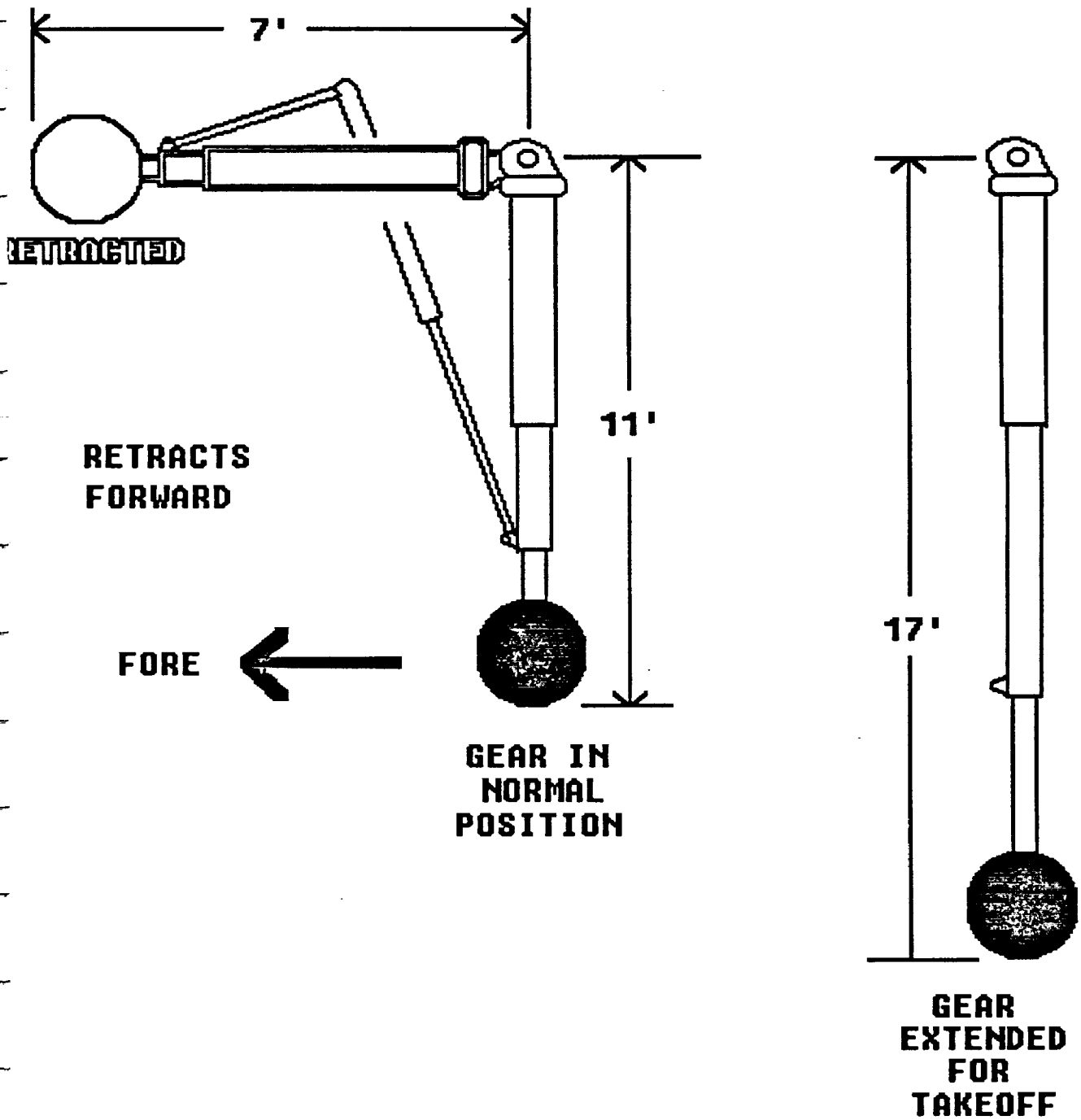

Figure 40 - Nose Gear Schematic

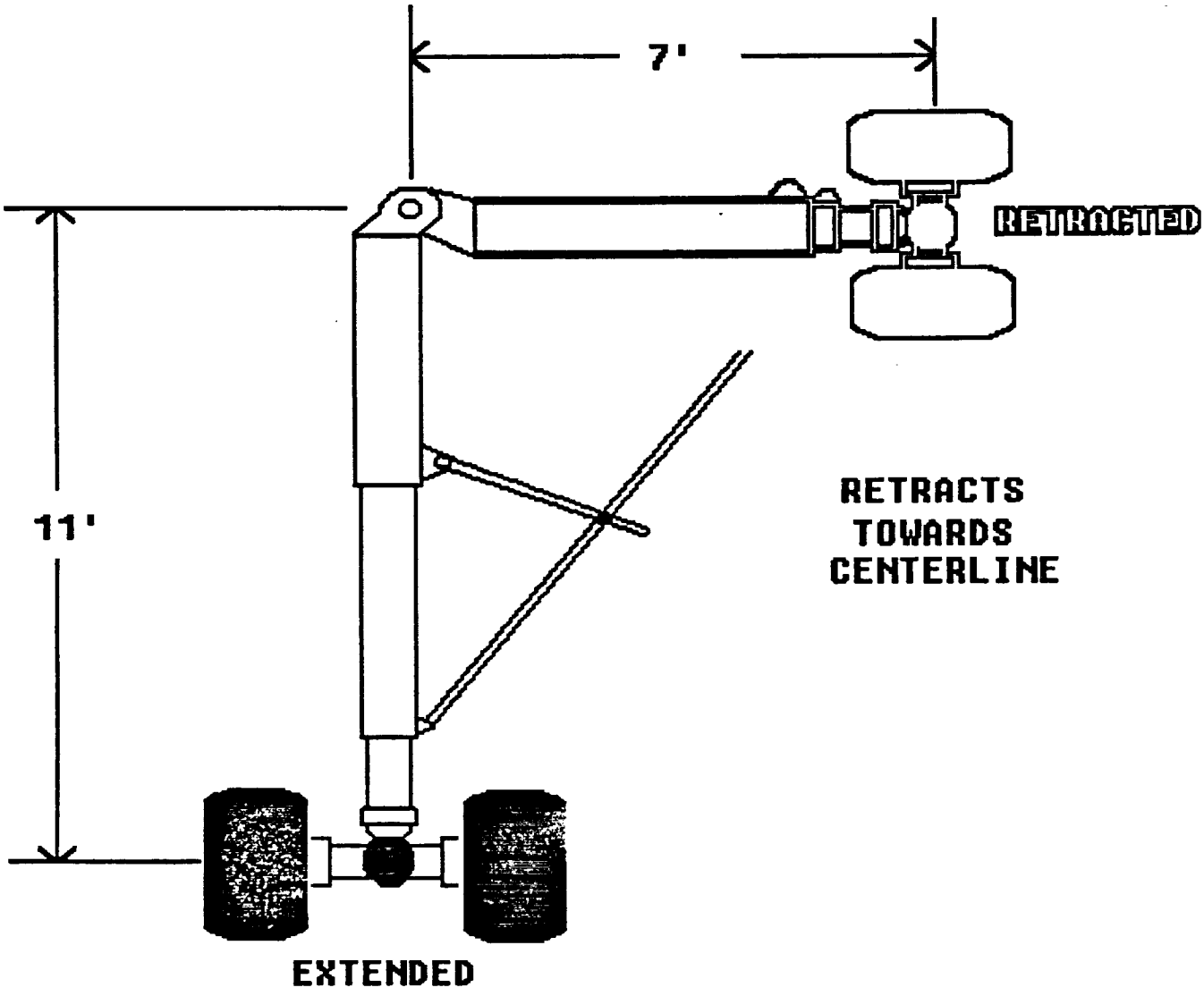

Figure 41 - Main Gear Schematic

10.3 TANK AND INSULATION SYSTEM

The primary goal of the liquid hydrogen tank insulation system is to minimize the hydrogen boil-off while also minimizing the insulation weight and thickness. One may almost completely insulate the tanks and prevent all boil-off but have such a thick insulation and weight that the system would be impractical. Some boil-off must be allowed, but no more (in weight) than can be prevented by the same amount of weight in increased insulation.

An inert purge gas is used in the area between the tanks and the structure of the aircraft. The gas purge system carries away hydrogen leakage from the system lines, prevents liquification of the surrounding gas on the tank surface (cryopumping), and condensation of water on the tank wall. The purge gas also fills the area with a low conductivity gas which helps with the insulation process.

Since the aircraft has an active cooling system, the tanks have to be insulated from temperatures around 300-400 degrees F. This temperature allows for thinner insulation to be used, reserving the space for other uses.

The three possible insulation systems were a helium gas purge non-sealed fibrous insulation, a nitrogen purge sealed insulation system, and a carbon dioxide frost purge system with a non-sealed fibrous insulation.

The nitrogen gas can only be used for the unsealed insulation because the gas would condense at liquid hydrogen temperatures.

Although the lightest possible would be the foam insulation with a nitrogen gas purge, the system would require an additional tank of nitrogen to be carried on board to supply the nitrogen. The sealed foam insulation has not been proven to be effective over many fillings of the cryogenic fuel tank.

The helium purge system with the non-sealed fibrous insulation would also require a separate tank of helium be carried on board and it weighs more than the nitrogen purge and carbon dioxide frost systems.

The system of choice is the carbon dioxide frost purge insulation. This system doesn't require any separate tank for the carbon dioxide gas. Carbon dioxide is cryodeposited to a maximum thickness in the outer layer of the insulation. As the pressure is reduced from increasing altitude and temperature rise due to aerodynamic heating, the carbon dioxide frost sublimes and fills the cavity between the aircraft structure and the tanks preventing cryopumping, condensation due to moisture, and carries away any hydrogen leakage (see Figure 42).

The fuel tanks are made of titanium and filled at an initial pressure of 17 psi (1.15 atm) with a venting pressure of 25 psi (1.7 atm). These pressures are from the hydrogen gas within the tank, therefore no external pressure device is needed. The weight estimate is for the outside skin only and does not include fuel line, hydrogen pump, or inside baffle weights.

A break down for the insulation and tank weights is shown in Table 18.

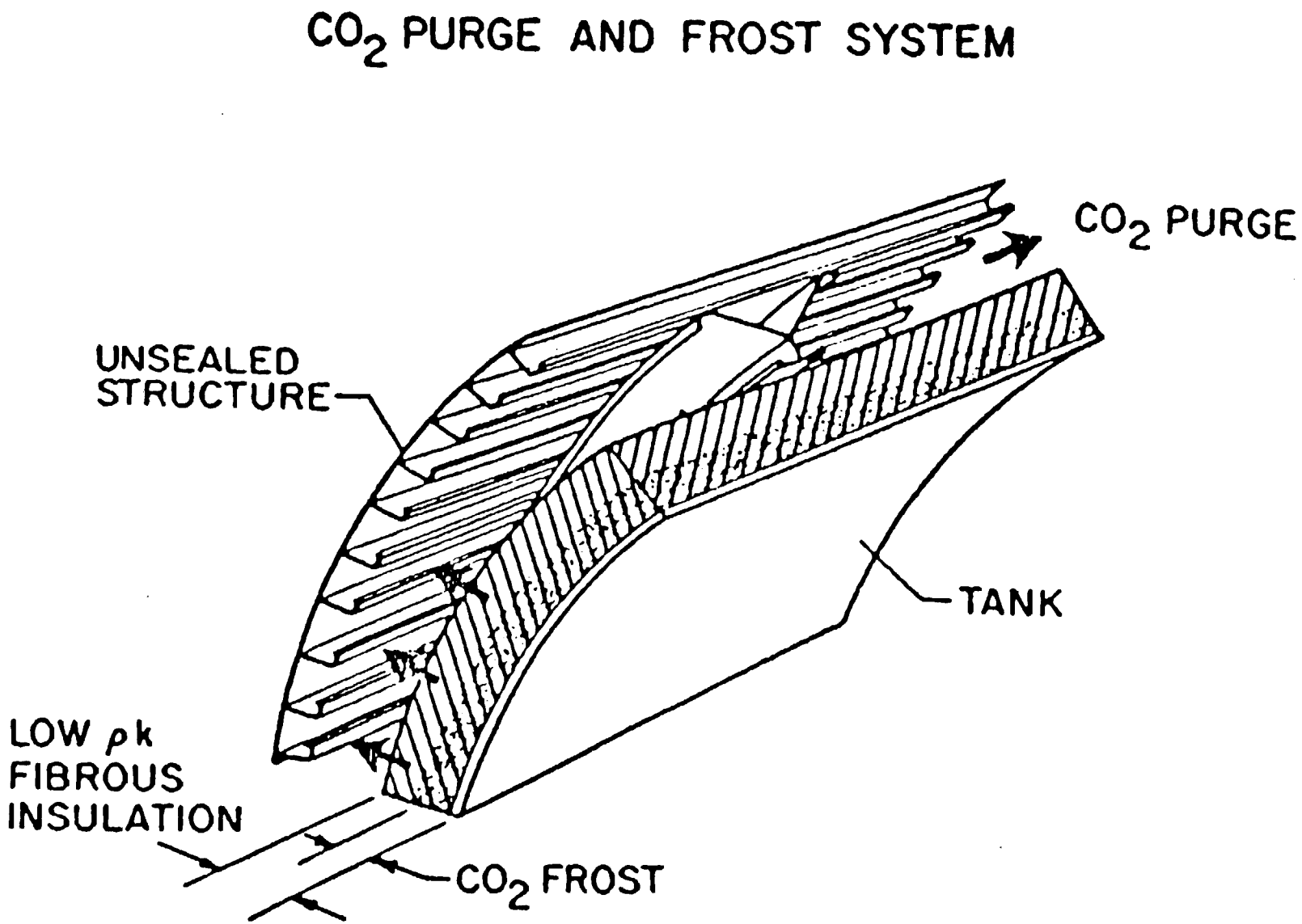

Figure 42 - CO_2 Purge and Frost System

Table 18 - Fuel Tank Specifications

Tank Material	Titanium
Tank Pressure (initial)	1.15 atm
(venting pressure)	1.70 atm
Exposure Time (discluding ground hold)	5000 s
Exposed Area	4800 ft^2
Insulation Type	CO_2 Frost System
Insulation Thickness	1 in
Weights	
Boil-Off (in flight)	864 lbs
(30 min ground hold)	750 lbs
Insulation System	6,816 lbs
Tanks	4,800 lbs
TOTAL	13,200 lbs

10.4 COOLING SYSTEM

The only cooling systems considered were ones that would allow the skin temperature level to be such that a viable skin material can be used. There were three different cooling systems evaluated for this project. They are transpiration cooling, convection cooling using the fuel as a coolant, and convection cooling using a separate coolant and the fuel as a heat sink.

The transpiration cooling system works by injecting a cool fluid directly into the boundary layer through the porous skin. Transpiration is quite effective because it acts as an insulator between the hot air and the surface, greatly reducing the heat flux to the skin. The problem with this is that the coolant is not recirculated, but lost after it is used, thus the total amount of coolant used during the mission must be carried. This can mean as

much as 20,000 lbs of coolant alone. Due to this large weight and the problems of the actual distribution system, we judged transpiration cooling as unacceptable for our mission.

This means that either of the convection systems will be used. The advantages to using the fuel as a coolant are that, a heavy heat exchanger is not needed and as long as the fuel is already on board, why not use it. The disadvantages are that the distribution system and pumps would have to be more complex and heavy to allow for colder temperatures and higher pressures, and pumping fuel all over the aircraft is potentially dangerous. Using a separate coolant has the advantage in that it can be a liquid at normal temperatures and be denser than the fuel to allow for lower flow rates. Basically the difference is the weight of a heat exchanger versus the weight of a more complex distribution system. Based on research we did we came up with a cooling system that incorporates a separate coolant is slightly lighter for our particular mission. This also follows our desire not to pump fuel all over the aircraft.

Now that a specific cooling system has been decided on, the temperature distribution and heat transfer coefficient have to be determined for the aircraft. The leading edge of the configuration needed to be aerodynamically sharp to correctly set up the attached shock system. But how sharp is sharp at Mach 6. Due to this problem a leading radius of .125" was chosen because it was deemed the smallest radius that could be effectively cooled in combination with heat shielded leading edges.

All the heat transfer coefficients were calculated assuming

no crossflow effects exist. In all laminar areas heat transfer coefficients were calculated from equations obtained using curve fitting techniques from existing experimental data. Calculation of turbulent heat transfer coefficients was done by using the Von Karman form of the Reynolds analogy in conjunction with Spalding and Chi's skin friction coefficients. No attempt was made to model the transition from laminar to turbulent flow. Once the local Reynolds number exceeded the transition Reynolds number of 500,000 the flow was assumed to be completely turbulent. Assuming no heat conduction through the skin, the local temperature can be found by the local convective and radiative heat balance. The skin temperature distribution for the upper and lower surfaces were found by assuming a worst heating case for each surface. This corresponds to the upper surface parallel to the free stream and the lower surface at an angle of attack of ten degrees. The surface temperature distribution is shown in Figure 43 for these cases. See Appendix D for the methods used to calculate the skin temperature distribution.

Using the temperature distribution given by the above method the surface area can be divided into small finite areas, each with an average temperature. Assuming that no cooling will be used for areas that have an average skin temperature less than 800°F (see Figure 44), a liquid silicon based coolant will be used due to its stability up to coolant temperatures of 400°F (see Figure 45). Coolant flow rates, fuel flow rates, and system weights can be calculated by a numerical method outlined in Appendix D. These values are outlined in Table 19:

Table 19 - Cooling System Specifications

Weights	
Liquid Silicon	1103 lbs
Distribution System	1655 lbs
Heat Exchanger	3279 lbs
Pumps	1200 lbs
TOTAL	7687 lbs
Coolant Flow Rate	6005 lb/hr
Fuel Flow Rate	49,162 lb/hr

10.5 MATERIALS

Suitable materials that can take these temperatures must now be evaluated. The outside skin material must have a high emissivity along with good high temperature characteristics. An alloy of 80Ni-20Cr is the best suited for this purpose, due to its high emissivity at high temperatures (ϵ = .89). The materials on the nose cap and leading edges must have good thermal loading and reusability characteristics. Carbon-carbon composites meet the temperature requirements, but due to oxidation erosion they must be replaced every flight. A JTA composite (a carbon composite that contains traces of zirconium, silicon, and boron) forms a protective coating on the outer surface as it oxidizes, thus greatly reducing the erosion and increasing the thermal loading life of the composite. The JTA composite was estmated to last 15 missions, as opposed to the 1 mission for the carbon-carbon composite, before it would need replacing. For this reason a JTA composite was chosen for the leading edge and nose cap materials.

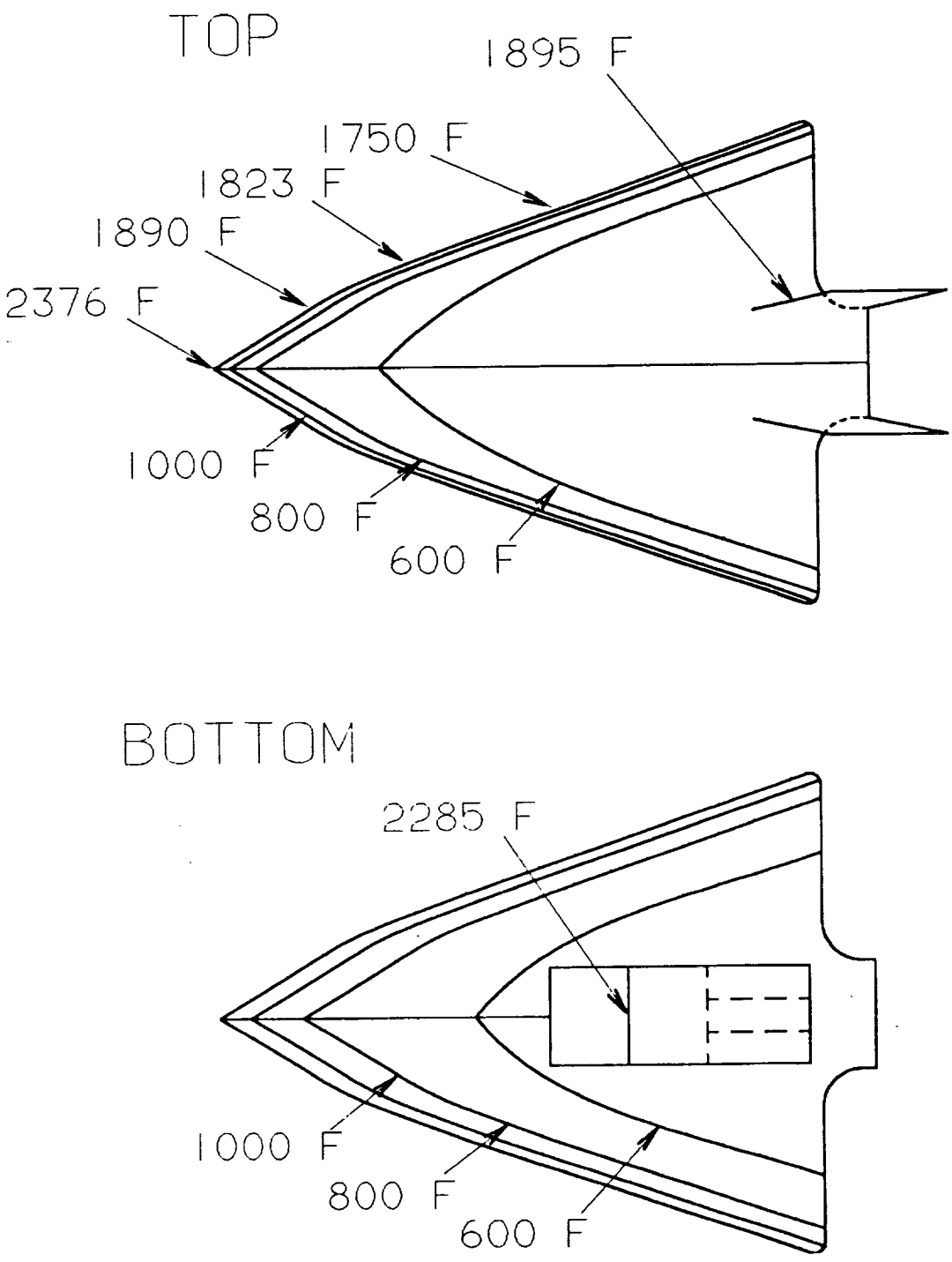

Figure 43 - Skin Temperature Distribution

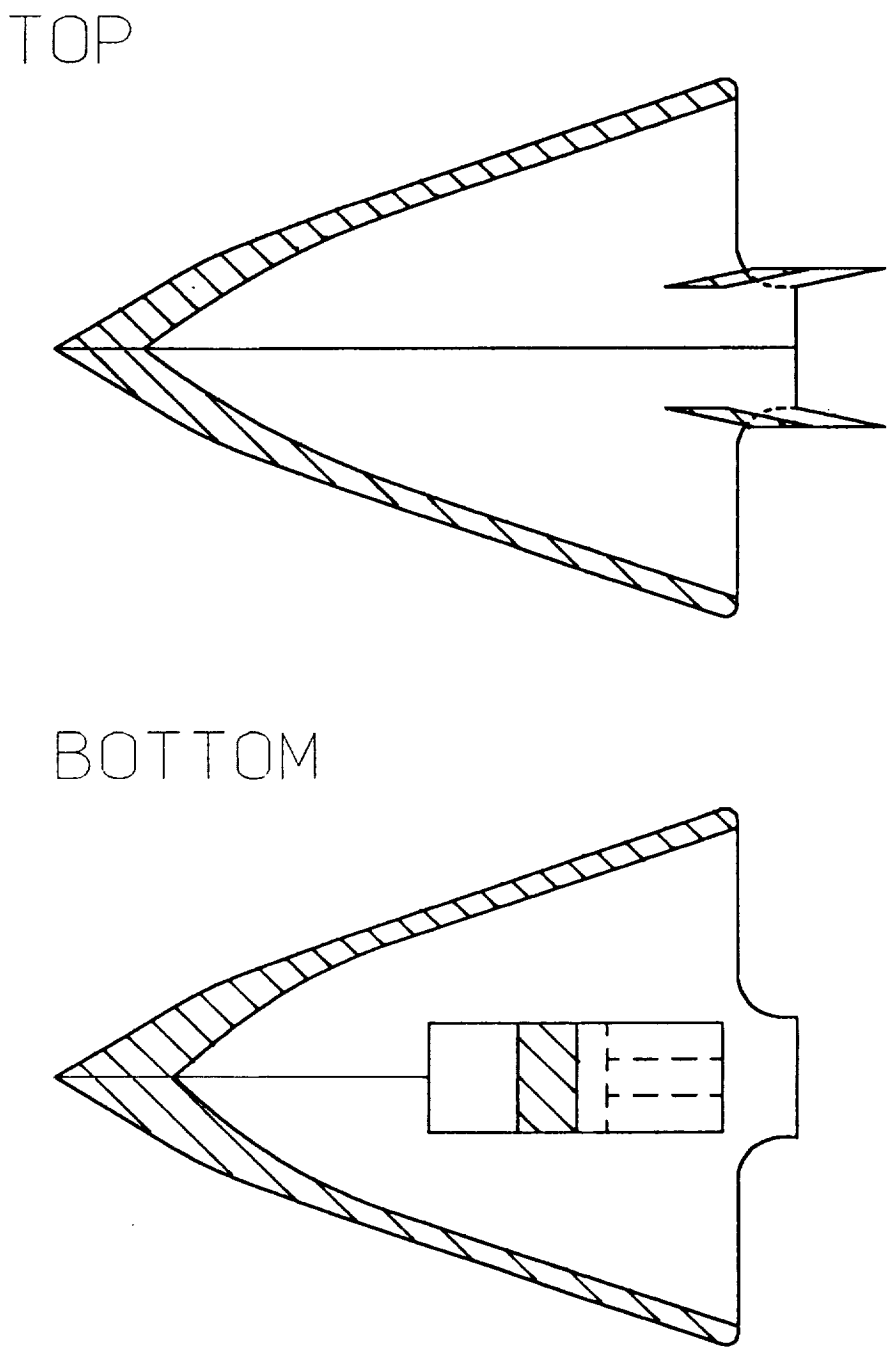

Figure 44 - Cooling System Placement

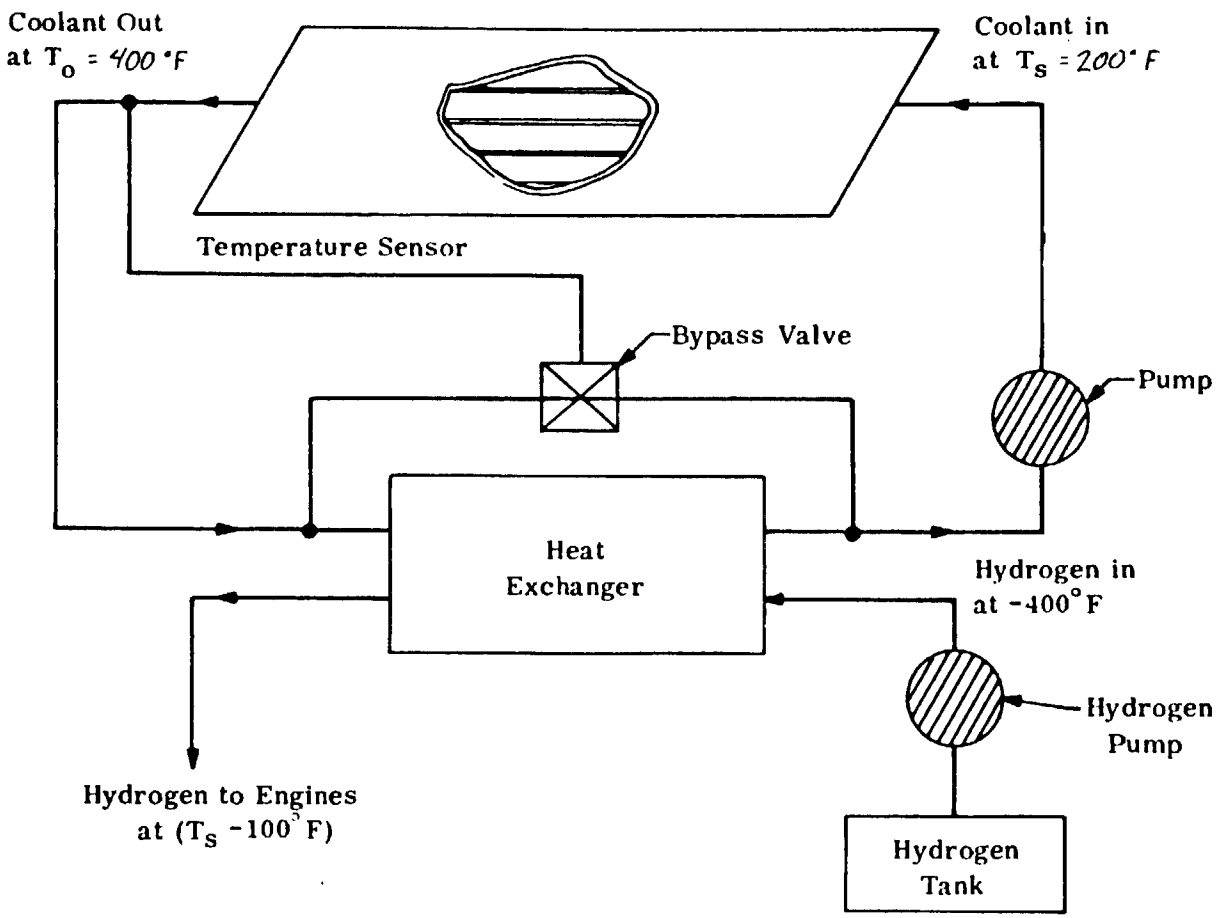

Figure 45 - Cooling System Schematic

The nickel alloy exhibited good thermal protection characteristics, but was lacking as a structural material with a lower yield strength and strength-to-weight ratio than a titanium alloy. For this reason, the nickel alloy needed to be bonded to a structural titanium alloy.

The process to be used was explosive welding. (see Figure 46) This process joins the two (or more) metals together on a molecular level, producing a bond even stronger than the original materials. Explosive welding produced long-lasting bonds at relatively low cost. (Reference 33) Due to the high emmisivity of the nickel alloy, the active cooling system needed to cover a 75% smaller area than if only titanium were used on the outer skin. For this reason, a metal composite skin was chosen for this project. Through an initial thermal expansion analysis, the thermal stresses created during atmospheric heating were judged to be acceptable. The skin was modelled as a microstructural isotropic layer of three thin metal foils. For longer life and durability, a thin layer of niobium must be sandwiched between the nickel and titanium alloys.

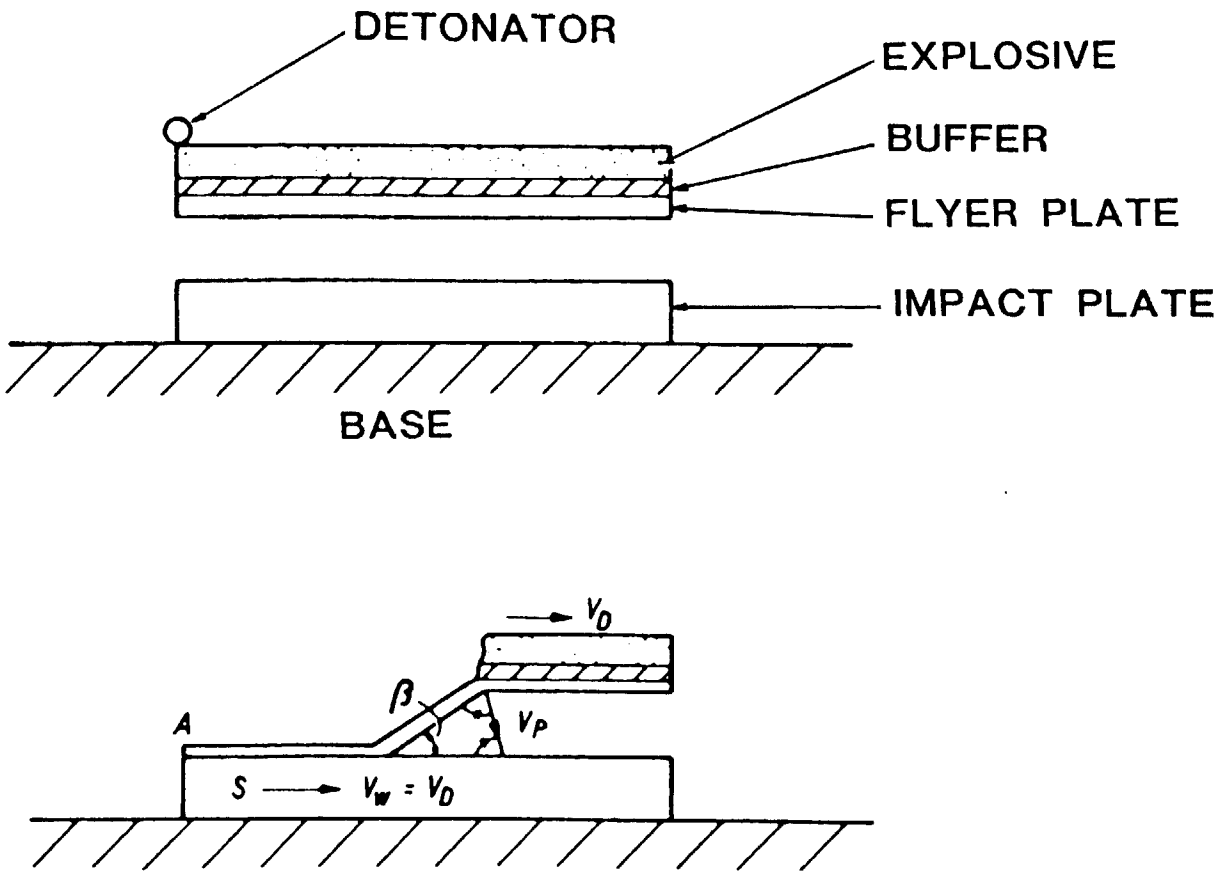

Figure 46 - Explosive Welding Schematic

11. CONCLUSIONS

During the course of this project, a conceptual hypersonic business jet was examined. The main areas of concentration include: aerodynamics, propulsion, stability and control, mission profile, and atmospheric heating.

We believe that a waverider design in combination with efficient turbofanramjets, utilizing a dual fuel scheme, turned out to be most feasible design from all the different designs examined.

As a direct result from this project there are specific conclusions that can be drawn. These include:

1. The 6500 nautical mile range of the proposed aircraft includes most of the world's flight routes (including the long transpacific routes)
2. The waverider concept is very efficient for crusing at Mach 6 and at high altitudes.
3. Atmospheric heating can be adequately dealt with using a combination of active (convective) and passive (radiative) cooling system.
4. The aircraft is statically stable, but an augmentation system will be needed.
5. Although the aircraft is expensive, an executive who values his or her time and makes frequent long distance trips could easily be sold on the idea of such an aircraft.

In addition a few recommendations for future effort are listed:

1. An in depth study of the handling qualities of the dynamic modes needs to be accomplished in order to determine the extent of augmentation.
2. An airframe design and stress analysis needs to be done to determine the mechanical and thermal loads, load paths, and required strengths of structural members.
3. Accurate subsonic and off-design supersonic testing needs to be carried out in order to determine the aerodynamic qualities of waveriders through all flight regimes.

Assuming the successful completion of the recommended studies, a relatively large scale model should be fabricated and experimentally evaluated under conditions similar to those experienced in hypersonic flight. This evaluation would give more realistsic weight and cost estimates, along with accurate heat transfer and aerodynamic data applicable to this specific project.

Appendix A

APPENDIX A - COMPUTER PROGRAMS FOR MISSION PROFILE AND PROPULSION

A.1 PROGRAM PROFILE.FOR

The fuel burned depends upon the aircraft gross weight, engine performance through the mission profile, and drag. In the program, the profile is separated into five stages:

1. TAKEOFF
2. CLIMB ON MAX. AFTERBURNER
3. CRUISE
4. DESCEND ON MINIMUM POWER
5. LOITER

Climb and descend are divided into 10,000 ft. intervals. The first interval is 0-5000; the second, 5000-15000; the third, 15000-25000, etc. At each interval, the program calculates performance based on the mean altitude and Mach number. These performance parameters are:

$$\text{THRUST} = W \left(\frac{1/6 + \cos\theta}{L/D}\right) + \sin\theta$$

$$\text{TIME} = \frac{U_2 - U_1}{a}$$

$$\text{DISTANCE} = \frac{U_2 + U_1}{2} * \text{TIME}$$

$$\text{FUEL} = \text{SFC} * \frac{\text{TIME}}{3600} * \text{THRUST}$$

If the thrust required is higher than that available, subroutine ADAPT is called to change the ascent angle and recalculate.

Acceleration through Mach 1 is at a level 1/10 g acceleration.

Cruise and loiter are divided into 20 intervals, with

$$\text{THRUST} = \frac{W}{L/D}$$

Program output is the following:

Fuel burned during mission profile

Climb angles at each altitude

Range

Flight times

A.2 PROGRAM INLET.FOR

This program simulates the performance of the inlet by calculating flow conditions through a series of oblique shocks. No considerations are given to frictional or boundary layer losses.

Inputs:

Wedge angle for each ramp

Ambient conditions

Outputs:

Conditions behind each shock

Coordinates of cowl lip shock intersection

See NACA Report 1135 for details of oblique shock equations.

A.3 PROGRAM NOZZLE.FOR

Essentially, Nozzle.for is a modification of a minimum length nozzle program using the method of characteristics, by modelling the expansion around an expansion surface on top and a slipline on bottom.

Inputs:

Exit Mach

Number of characteristics (n<15)

Nozzle stagnation pressure

Pressure at slipline

Outputs:

Node conditions

Wall coordinates

The program calculates the Prandtl-Meyer angle at the exit and at the slipline. The expansion on top is the difference of these.

Beyond this point, the only difference from a minimum length nozzle problem is the node numbering scheme.

Appendix B

APPENDIX B - MAXWARP DATA

B.1 MAXWARP INPUT DATA

```
WAVERIDER FROM FLOW OVER 1/2 POWER-LAW BODY: M=6, Alt.=100,000 ft

    1       POW-LAW BODY: IGEM   = body geometry:
    0.500                 POWER  = exponent of power-law equation
     .160                 YBL    = slenderness ratio (base ht./l)
   35.0                   LENGTH = length of waverider (m)
    0.05                  ZSL    = power-law body nosetip / length
    1.4      FLOW FIELD:  G      = ratio of specific heats
  288.                    RGAS   = specific gas constant (J/kg/K)
    6.                    MFREE  = freestream Mach number
 1101.71                  PFREE  = freestream pressure (N/m2)
    0.016432              RFREE  = freestream density (kg/m3)
    1       SPACE MARCH:  IFLOW  = compute flow field only (1=yes)
    0.95                  FUDGE  = Courant number for step size
    1                     IC     = print initial conds.? (0,1=yes)
    1                     NDIM   = non-dim results? (0=no,1=yes)
   10.0                   ZPRINT = Z print spacing (meters)
   35.      WAVERIDER:    ACLEN  = aircraft length (m)
    1                     IVISC  = inviscid (=0) or viscous (=1)
    0                     IBL    = bound layer (0=trans)
  611.111                 TWALL  = aircraft wall temperature (K).
    1       CONSTRAINTS:  KSLR   = SLR constraint active?(1=yes)
    0.085                 SLRMIN = min slend ratio (base/length)
    1                     KBOX   = BOX constraint active?(1=yes)
    0.1                   BOXMIN = min box size (semi-span/length)
    1.0                   BOXMAX = max box size (semi-span/length)
    0                     IVOL   = vol constraint active?(1=yes)
    0.                    VOLMIN = minimum volume (cubic meters)
    0.                    VOLMAX = maximum volume (cubic meters)
    1     OPTIMIZATION:   IOPT   = optimize designs?  (0=no,1=yes)
    1                     MIN    = maximize L/D (=1), min CD (=2)
    50                    MLEVEL = max iterations allowed
    1                     MPRINT = # of iterations between output
    0       PROPULSION:   IENGN  = engine-airframe integr(1=yes)
    1         GRAPHICS:   IGRAF  = (0=no, 1=PLOT-10, 2=GENTRY)
    1                     ITRIP  = transition line picture(1=yes)
    1     PRINT SWITCH:   IBASIS = leading edge data  (0,1=yes)
    1                     ILE    = leading edge coords (0,1=yes)
    1                     IVIOLT = violation of constraints(1=yes)
```

B.2 MAXWARP OUTPUT

WAVERIDER FROM FLOW OVER 1/2 POWER-LAW BODY: M=6, Alt.=100,000 ft

---------- FLIGHT CONDITIONS ----------

Mach no.	=	6.00000E+00	
Pressure	=	2.30088E+01	lbs/ft^2
Density	=	3.18849E-05	$slugs/ft^3$
Temperature	=	4.19008E+02	deg R
Dynamic pressure	=	5.79822E+02	lbs/ft^2
Reynolds number	=	6.94612E+07	

---------- GENERATING BODY FOR FLOW FIELD ----------

Base-to-length ratio	=	1.52381E-01	
Length	=	4.00079E+02	ft
Cone nosetip length	=	3.81028E+01	ft
	=	9.52381E-02	(fraction of body length)
Cone semi-apex angle	=	1.96857E+01	deg
Shock wave angle	=	2.37439E+01	deg

---------- AIRCRAFT DIMENSIONS ----------

Aircraft length	=	1.14829E+02	ft
Base height / length	=	8.54562E-02	
Semi-span / length	=	3.93526E-01	
Planform area	=	5.45449E+03	ft^2
Base area	=	4.41280E+02	ft^2

Wetted area (upper surface)	=	5.97204E+03	ft^2
Wetted area (lower surface)	=	5.61310E+03	ft^2
Total wetted area	=	1.15851E+04	ft^2

Aircraft volume	=	1.88234E+04	ft^3
Volumetric efficiency	=	1.29731E-01	

---------- INVISCID AERODYNAMIC FORCES ----------

CLpl = 7.64279E-02	CDpl = 5.80764E-03	CMpl = -2.29927E-02
CLpu = -3.96825E-02	CDpu = 0.00000E+00	CMpu = 0.00000E+00
CLpc = 0.00000E+00	CDpb = -3.21040E-03	CMpb = -2.46802E-03
CLp = 3.67453E-02	CDp = 2.59724E-03	CMp = -2.54607E-02
L/D = 1.41479E+01		

```
------------------ VISCOUS AERODYNAMIC FORCES ------------------

 Local transition Reynolds number                 =  3.23399E+06
 Upper surface transition distance (from l.e.) =  5.34625E+00 ft

CLfl = -1.34739E-04    CDfl =  1.61699E-03    CMfl = -5.94407E-05
CLfu =  0.00000E+00    CDfu =  1.02781E-03    CMfu = -6.10291E-05
CLf  = -1.34739E-04    CDf  =  2.64480E-03    CMf  = -1.20470E-04
CL   =  3.66106E-02    CD   =  5.24203E-03    CM   = -2.55812E-02
L/D  =  6.98404E+00


---------------------- HEAT TRANSFER DATA ----------------------

 Aircraft wall temperature =  1.10000E+03 deg R
```

Appendix C

APPENDIX C - STABILITY AND CONTROL

C.1 CONTROL SURFACE SIZING

C.1.1 VERTICAL STABILIZERS

$(C_{n\beta})_{vs}$ is proportional to V_{vs}, the vertical tail volume coefficient, where:

$$V_{vs} = \frac{l_{vs}\, S_{vs}}{S_{wet}\, b}$$

S_{vs}, the area of the vertical stabilizers, was varied until $(C_{n\beta})_{vs}$ was close to 0.19. As the stabilizer geometry changed, l_{vs}, the distance from the CG to the C_p of the stabilizers, changed also.

C.1.2 RUDDERS (Source: Nicolai, Reference 2)

C.1.2.1 Crosswind TO and landing

$C_n = C_{n\beta}\,\beta + C_{n\delta r}\,\delta r = 0$

where $\beta = 11.5^\circ$, $\delta r = +/-20^\circ$, $C_{n\beta} = .2$

Solving: $C_{n\delta r} = 0.1150.$

$C_{n\delta r} = .9(C_{L\alpha})_{vs}\, V_{vs}\tau$

Solving: $\tau = 0.637$ ($\tau = .64$, from Figure 21.12, Ref 2)

C.1.2.2 Engine out

$$C_n = -\left(\frac{T - D_e}{qSb}\right) + C_{n\delta r}\,\delta r.$$

T = 21,333 lbs thrust for one unagmented engine at takeoff. Center engine causes no sidslip.

D_e = drag of the unstarted engine, approximately 10% of Thrust

q = 100.64 for a sea level takeoff

$\delta r = +/-20^\circ$ max

Solving: $C_{n\delta r} = .00013$

Solving again: $\tau = 0.007$ (This requires very little rudder)

C.1.2.3 Adverse yaw

This passenger jet will not be making the abrupt aileron rolls, therefore this requirement is not addressed.

C.1.3 ELEVONS

C.1.3.1 Roll Control (Source: Roskam, Reference 31)

Geometric parameters:

MAC at elevon location = 66.67, $c_f = 3$, $c_f/MAC = .045$,

$b_f = 30$, $\Lambda = 70^\circ$, $b_i = 12$ ft, $b_o = 42$ ft, $\beta = 0.954$,

$\eta_i = 12/45 = .267$, $\eta_o = 42/45 = .933$

K=.455 (From Figure 11.3, Ref 31)

where

$$\frac{\beta A}{K} = 2.953 \quad \text{(read \& averaged from } \frac{\beta A}{K} = 2,\ 4\text{)}$$

$$\frac{\beta C l_\delta}{K} = 0.265 \qquad \text{(from Figure 11)}$$

$$C_{l_\delta} = \left(\frac{K}{\beta}\right)\left(\frac{\beta C_{l_\delta}}{K}\right) = 0.1265.$$

$$C_{l_\delta} = \alpha_\delta \; C_{l_\delta} = 0.0258$$

where $\alpha_\delta = (1.75)\ (.35)$ (from Figures 10.5-10.6)

For differentially deflected flaps, (left and right):

$$C_l = \left(\tfrac{1}{2}(C_{L\delta})_{left} + \tfrac{1}{2}(C_{L\delta})_{right}\right)\ (\delta_{left} - \delta_{right})$$

$$\delta a = \tfrac{1}{2}(\delta_{left} - \delta_{right})$$

$$C_l = C_{l_\delta}\ \delta_a$$

Solving: $C_{l_{\delta a}} = C_{l_\delta} = 0.0258/rad$

C.1.3.2 Roll Rates (p)

$$p = \frac{L_{\delta a}\ \delta_a}{L_p}$$

where, $L_{\delta a} = \dfrac{qSC_{l_{\delta a}}}{I_{xx}}$ & $L_p = \dfrac{qSb^2 C_{lp}}{2I_{xx}V}$

$$p = \frac{2C_{l_\delta} aV}{bC_{lp}}\ \delta a$$

C.1.3.3 Elevators (Source: Nicolai, Reference 2)

For $\frac{c_f}{c} = .045$ & $\frac{t}{c} = .14$

$$\frac{dCl}{d\delta_f} = 1.75 \qquad \text{(from Figure 9.10)}$$

$$\alpha_{0L} = \frac{-dC_l}{d\delta_f}\,\frac{1}{C_{l\alpha}}\,\delta_f\,K' = 0.5833\,\delta_f\,K'$$

where, K' is a correction factor from Figure 9.9,

and $\frac{cf}{c} = 0.45$ was extrapolated.

Table C1. Results for Full Span Flap Deflection

δ_f (°)	K'	α_{0L} (°)	C_L
10	1.0	-5.83	0.3
20	0.91	-10.61	0.25
30	0.73	-12.78	
40	0.675	-15.75	

From Table C1,

$$\frac{C_L}{\delta_e} = 1.576/\text{rad}$$

and if the full span is deflected between 0 and 20 degrees, for quarter span elevators, $C_{L\delta e} = 0.394$.

C.2 TRIMMING (Source: Nicolai, Reference 2)

An aircraft is trimmed when $C_{mcg} = 0$. The equation that governs trim accounts for C_{mac}, the lift vector moment, the drag vector moment, the boattail lift vector moment, the thrust moment, and the inlet air moment:

$$C_{mcg} = C_{mac} + SM\ C_L + \frac{z}{c}C_D - \frac{x_{bt}}{c}C_{Lbt} + \frac{T_{zt}}{qSc} - (C_{mcg})_{inlet}$$

$C_{m\delta e}$ was found by differentiating both sides of this equation with respect to elevator deflection angle.

C.3 STABILITY AND CONTROL DERIVATIVES

C.3.1 DEFINING CONSTANTS

$$V_{vs} = \frac{l_{vs}\ S_{vs}}{b\ S}$$

$$c1 = 0.724 + b_s + 0.009\ AR$$

$$f1 = (4\pi AR)^{-1}$$

$$e1 = \frac{\tan\Lambda}{\pi AR\ (AR + 4\cos\Lambda)}$$

$$d1 = \cos\Lambda - \tfrac{1}{2}AR - \frac{AR^2}{8\cos} + \frac{6x\ \sin\Lambda}{c\ AR}$$

$$g1 = \frac{AR\ x_b}{2\ c} + 2\left(\frac{x_b}{c}\right)^2 \left(\frac{1}{AR + 2\cos\Lambda}\right)$$

$$h1 = \frac{AR^3\tan^2\Lambda}{24(AR + 6\cos\Lambda)}$$

C.3.2 DERIVATIVES

$$C_{n\beta} = V_{vs} C_{L\alpha}\ c1\ C_L^2\ (f1 - e1\ d1)$$

$$C_{l\beta} = -C_{l\alpha}\ c1\ \frac{S_{vs} z_{vs}}{S\ b} - .198 - .43$$

$$C_{n\delta r} = \frac{C_{n\beta}\ \beta}{\delta_r}$$

$$\tau = \frac{C_{n\delta r}}{.9 C_{L\alpha} V_{vs}}$$

$$C_{l\delta a} = \frac{p\ b}{2\beta V_{TO} \delta_a}$$

$$C_{Yp} = \frac{dC_{Yp}}{dC_L} C_L + \frac{2z - z_p}{b} \frac{dC_Y}{b_{vw}} - 0.1018$$

$$C_{nr} = C_L^2 \left(1 + \frac{C_{D0}}{\pi AR}\right) + .09 + \left(\frac{2}{b^2}\right)(l_{vs}\cos\alpha + z_p \sin\alpha)^2 \frac{dC_Y}{b_{vw}}$$

$$C_{np} = \left(\frac{L_{vs}\cos\alpha + z_p \sin\alpha}{b}\right)\left(\frac{2z - z_p}{b}\right) \frac{dC_Y}{b_{vw}}$$

C.4 STATIC MARGIN TABLES

Table C2 - Static Margin at Take-Off

	Weight (lb)	CG (ft)	W * CG
JP + TANKS	38,516	41.33	1,591,866.28
LH_2 FUEL	36,854	88.39	3,257,525.06
ENGINES	21,653	102.00	2,208,606.00
PAYLOAD	2,500	91.00	227,500.00
CREW	440	74.15	32,626.00
COOLING SYSTEM	7,687	32.52	249,981.24
INLET	12,000	78.80	954,600.00
LH_2 TANKS	11,109	88.39	981,924.51
STRUCTURE	42,935	76.67	3,291,826.45
MAIN GEAR	2,651	101.00	267,651.00
NOSE GEAR	1,326	32.00	42,432.00
VERT. STABILIZERS	1,386	120.00	166,320.00
AVIONICS	4,869	60.00	282,000.00
	172,957		12,694,918.54

CG LOCATION	73.39928
AC LOCATION	77.03000
CP - CG	3.63072
$(CP - CG)_{NON-DIM}$	4.73573

Table C3 - Static Margins at the Start of Cruise

	Weight (lb)	CG (ft)	W * CG
JP + TANKS	14,999	38.00	569,962.00
LH_2 FUEL	29,649	88.39	2,620,675.11
ENGINES	21,653	102.00	2,208,606.00
PAYLOAD	2,500	91.00	227,500.00
CREW	440	74.15	32,626.00
COOLING SYSTEM	7,687	32.52	249,981.24
INLET	12,000	78.80	954,600.00
LH_2 TANKS	11,109	88.39	981,924.51
STRUCTURE	42,935	76.67	3,291,826.45
MAIN GEAR	2,651	101.00	267,651.00
NOSE GEAR	1,326	32.00	42,432.00
VERT. STABILIZERS	1,386	120.00	166,320.00
AVIONICS	4,869	60.00	282,000.00
	141,335		10,982,164.31

CG LOCATION	77.70308
AC LOCATION	78.67000
CP - CG	0.96692
$(CP - CG)_{NON-DIM}$	1.26120

Table C4 - Static Margins at the End of Cruise

	Weight (lb)	CG (ft)	W * CG
JP + TANKS	14,999	38.00	569,962.00
LH_2 FUEL	273	88.39	24,130.47
ENGINES	21,653	102.00	2,208,606.00
PAYLOAD	2,500	91.00	227,500.00
CREW	440	74.15	32,626.00
COOLING SYSTEM	7,687	32.52	249,981.24
INLET	12,000	78.80	954,600.00
LH_2 TANKS	11,109	88.39	981,924.51
STRUCTURE	42,935	76.67	3,291,826.45
MAIN GEAR	2,651	101.00	267,651.00
NOSE GEAR	1,326	32.00	42,432.00
VERT. STABILIZERS	1,386	120.00	166,320.00
AVIONICS	4,869	60.00	282,000.00
	111,959		8,385,619.67

CG LOCATION	74.89902
AC LOCATION	78.67000
CP - CG	3.77098
$(CP - CG)_{NON-DIM}$	4.91887

Table C5 - Static Margins at the Start of Loiter

	Weight (lb)	CG (ft)	W * CG
JP + TANKS	12,397	35.00	433,895.00
LH_2 FUEL	0	88.39	0.00
ENGINES	21,653	102.00	2,208,606.00
PAYLOAD	2,500	91.00	227,500.00
CREW	440	74.15	32,626.00
COOLING SYSTEM	7,687	32.52	249,981.24
INLET	12,000	78.80	954,600.00
LH_2 TANKS	11,109	88.39	981,924.51
STRUCTURE	42,935	76.67	3,291,826.45
MAIN GEAR	2,651	101.00	267,651.00
NOSE GEAR	1,326	32.00	42,432.00
VERT. STABILIZERS	1,386	120.00	166,320.00
AVIONICS	4,869	60.00	282,000.00
	109,984		8,279,422.20

CG LOCATION	75.27842
AC LOCATION	77.03000
CP - CG	1.75158
$(CP - CG)_{NON-DIM}$	2.28466

Table C6 - Static Margins When Fully Fueled

	Weight (lb)	CG (ft)	W * CG
JP + TANKS	41,959	41.33	1,734,165.47
LH_2 FUEL	36,854	88.39	3,257,525.06
ENGINES	21,653	102.00	2,208,606.00
PAYLOAD	2,500	91.00	227,500.00
CREW	440	74.15	32,626.00
COOLING SYSTEM	7,687	32.52	249,981.24
INLET	12,000	78.80	954,600.00
LH_2 TANKS	11,109	88.39	981,924.51
STRUCTURE	42,935	76.67	3,291,826.45
MAIN GEAR	2,651	101.00	267,651.00
NOSE GEAR	1,326	32.00	42,432.00
VERT. STABILIZERS	1,386	120.00	166,320.00
AVIONICS	4,869	60.00	282,000.00
	176,379		12,837,217.73

CG LOCATION	72.77334
AC LOCATION	77.03000
CP - CG	4.25666
$(CP - CG)_{NON-DIM}$	5.55216

Table C7 - Static Margins When Dry

	Weight (lb)	CG (ft)	W * CG
JP + TANKS	1,014	41.33	41,908.62
LH_2 FUEL	0	88.39	0.00
ENGINES	21,653	102.00	2,208,606.00
PAYLOAD	2,500	91.00	227,500.00
CREW	440	74.15	32,626.00
COOLING SYSTEM	7,687	32.52	249,981.24
INLET	12,000	78.80	954,600.00
LH_2 TANKS	11,109	88.39	981,924.51
STRUCTURE	42,935	76.67	3,291,826.45
MAIN GEAR	2,651	101.00	267,651.00
NOSE GEAR	1,326	32.00	42,432.00
VERT. STABILIZERS	1,386	120.00	166,320.00
AVIONICS	4,869	60.00	282,000.00
	98,601		7,887,435.82

CG LOCATION	79.99347
AC LOCATION	77.03000
CP - CG	-2.96347
$(CP - CG)_{NON-DIM}$	-3.86539

Appendix D

APPENDIX D - AERODYNAMIC HEATING

Aerodynamic heat flux distribution to the surface of an aircraft is a function of velocity, altitude, angle of attack, sweep angle, and radius of curvature of the leading edge and nose cap. The method described is divided into three parts: 1) the heat flux at the stagnation line, 2) the ratio of the local laminar heat flux to the stagnation heat flux aft of the stagnation line, and 3) the turbulent heat flux after a Reynolds number of 500,000 was exceeded. This allowed for the use of different methods for each part, providing for a greater overall accuracy.

D.1 LAMINAR HEAT FLUX

All Laminar heat transfer coefficients were calculated using the method described in Reference 36, outlined as follows:

D.1.1 STAGNATION POINT

$$h_0 = \left(\frac{.1055}{r_o^{1/2}}\right) \left(\frac{\rho_\infty}{\rho_{atm}}\right)^{1/2} \left(\frac{U_\infty}{10000}\right)^{1.16}$$

D.1.2 STAGNATION LINE

$$\frac{h_{le}}{h_0} = 1.0086 \left(\frac{P_f^{.8}}{r_o^{.2}}\right) (.72 \sin^{1.5}\alpha + .04 \cos\alpha)$$

where

$$P_f = \frac{1.33\ M_\infty^2\ \cos\Lambda_{le} + 1}{(1.33\ M_\infty^2 + 2.5)\ (\cos^2\Lambda_{le} - .0019)}$$

$$\Lambda_{le} = \sin^{-1}(\sin\Lambda \cos\alpha)$$

D.1.3 FLAT SURFACE

$$\frac{h_{fs}}{h_0} = \left(\frac{P_f\ (1 + 2\ N)}{3\ X}\right)^{1/2} \left(\frac{1.7\sin\beta - .86\sin\beta + .06}{M_\infty^2 \sin\beta + 1}\right)$$

where

$$P_f = \frac{1.33\ M_\infty^2 \sin^2\beta + 1}{(1.33\ M_\infty^2 + 2.5)\ (\sin^2\beta + .0019)}$$

$$\Lambda_{le} = \sin^{-1}(\sin\Lambda \cos\alpha)$$

$$N = \frac{.195\ \sin\alpha\ \tan\Lambda_{le}}{\sin\Lambda_{le}}$$

$$\beta = \sin^{-1}(\sin\alpha\ \cos\phi)$$

D.2 TURBULENT HEAT FLUX

All the turbulent heat transfer coefficients were calculated using the method described in References 3 and 4, outlined as follows:

$$h_t = \frac{C_f\ C_p\ U_\infty P_\infty}{2\ R\ T_\infty}\left(1 + 5\left(\frac{F_c\ C_f\ .5}{2}\right)\ (P_R - 1 + \ln\left(\frac{5P_R + 1}{6}\right))\right)$$

D.3 SKIN TEMPERATURE DISTRIBUTION

The local skin temperature distribution was calculated by iteratively solving the local heat balance equation:

$$h_i(T_{aw} - T_w) = \epsilon\sigma T_w^4$$

D.5 LIQUID CONVECTION

The skin temperature distribution on the surface was divided into 300 finite areas, where each area had an average temperature. From these finite areas the flow rates and weights can be calculated by the method in Reference 3 and 4, outlined as follows:

$$\text{Coolant Flow Rate (lb/hr)} = \frac{h_i\ (T_r - T_w)\ A_i - \epsilon\sigma T_w^4}{C_{pc}\ \ 200}$$

$$\text{Heat Exchanger Weight (lb)} = 5.75 \times 10^{-5}(CFR)\ C_{pc}\ 200$$

$$\text{Fuel Flow Rate (lb/hr)} = \frac{CFR}{370}\ \frac{C_{pc}}{C_{pf}}$$

$$\text{Distribution System Weight (lb)} = .3\ \Sigma\ A_i$$

Appendix E

APPENDIX E - SUBSONIC TESTING

The subsonic testing was carried out at The Ohio State University Aeronautical and Astronautical Research Laboratory. A 15½ inch model, mounted on a sting balance, was tested in the 3' x 5' subsonic wind tunnel at air speeds of 152 - 158 ft/s. The model was swept through different angles of attack, where normal and axial forces were measured from strain gauges in the sting balance. These forces are then resolved into C_L, C_D, and C_M through a computer link-up with the balance. Atmospheric temperature, pressure, and angle of attack are inputed into the program. The program then computed the dynamic pressure using a pitot probe input for the wind tunnel pressure, and it automatically resolved the strain gauge loads into aerodynamic coefficients.

The main difficulty with the testing, was that the zero load value on one of the normal strain gauges floated considerably while the test was in progress. To minimize this error, the model was quickly swept through 6 angles of attack within 2 - 3 minutes. Then the wind tunnel was shut down and the zero load values re-calibrated. The model was then again swept through 6 angles of attack, starting at a higher angle.

This procedure gave 6 sets of points for each angle of attack, with the data for the last 2 angles of the 6 being unreliable. The posed the problem of how to reduce the data. The method chosen was a weighting function method, outlined as follows:

When the data for the angle that was being reduced was first it was weighted 1, when it was second ; 0.5, and third ; 0.25.

i.e. for this set of data:

RUN	α	C_L
7	2	0.1525
	4	0.2421
	6	0.3429
	8	0.4471
	10	0.5474
	12	0.6543
8	4	0.2421
	6	0.3313
	8	0.4292
	10	0.5625
	12	0.6428
	14	0.7396
9	6	0.3480
	8	0.4536
	10	0.5585
	12	0.6603
	14	0.7681
	16	0.8779

then, for $\alpha = 6^{\circ}$,

$$C_L = \frac{0.3480 + .5\ (0.3313) + .25\ (0.3429)}{1.75} = 0.34250$$

See Table E.1 for aerodynamic coefficients found from the subsonic experimental test of the proposed configuration.

Table E.1 - Subsonic Test Data of the Proposed Configuration

α (deg)	C_L	C_D	C_{mac}	L/D
-8	-0.26063	0.05200	0.04324	-5.01212
-6	-0.18120	0.04006	0.02453	-4.52322
-4	-0.09661	0.03190	0.00933	-3.02853
-2	0.00472	0.02818	-0.00044	0.16749
0	0.09074	0.02950	-0.01231	3.07593
2	0.15750	0.03749	-0.02733	4.19579
4	0.24220	0.05331	-0.04465	4.54324
6	0.34250	0.07601	-0.06301	4.50599
8	0.44537	0.10667	-0.08560	4.17521
10	0.55447	0.14512	-0.11011	3.82077
12	0.64733	0.19430	-0.13097	3.33160
14	0.74491	0.24817	-0.16557	3.00161
16	0.86406	0.31609	-0.19375	2.73359
18	0.96307	0.38844	-0.22232	2.47933
19	1.00561	0.42549	-0.23368	2.36342
20	1.04099	0.46674	-0.24902	2.23034
21	1.08113	0.50593	-0.25966	2.13692
22	1.11526	0.54662	-0.27022	2.04028
23	1.12080	0.57493	-0.28278	1.94945
24	1.16390	0.61910	-0.29650	1.87999
25	1.19938	0.67266	-0.29854	1.78304
26	1.24200	0.72556	-0.30451	1.71178
27	1.26950	0.76990	-0.31142	1.64892
28	1.29650	0.82110	-0.31484	1.57898
29	1.29839	0.85929	-0.31669	1.51100
30	1.30743	0.89680	-0.31456	1.45788
31	1.30843	0.93607	-0.31255	1.39779
32	1.28490	0.95830	-0.30532	1.32560
33	1.24453	0.96930	-0.29108	1.28395
35	1.18340	0.99440	-0.26504	1.19006

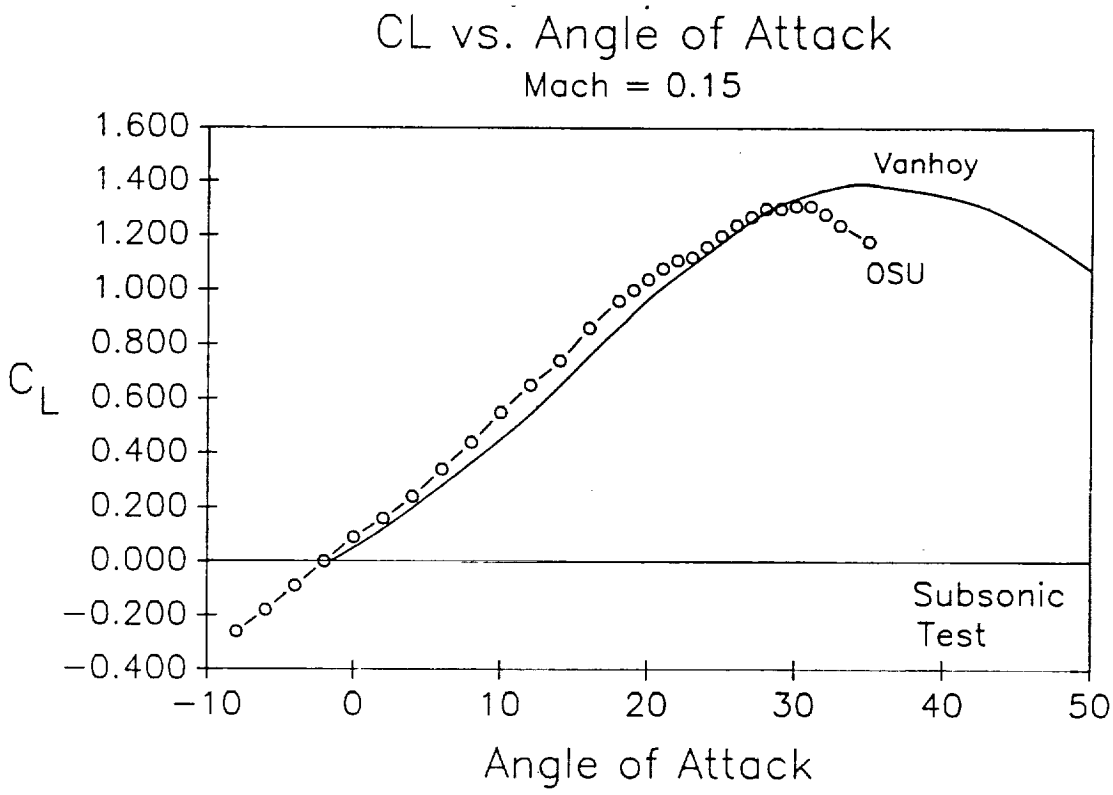
CL vs. Angle of Attack
Mach = 0.15
1.600
1.400
1.200
1.000
0.800
0.600
0.400
0.200
0.000
−0.200
−0.400
C_L
−10
0
10
20
30
40
50
Angle of Attack
Vanhoy
OSU
Subsonic
Test

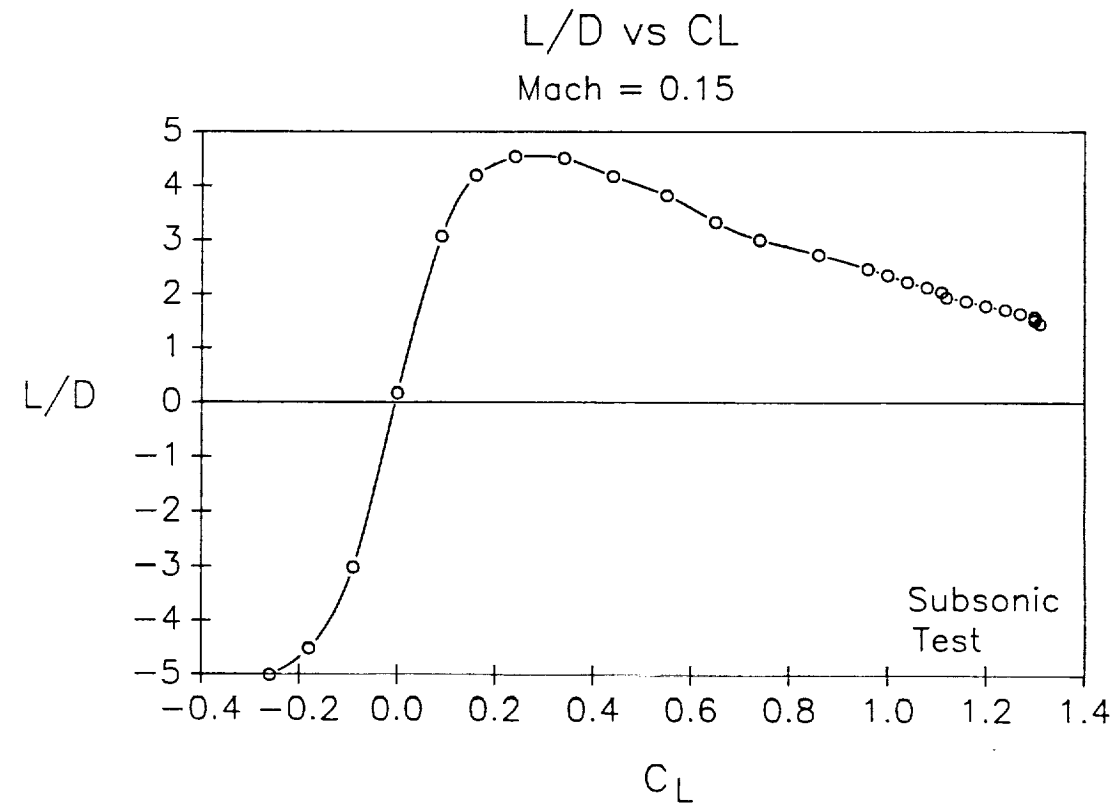
L/D vs CL
Mach = 0.15
5
4
3
2
1
0
−1
−2
−3
−4
−5
L/D
−0.4
−0.2
0.0
0.2
0.4
0.6
0.8
1.0
1.2
1.4
C_L
Subsonic
Test

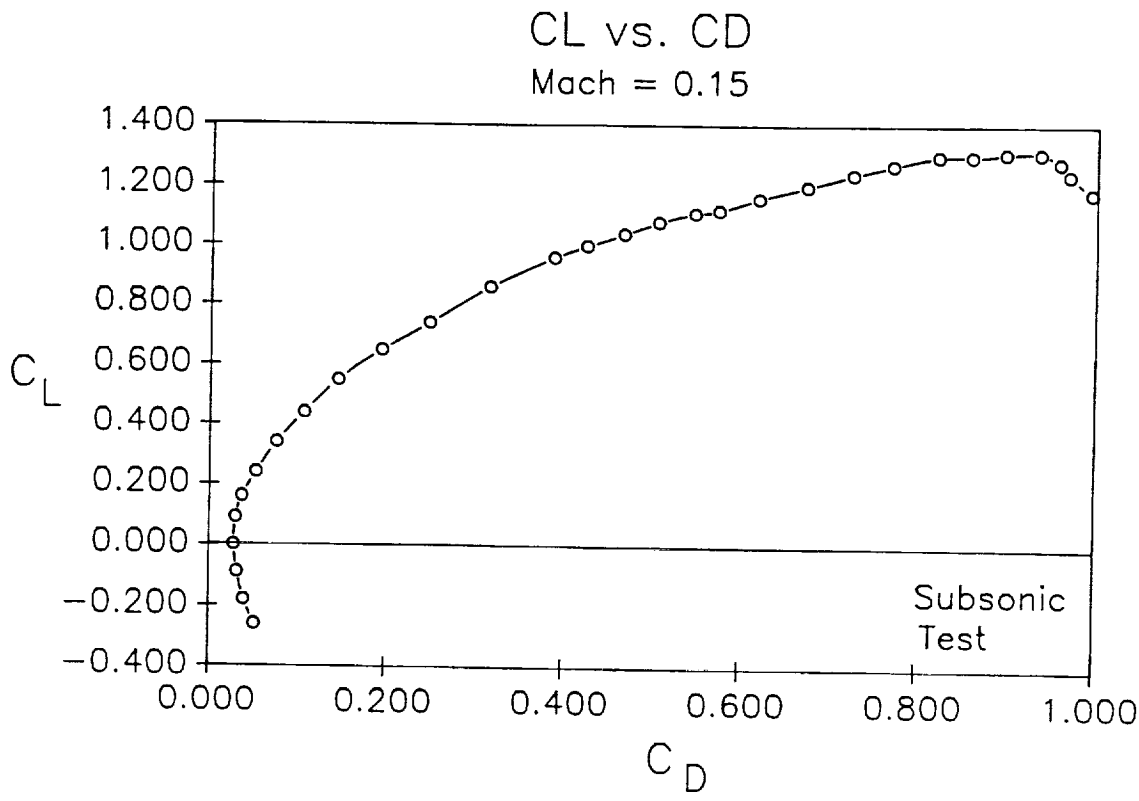
CL vs. CD
Mach = 0.15
1.400
1.200
1.000
0.800
0.600
0.400
0.200
0.000
−0.200
−0.400
C_L
0.000
0.200
0.400
0.600
0.800
1.000
C_D
Subsonic
Test

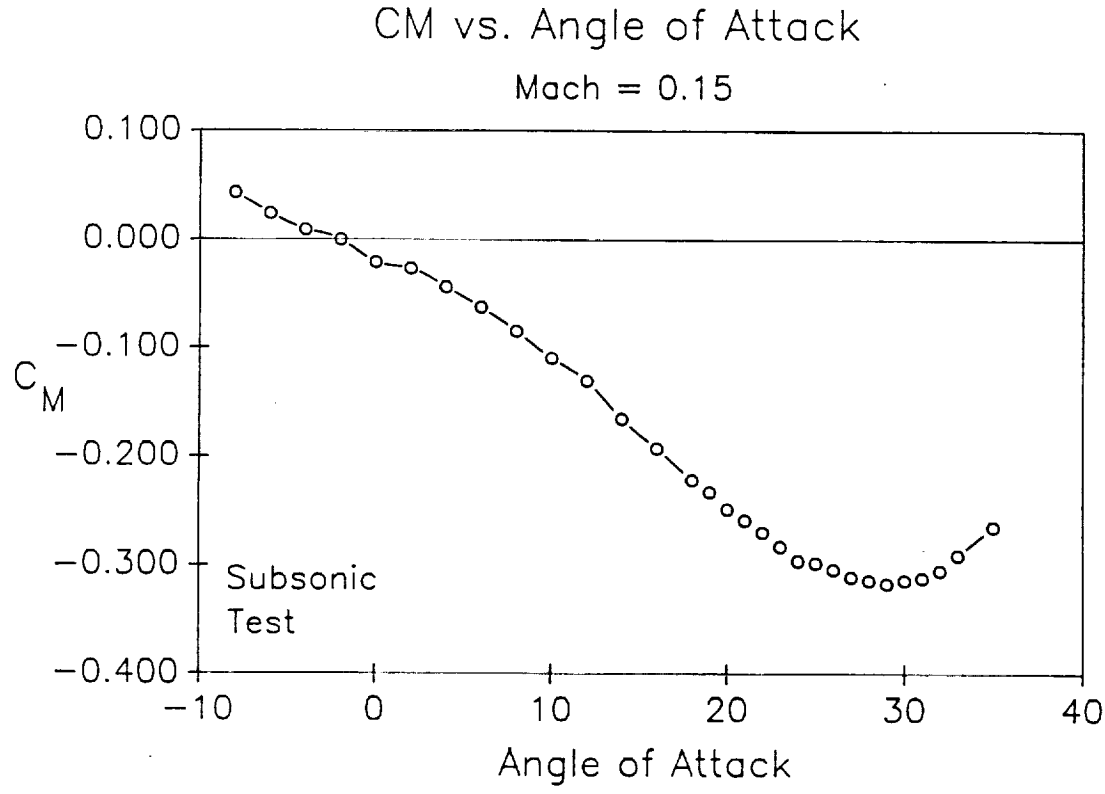
CM vs. Angle of Attack
Mach = 0.15
0.100
0.000
−0.100
−0.200
−0.300
−0.400
C_M
−10
0
10
20
30
40
Angle of Attack
Subsonic
Test

REFERENCES

1. Anderson, J.D., "Modern Compressible Flow with Historical Perspective," McGraw-Hill Inc., New York, 1982.

2. Nicolai, L.M., "Fundementals Of Aircraft Design," METS Inc., San Jose, 1984.

3. McConarty, W.A. and Anthony, F.M., "Design and Evaluation of a Active Cooling System for a Mach 6 Cruise Vehicle Wings," NASA CR-1916, December, 1971.

4. Helenbrook, R.G., McConnerty, W.A., and Anthony, F.M., "Evaluation of Active Cooloing Systems for a Mach 6 Hypersonic Transport Airframe," NASA CR-1917, December, 1971.

5. Resholko, E. and Cohen, C.B., "Heat Transfer at the Foward Stagnation Point of Blunt Bodies," NACA Report 3513, 1955.

6. Lees, L., "Laminar Heat Transfer over Blunt-Nosed Bodies at Hypersonic Speeds," Jet Propulsion, Vol. 26, No. 4, April 1956, pp. 259-269.

7. Neal Jr., L. and Bertram, M.H., "Turbulent-Skin-Friction and Heat-Transfer Charts Adapted from the Spalding Chi Method," NASA TN-D-3969.

8. Spalding, D.B. and Chi, S.W., "The Drag of a Compressible Turbulent Boundary Layer on a Smooth Flat Plate with and without Heat Transfer," Journal of Fluid Mechanics, Vol. 18, Part 1, January 1964, pp. 117-143.

9. Small, W.J., Fetterman, D.E., and Bonner, T.F., "potential of Hydrogen Fuel for Future Air Transportation Systems," ASME 73-ICT-104, 1973.

10. Pratt, D.T., Allwine, K.J., and Malte, P.C., "Hydrogen as a Turbojet Engine Fuel-Technological, Economical, and Enviromental Impact," from the 2nd International Symposium on Air Breathing Engines, 1974.

11. Waters, M.H., "Turbojet-Ramjet Propulsion System for All-Body Hypersonic Aircraft," NASA TN-D-5993, 1971.

12. Strack, W.C., "Aeropropulsion Opportunities for the 21st Century," NASA TM 88817, 1986.

13. Langley Research Center, "Vortex Flow Aerodynamics," Vol. 1, NASA CP 2416, 1985.

14. Hoerner, S.F., "Fluid-Dynamic Lift," Hoerner Fluid Dynamics, 1985.

15. Hoerner, S.F., "Fluid Dynamic Drag," Hoerner Fluid Dynamics, 1965.

16. Wentz, W.H.,"Wind Tunnel Investigations of Vortex Breakdown on Slender Sharp-Edge Wings," PhD Dissertation, Wichita State University, 1969.

17. Soltani, M.R., "Experimental Measurements on an Oscillating 70 deg Delta Wing in Subsonic Flow," AIAA-88-2576-CP, 1988.

18. Polhamus, E.C., "Predictions of Vortex Lift Characteristics by a Leading-Edge Suction Analogy," NASA Langley, April 1971.

19. Schrader, K.F., Reynolds, G.A., and Novak, C.J., "Effects of Mach Number and Reynolds Number on Leading-Edge at High Angles of Attack," AIAA-88-0122.

20. Williams, L.J., "Estimated Aerodynamics of All-Body Hypersonic Aircraft Configurations," NASA TM X-2091, March 1971.

21. Squire, L.C., "Calculations of the Pressure Distribution on Lifting Conical Wings with Applications to the Off Design Behavior of Wave-Riders," Cambridge University, 1968.

22. Bowcott, K.G., Anderson, S.D., and Capriotti, D., "Viscous Optimized Hypersonic Waveriders," University of Maryland, AIAA 87-0272, 1987.

23. Seddon, J. and Spence, A., "The Use of Known Flow Fields as an Approach to the Design of High Speed Aircraft," London, 1968.

24. Roskam, J., "Airplane Design, Part IV: Layout Design of Landing Gear and Systems," University of Kansas, 1986.

25. Arnaiz, H.H., "Flight-Measured Lift and Drag Characteristics of Large, Flexible, High Supersonic Cruise Airplane," NASA TM X-3532, May 1977.

26. Cubbage, J.M. and Kirkham, F.S., "Investigation of Engine-Exhaust-Airframe Interference on a Cruise Vehicle at Mach 6," NASA TN D-6060, January 1971.

27. Mattingly, J., Heiser, W., and Daley, D., "Aircraft Engine Design," AIAA, Inc., New York, 1987.

28. Kunkler, H., "The Influence of Air-Precooling Before Compression in Air-Breathing Engines of a Space-Launcher," from the 5th International Symposium on Airbreathing Engines, 1981.

29. Dusa, D.J., "Exhaust Nozzle System Design Considerations for Turboramjet Propulsion Systems," from the 9th International Symposium on Airbreathing Engines.

30. Roskam, J., "Airplane Flight Dynamics and Automatic Flight Controls," Part 1, University of Kansas, 1979.

31. Roskam, J., "Methods for Estimating Stability and Control Derivatives of Conventional Subsonic Airplanes," University of Kansas, 1971.

32. Ellison, D.E., "USAF Stability and Control Handbook (DATCOM)," Air Force Flight Dynamics Laboratory, AFFDL/FDCC, Wright-Patterson AFB, August 1968.

33. Blazynski, T.Z., "Explosive Welding," Applied Science Publishers LTD.,Essex England,1983

34. Deribas, A.A., "Treatment of Materials By Explosive Energy," Combustion, Explosion, and Shockwaves, Vol. 23, No. 5, pp.148-158, September-October 1987.

35. Vanhoy, D., "Low Speed Wind Tunnel Testing of a Mach 6 Viscous Optimized Waverider," University of Maryland, July 1988.

36. "Conceptual Design Aerodynamic Heating Analysis (CDHEAT)"

37. Seddon, J. and Goldsmith, E.L., "Intake Aerodynamics," AIAA, Inc., New York, 1986.

38. Kuethe, A.M. and Chow, C.Y., "Foundations of Aerodynamics," John Wiley and Sons, New York, 1986.

39. Corda, S., "Viscous Optimized Hypersonic Waveriders Designed from Flows Over Cones and Minimum Drag Bodies," PhD Dissertation, University of Maryland, 1988.